공학박사학위논문

다양한 설계 요소를 고려한 풍력터빈 블레이드 최적 설계

Optimal Design of Wind Turbine Blade considering Multiple Variables using the Response Surface Method

2021 년 2 월

서울대학교 대학원

기계항공공학부

이 상 래

다양한 설계 요소를 고려한 풍력터빈 블레이드 최적 설계

Optimal Design of Wind Turbine Blade considering Multiple Variables using the Response Surface Method

지도교수 신 상 준

이 논문을 공학박사 학위논문으로 제출함

2020 년 10 월

서울대학교 대학원

기계항공공학부

이 상 래

이상래의 공학박사 학위논문을 인준함

2020 년 12 월

위 원 장 : 윤 준 진

부위원장 : 申 尙 埈

위 원 : 유 기 완

위 원 : 백 인 수

위 원 : 김 용 협

Abstract

As the size of the wind turbines becomes larger, the optimal design of the blades becomes more significant. Design of a wind turbine blade is performed through the procedures of aerodynamic design, structural design, load analysis, structural integrity evaluation. And then the design will be finalized when the final aerodynamic and structural performances satisfy the target specification set at the conceptual design stage. From the perspective of a blade aerodynamic design, target output, efficiency, axial load and noise are the key factors of the design. With regard to the structural design of the blade, weight, tip deflection, safety margin from extreme, fatigue failure, and buckling load coefficient are the major design parameters to be considered. However, each design factor has an interactive relationship, not independent. Therefore, it is important to reduce the number of repetitive designs to minimize the blade development period, and for this, aerodynamic and structural designs of the blade should be carried out appropriately.

This thesis describes an improved optimization scheme for the blade aerodynamic design under realistic conditions, while considering multiple design parameters. The relationship between the objective function and the design parameters, such as the chord length, maximum chord and twist angle, are obtained by using the second-order response surface methodology (RSM). The identified parameters are organized to optimize the aerodynamic design of the blades. Meanwhile, from the standpoint of the structural design, the present research presents a methodology to perform blade structural design of large-

size wind turbine blade by using structural specific results of a baseline blade with proven structure based on the classical lamination theory (CLT) and the one-dimensional beam formulation. In addition, with an optimal structural design scheme using Variational Asymptotic Beam Section Analysis (VABS), the optimal design for blade structure is carried out. By the proposed design scheme, it will be possible to do a state-of- the-art design. It is reachable in a short period of time with small computer resources and effort. As a result, this design method is expected to provide optimal design for the wind turbine blade.

Keywords: Wind Turbine; Rotor Blade; Optimization; Aeroelastic Analysis; Blade Element Momentum Theory (BEMT); Response Surface Methodology (RSM); Design Parameters; Spar Cap; Classical Lamination Theory; Variational Asymptotic Beam Section Analysis (VABS); Finite Element Analysis(FEA); CFD; Bending- Torsion Coupling; Preliminary Structural Design; Annual Energy Production (AEP)

Student Number: 2013-30951

Contents

List of Figures

List of Tables

Chapter 1

INTRODUCTION

1.1 Wind Turbine and its Blades

Wind turbine is a complex engineering hardware, subjected to highly fluctuating and irregular wind loads. Although the wind turbines have continued to grow in terms of the dimension, power, and complexity, an optimal design of the wind turbine blade will still be one of the important tasks. In recent years, wind power is widely distributed as an alternative of fossil fuels. As it is demonstrated by the fact, the world wind power market has grown by 30% per a year since 1996[1]. When the initial wind turbine was launched, it was very small in size, but 70m or larger rotor blade is being realized in order to obtain efficiency in terms of the scale in recent years as shown in Fig 1.1. Additionally, their rotor swept area also has increased by 20 times and the capacity has also risen by approximately 100 times [2]. Rotor

swept area is a scale of the full sweep of the turbine blades. Greater rotor swept area suggests that the turbine be capable of capturing more amount of the wind. Therefore, the manufacturers seek to create turbines that is capable of generating more energy both by reaching the faster wind speeds in loftier heights, and by increasing the size. The bigger the blades, the more energy the turbine may generate.

1.2 Literature Review

There exist a number of considerations when designing the blades for the wind turbine. Regarding the aerodynamic design, which signifies the shape design of the blade, the design has usually been conducted using a simple methodology such as blade element momentum theory (BEMT). Various design methods have then been applied for an optimal design for the blades, and response surface method (RSM) is adopted in this thesis. There exist many methodologies to design the blade structure. This thesis focuses on an optimal cross-sectional design of the blade, in detail, an optimal design of the spar cap, which is the core component of the blade structure. For blades with completed structural design, a study will be also conducted on how to convert the blades to an equivalent beam representation for load analysis. Therefore, a literature survey will be carried out focusing on those aspects.

Blade Element Momentum Theory (BEMT)

For the designing and performance estimation of the blades, numerous

researchers used BEMT, which was originally developed for propellers by Glauert [3]. The BEMT was combined with the axial momentum and blade element theory to analyze the wind turbine performances. Many researchers predicted the wind turbine performance by combining the above two theories [4-8]. Mostafa et al. [9] showed an aerodynamic performance improvement of the wind turbine blade by the cavity shape optimization. Ozge and Ismail [10] explained an aerodynamic shape optimization methodology based on the genetic algorithm and BEMT. Wei et al. [11] presented an integrated method for designing the airfoil families of the large wind turbine blades using BEMT. Krishnil et al. [12] designed and optimized the airfoils for 20 kW wind turbine using the multi-objective genetic algorithm. BEMT was applied all along the blade span to calculate the turbine aerodynamic performances to optimize the horizontal axis wind turbine blade by Vincent et al. [13]. Bai et al. [14] studied to develop a small-scale horizontal-axis wind turbine (HAWT) suitable for the local wind conditions of Tainan, Taiwan using BEMT for the turbine blades airfoils. Thus, basically, the BEMT theory has been the easiest and fastest applicable theory in the design of the blades for wind turbine, but there was a limit to the aerodynamic design of blade that should have the greatest efficiency.

Response Surface Methodology (RSM)

The limitations of these BEMT theories are identified and the blade aerodynamic optimal design using RSM is considered for the purpose of supplementing them. RSM is a statistical method for investigating the

relationship between multiple design variables and fewer response variables. Li et al. [15] presented an aerodynamic optimization of wind turbine airfoils using the response surface techniques. An improved aerodynamic optimization technique for two-dimensional wind turbine airfoils is presented. Toft et al. [16] assessed the structural integrity of a wind turbine using the RSM. Tabatabaeikia et al. [17] studied an optimization of a wind turbine based on both computational and experimental method. In their study, as an analytical procedure for the optimization method, RSM was utilized using multivariate statistical techniques. Huang et al. [18] presented an optimal blade setting angle of a tidal turbine using the RSM and validated it with an experimental method. Sun [19] presented a wind turbine airfoil design using the RSM under various operating conditions. In particular, most of the literatures have focused on the optimization of the airfoil profile or active twist rotors, etc. However, in addition to those factors, there were more possibilities for aerodynamic design for improving the efficiency of the blade, and further study would be needed.

Optimal Cross-Sectional Design

Apart from the blade aerodynamic design mentioned so far, there are also considerations for various design methods in the field of blade structural design. In relation to the structural design of the blade, many studies have been processed in rotorcraft [20] and aeronautical engineering field for the structural optimization. Eun et al. [21] suggested a design optimization procedure for blade sections to improve the existing cross-sectional design. Lim et al. [22] developed a rotor optimization framework for a compound

rotorcraft with a lift offset using a multilevel optimization approach. Friedmann et al. [23] examined the composite beam cross-sectional analysis based on the variational asymptotic approach, cross-sectional analysis, and optimal structural design were performed. Kovalovs, et al. [24] conducted numerical optimization of helicopter rotor blade design for active twist control based on the optimal cross-sectional design approach. Seoul National University Flap (SNUF) blade with a trailing-edge flap was investigated and improved using the optimal cross-sectional design [25]. Thus, in relation to the cross-sectional design approach of the blade design, many studies have been conducted already in helicopter and aeronautical engineering fields. When it comes to the design of wind turbine blades, it may be a good design approach to reference them without any clear methodology being presented.

Optimal Design of a Spar Cap

In the extension of the structural design, the blade structure has a crucial impact on the blade stiffness of a wind turbine. In addition, the spar cap is the most important design consideration factor in the blade structure for wind turbine. Therefore, careful design and evaluation should be carried out. Perry, et al. [26] presented structural design of the spars for 100-m biplane wind turbine blades. Analysis is developed for those spars. Barnes and Morozov [27] conducted structural optimization of composite wind turbine blade structures with variations of internal geometry configuration and compared to investigate the effect of allowing various aspects of the internal structural geometry and spar cap. Maheri, et al. [28, 29] presented combined

analytical/FEA-based method for coupled aero-structure simulation of wind turbines utilizing bending-twist adaptive blades. Barr, et al. [30] optimized tow-steered composite wind turbine blades for static aeroelastic performance with variable-angle tow composite materials and enabled coupled bending-twist deformations under aerodynamic loads. Additionally, an optimization of the spar caps in wind turbine blades is examined by Liao et al. [31]. In particular, most researches in the past yielded optimal spar cap design by a number of iterations, which consumed a lot of time and computational resources. Therefore, comparison and obtaining information of the blade characteristics, such as stiffness, weight and thickness, from the existing blades will be a useful method. This will be an efficient approach in verifying the design when one's own blade design results are not sufficiently accumulated

This thesis presents a multiple parametric blade design methodology with maximum efficiency using the second-order RSM based on the BEMT. The ultimate goal of the RSM application is obtaining the best blade performance by identifying the design variables that significantly affect the blade efficiency, such as chord length, max chord length and twist angle, etc., and designing the blades with the maximum efficiency and maximum energy production through the optimal combination of these variables. Additionally, a methodology to perform a blade structural design of a large wind turbine blade by using structural specific results of a baseline blade with a proven structure and aerodynamic characteristics are also presented. The methodology is based on classical lamination theory (CLT) and optimal cross-sectional design approach.

Furthermore, the structural optimal design is focused on the spar cap.

1.3 Summary of Chapters

The purpose of this research is to design the optimal aero-structural design of a 2 MW class wind turbine blade and to check and verify its performance and structural integrity through design evaluation based on international standard (IEC) and the guideline of certification institutions [32].

The following is a brief summary of the organization of present dissertation:

- In Chapter 2, objective and scope of this thesis are presented. Design of a wind turbine blade is performed through the procedures of aerodynamic design, structural design, load analysis and structural integrity evaluation. Among them, aerodynamic and structural design are the most important design procedures for blade design. Thus, the details of blade aerodynamic design and structural design, which are carried out intensively in this thesis, are explained using the design flow chart.

- In Chapter 3, regarding the blade design, various theoretical back grounds are described related to aerodynamic design, structural design, load analysis and structural evaluation. In the case of blade

aerodynamic design, the theory of BEMT, RSM, etc. is applied to carry out the initial and optimal design, respectively. For structural design of the blade, the optimized number of the spar cap layers, a parametric study for the axial and twist coupling stiffness coefficients for each material design is introduced. In addition, in relation to the blade design evaluation, it describes the evaluation method, type and failure criteria, etc.

- Chapter 4 describes an improved optimization framework for the blade aerodynamic design under realistic conditions, while considering multiple design parameters. The relationship between the objective function and the design parameters, such as the chord length, maximum chord and twist angle, are obtained by using the second-order RSM. Moreover, the identified parameters are organized to optimize the aerodynamic design of the blades.

- Chapter 5 presents a methodology to perform blade structural design of large-size wind turbine blade by using structural specific results of a baseline blade with proven structure based on the CLT, focused on the spar cap. In addition, for the sectional optimum design of the blade, it is divided several sections and improvements in the structural blade design are attempted for each section based on the optimal cross-sectional design approach.

- In Chapter 6, load calculation for blade design and integrity evaluation are is conducted. In this thesis, 2MW- rated turbines are selected as reference models and the load value used in blade design is calculated using the BEMT-based GH-BLADE program. To check the streamlines and pressure distribution depending on the wind velocity on the blade surface, calculations using computational fluid dynamics (CFD) are also performed and compared with BEMT results. In addition, design evaluation such as Fiber failure, inter fiber failure, stability, modal analysis, maximum tip deflection examination is carried out. Fatigue life evaluation of the fatigue limit state (FLS) condition is also processed. Through this, the reliable design of the blade is completed.

Finally, conclusions and recommendation for the future work are presented in Chapter 7.

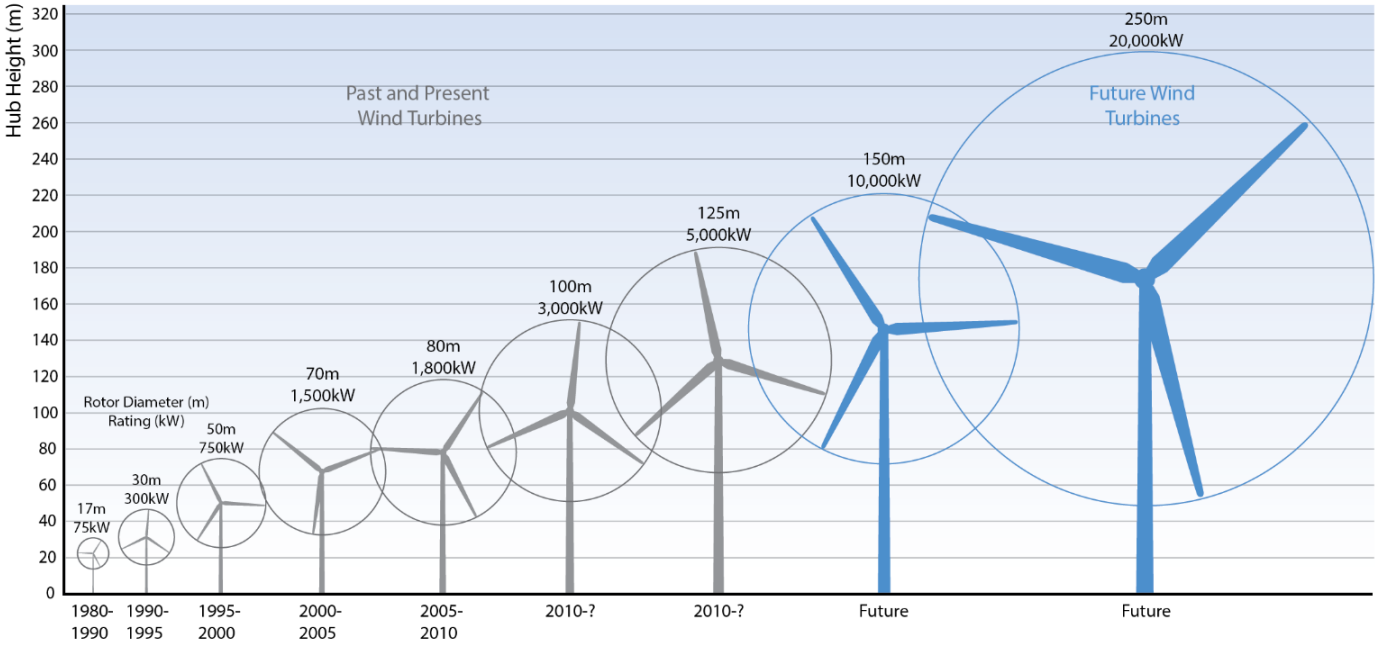

Figure 1.1. Growth in size of typical commercial wind turbines [33]

Chapter 2

OBJECTIVE AND SCOPE

2.1 Wind Turbine Blade Design

Designing of a wind turbine blade is performed through the procedures of aerodynamic design, structural design, load analysis and structural integrity evaluation, and the design is finalized when the final aerodynamic and structural performances satisfy the target specification.

After the design specifications of a blade are decided, at the aerodynamic design stage, usually selects the candidate group of airfoil and conducts basic aerodynamic design and performance analysis by obtaining reliable airfoil performance data through tests or numerical analysis. Initial aerodynamic design is generally conducted by BEMT, and goes through a design optimization process based on the evaluation results of output, efficiency, and load. If the design conditions are satisfied and the aerodynamic design is

completed in the optimal design process, the final aerodynamic design information such as twist angle, chord length distribution and surface model, etc, are sent to the structural design stage.

In the structural design stage, a design concept is decided considering used material, manufacturing procedures, and internal structure concept such as spar cap, shear web, root connection, etc. If the structural design of the blade is completed, the structural design is verified through a structural integrity evaluation based on international standards or industrial guidelines.

In the meantime, at the load calculation stage, it is needed to define the design load case. From the perspective of a wind turbine, various cases that can be experienced during the life time of 20 years should be set, and a design load case should be set in consideration of these situations. Subsequently, a variety of load analysis programs based on BEMT are used to calculate the load to be used for blade design and evaluation

On this wise, the blade design needs to be repeatedly performed aerodynamic design, structural design, load analysis and design evaluation, so the blade design should be performed in an integrated manner to ensure optimal design results can be obtained by taking into account various design conditions.

2.2 Optimal Aerodynamic Design of the Blade

With regard to optimal aerodynamic blade design, a flowchart of the present process is shown in Fig 2.1. First, based on BEMT, the shape design of the

blades, i.e., the aerodynamic design, is carried out as a baseline blade. To check the adequacy of the aerodynamically designed blade, the blade will be examined regarding whether it is applicable to an actual turbine based on various parameters such as blade efficiency, power production, and thrust, obtained using commercial load calculation program, GH Bladed. In this process, it is important to identify the design variables that affect blade efficiency in the blade design procedure.

Next, using the identified design variables, the best combination of the design variables that can yield the maximum blade efficiency will be obtained. It is identified that the blade chord length and the built-in twist angle will be the most significant design variables, and the design process to determine the optimal combination of those will be conducted. Meanwhile, as a first step in the optimal design using the RSM, several calculation locations are chosen along the length of the blade. In the case of a substantial change in the geometry of the blade, a significant amount of computation is performed by placing the calculation locations more densely. For the computation of the RSM, the ranges and levels of the variables for the chord length and built-in twist angle are assigned for each calculation location. At each calculation location, various combinations of the chord length and twist angle are presented using the RSM, and the blade efficiency will then be estimated by GH Bladed based on those combinations. These computations are performed at each calculation location. The chord length and the twist angle, determined by the optimal combination at each location [4–7], finally represent the geometry of the blade as a result of the aerodynamic design.

As the final step, the blade efficiency, power production, and thrust are obtained using the optimal design blade again. If the results are within the blade design objective, the blade optimization will be completed. However, if they do not match, the redesign will be performed by changing the design parameters.

2.3 Optimal Structural Design of the Blade

In terms of the optimal design of the blade structure, schematic diagram of the structural design optimization procedure is shown in Fig 2.2. For blade structure optimization design, the optimal design is carried out through a two-step process.

First, the structural design procedure of large wind generator blades based on CLT is presented. By analyzing the existing blade, the optimized numbers of the spar cap layers in the blades are estimated. Moreover, a parametric study using the carbon fiber-reinforced plastics (GFRP) and glass fiber-reinforced plastic (CFRP) at multiple fiber orientation angles for the spar cap design is attempted with regards to the axial and twist coupling stiffness coefficients for each material design.

The next step is that the blade is divided several sections and improvements in the structural blade design are attempted for each section. This optimization framework for the sectional design is established on the basis of the Advanced Technology Rotor (ATR) optimization procedure as suggested in a previous

study [34]. An objective function is established to minimize the weight of the blade and the design variables are used such as ply number for spar cap, skin and shear web and shear web location. With this optimal design framework, the design of the blade structure is in progress and the design of the structure has been completed if the final constrain is satisfied through various iterative calculations. In addition, a cross sectional analysis is performed using VABS [35], which not only calculates the sectional properties compatible with linear and nonlinear beam analysis, but can also recovers the pointwise distribution of the three-dimensional displacement /stress/strain field. When compared with the FEA using three-dimensional brick elements, two to three orders of magnitude in computing time can be saved by using VABS, with little loss of the accuracy [36].

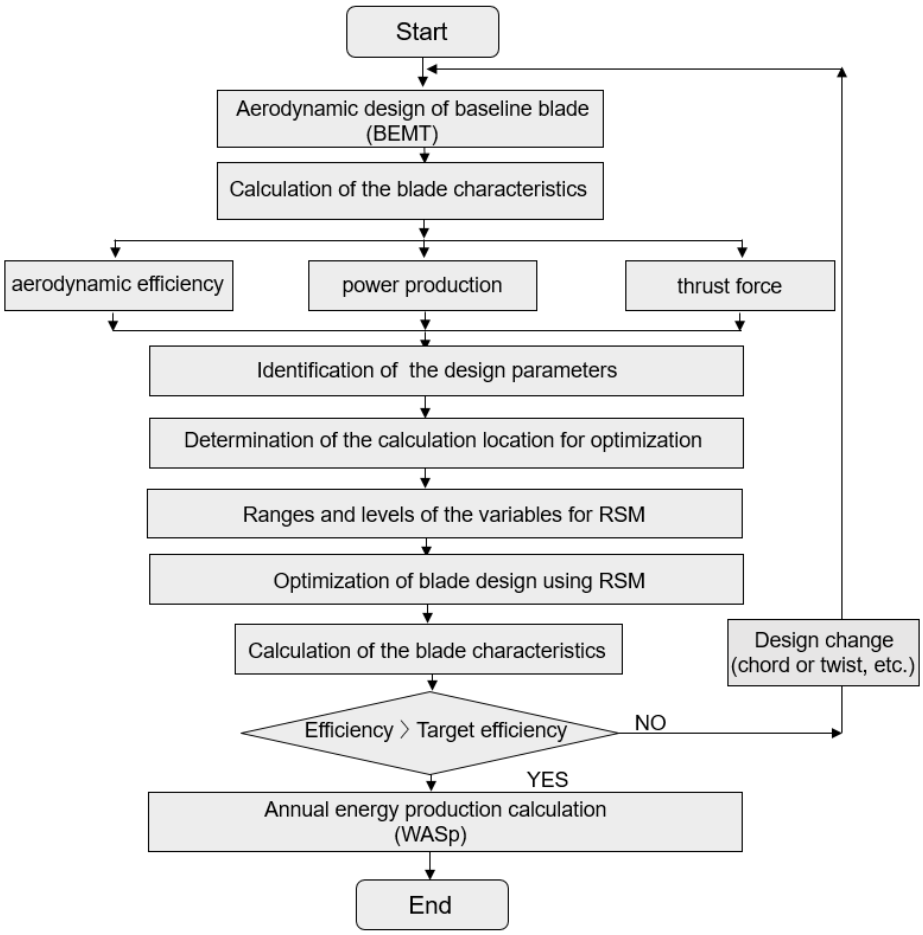

Figure 2.1. Flow chart of the aerodynamic design optimization procedure

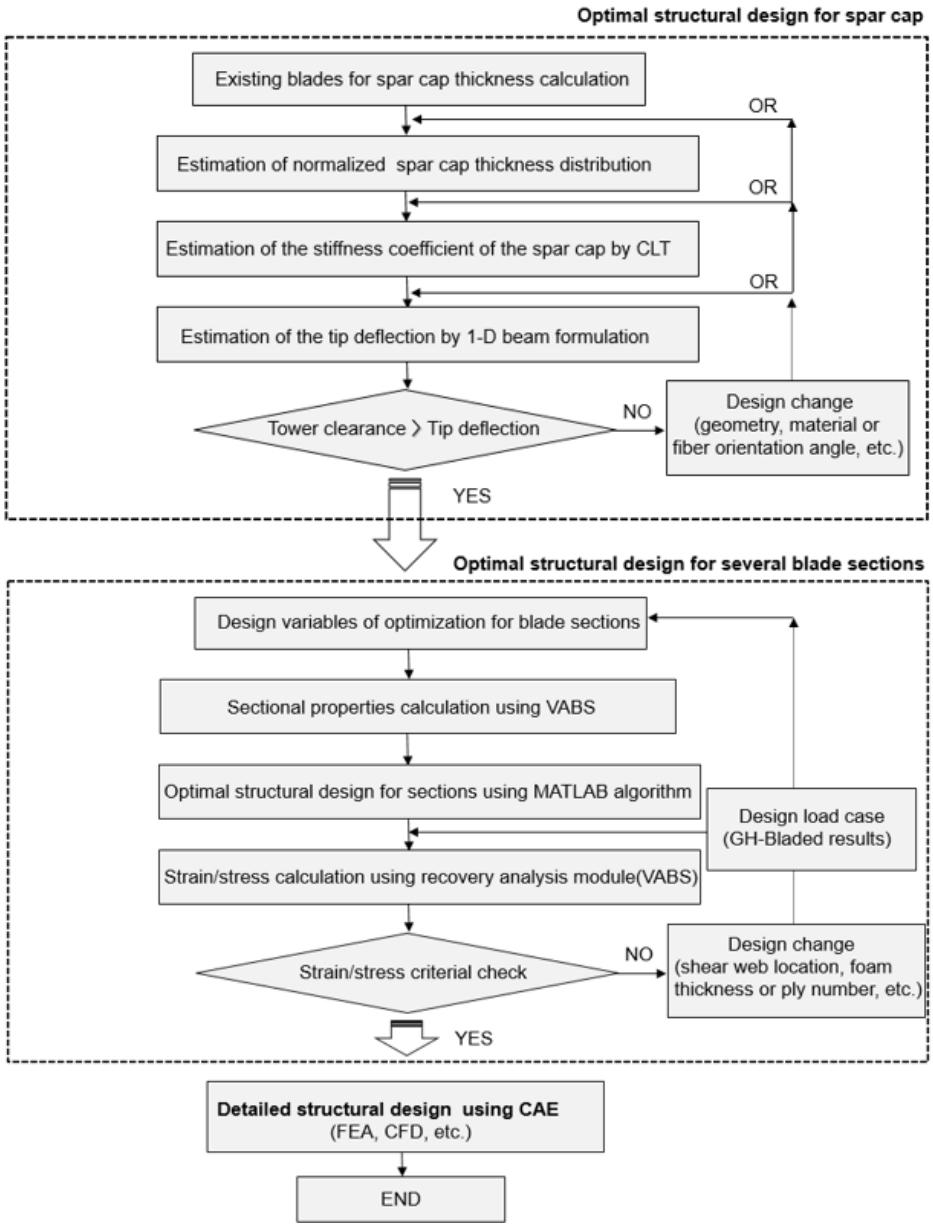

Figure 2.2. Schematic diagram of the structural design optimization procedure

Chapter 3

THEORETICAL METHOD

This chapter describes an improved optimization framework for blade design under realistic conditions based on the theorem. In the case of blade aerodynamic design, the theory of BEM is introduced for the baseline blade design and then RSM is applied to carry out the optimal design, respectively. Meanwhile, for the structural design of the blade, using the CLT, the optimized number of the spar cap layers, a parametric study for the axial and twist coupling stiffness coefficients for each material design is conducted. In addition, the design optimization procedure for blade sections to improve the existing cross-sectional design is followed with ATR. Furthermore, the method of extraction of the sectional properties from blade based on the blade sectional element concept, structural evaluation procedure including Ultimate Limit State (ULS), Fatigue Limit State (FLS) is presented.

3.1 Aerodynamic Design

BEMT has been used as a theory to predict blade performance, and this theory has the assumption that the wind is a one-dimensional, non-viscous, and incompressible flow. This theory has been applied in numerous studies dealing with the simulation of wind turbine performance [4–8]. In this way, the aerodynamic design for the blade is performed primarily using BEMT. However, in the case of BEMT theory, there are limitations in efficiency, power, etc., and in order to solve such limitation, RSM will be applied to the blades and the optimal design will be performed.

3.1.1 Blade Element Momentum Theory (BEMT)

Based on BEMT, wind turbine blades are considered as actuator discs and have no thickness, as shown in Fig 3.1. The definition of the power coefficient (C_P) is as follows:

$$C_P = \frac{Actual\ electrical\ power\ production}{Wind\ power\ in\ turbine} = \frac{P_{out}}{P_{in}} = \frac{P_{rotor}}{0.5\rho A_T V^3} \tag{3.1}$$

where ρ, A_T, and V are the air density, cross-section of the rotor, and wind velocity, respectively. The axial induction factor is introduced as

$$a = \frac{V - V_T}{V} \tag{3.2}$$

Regarding the upstream flow, it is assumed that the downstream flow is rotated at angular velocity ω while it is entirely axial. Taking into account

the tangent flow behind the rotor, a factor defined as a', the tangential induction factor, is introduced as follows:

$$a' = \frac{\omega}{2\Omega} \tag{3.3}$$

where ω is the induced tangential angular velocity of the flow and Ω is the angular velocity of the rotor, respectively.

The thrust by the annular element can be expressed as follows, and the power produced by the rotor, P, is found to be the product of the annular elemental torque and the angular velocity, described as follows:

$$dT = 4a(1-a)\frac{1}{2}\rho V^2 2\pi r dr(a), \quad P = \frac{\int_0^R 4a'(1-a)}{2}\rho V 2\pi r dr \Omega r^2 (b) \tag{3.4}$$

dr is a blade element of length and r is a distance from the rotor axis, shown in Fig 3.1, and the power coefficient, C_p, is given as follows.

$$C_p = \frac{8}{\lambda^2}\int_{\lambda_h}^{\lambda} \lambda_r{}^3 a'(1-a)\left\{1-\left(\frac{C_D}{C_L}\right)\cot\phi\right\} d\lambda_r \tag{3.5}$$

where λ is the tip speed ratio, λ_h is the speed ratio at the hub radius, and λ_r is the speed radius at rotor radius r.

$$\lambda = (\Omega R / V), \qquad \lambda_h = (\Omega R_h / V), \qquad \lambda_r = (\Omega r / V) \tag{3.6}$$

Several research studies have considered the effects of tip losses [11]. Prandtl's tip loss coefficient (C_t) is shown below.

$$C_t = \frac{2}{\pi}\cos^{-1}\left(\exp\left[-\left\{\frac{\left(\frac{B}{2}\right)\left(1-\frac{r}{R}\right)}{\frac{r}{R}\sin\phi}\right\}\right]\right) \tag{3.7}$$

The power coefficient, C_p, along with the tip loss coefficient of the blade can

be determined as

$$C_p = \frac{8}{\lambda^2}\int_{\lambda_h}^{\lambda} C_t \sin^2\phi(\cos\phi - \lambda_r \sin\phi)(\sin\phi + \lambda_r \cos\phi)\left\{1 - \left(\frac{C_D}{C_L}\right)\cot\phi\right\}\lambda_r^{\,2} d\lambda \tag{3.8}$$

By looking at Equation (3.8), it is obvious that the torque and power depend on the angle of attack, ϕ, which is determined by the inflow wind speed and the rotational speed of the turbine.

3.1.2 Aerodynamic Design

In the initial blade design phase, the design parameter, such as the diameter of the blade, D_{rotor}, rated speed, $\Omega_{blade,rated}$, and design tip speed ratio, λ_{design}, can be predicted by using Equations (3.9)- (3.11).

$$D_{rotor} = \sqrt{\frac{8P_{rated}}{\eta C_{p,estimated}\rho\pi V^3{}_{rated}}} \tag{3.9}$$

$$\Omega_{blade,rated} = \left(\frac{V_{tip}}{V_{rated\ wind\ speed}}\right) \tag{3.10}$$

$$\lambda_{design} = \left(\frac{\omega R}{V_{in}}\right) \tag{3.11}$$

After determining the design parameters is completed, the computation of the chord length and twist angle will be processed as follows [6].

(1) Compute the tip loss factor in Equation (3.7), (C_t)

(2) Calculation of the axial flow induction factor,

$$a_\mu = \frac{1}{3} + \frac{1}{3}C_t + -\frac{1}{3}\sqrt{1 - C_t + C_t^{\,2}} \tag{3.12}$$

(3) Check the convergence digit after iterative computations for C_t and a_μ

(4) Obtain the tangential flow induction factor, a'_μ

$$a'_\mu = \frac{a_\mu\left(1-\frac{a_\mu}{C_{t,\mu}}\right)}{\lambda^2{}_{design}\mu^2} \tag{3.13}$$

(5) Calculate the chord length, c_μ

$$c_\mu = \frac{2\pi}{N\lambda_{designC_{L,tip\ foil}}\mu^2}\frac{4\lambda^2{}_{design}\mu^2 a'_\mu R}{2\sqrt{(1-a_\mu)^2+(\lambda^2{}_{design}\mu(1+a'_\mu))^2}} \tag{3.14}$$

(6) Calculate the twist angle, θ_μ

$$\theta_\mu = \phi_\mu - \alpha_{tipfoil} \tag{3.15}$$

Through this procedure, the aerodynamic blade design for the wind turbine is completed, and its power and efficiency are obtained based on BEMT.

3.1.3. Response Surface Method (RSM)

RSM is an important statistical methodology for investigating the relationships among the variables, which is to set-up an estimated specific relation between the design parameters and their responses. The main purpose of RSM is to use a series of designed experiments to acquire a best response. It is used to maximize the performance of a product by optimizing the operating elements. Independent variables are assumed to be continuous and can be controlled by experiments with minor errors. It is needed to find an appropriate

assumption of the actual practical relationship between the individual variables and the responses. Generally, the second-order RSM model is used as follows.

$$Y = \beta_0 + \sum_{i=1}^{k}(\beta_i x_i) + \sum_{i=1}^{k-1}\sum_{j=2}^{k}(\beta_{ij} x_i x_j) + \sum_{i=1}^{k}(\beta_{ii} x^2{}_i) + \varepsilon \tag{3.16}$$

where Y is the response value of the system, β_0 is the regression coefficient intercept, β_i are the linear terms, β_{ij} are the quadratic terms, and β_{ii} are the interaction terms. x_i and x_j are the coded independent variables for the design parameters. In addition, k and ε are the number of the variables and the statistical error, respectively.

$$y = X\beta + \varepsilon \tag{3.17}$$

$$\begin{bmatrix} y_1 \\ y_2 \\ \vdots \\ y_n \end{bmatrix} = \begin{bmatrix} 1 & x_{11} & x_{12} & \cdots & x_{1k} \\ 1 & x_{21} & x_{22} & \cdots & x_{2k} \\ \vdots & \vdots & \vdots & \vdots & \vdots \\ 1 & x_{n1} & x_{n2} & \cdots & x_{nk} \end{bmatrix} \begin{bmatrix} \beta_1 \\ \beta_2 \\ \vdots \\ \beta_k \end{bmatrix} + \begin{bmatrix} \varepsilon_1 \\ \varepsilon_2 \\ \vdots \\ \varepsilon_k \end{bmatrix} \tag{3.18}$$

Using the least-squares method, Equations (3.17) and (3.18) are solved, and the equation coefficients are computed. After obtaining the equation coefficients, the response is estimated by solving the equations. In Section 3.1.2 and [5–7], the chord length and the twist angle distribution along the blade are recognized as the most important design parameters for the blade efficiency, and research on the optimal blade design is conducted by focusing on these two parameters using the RSM.

3.2 Structural Design

This chapter presents a procedure for the structural design of a large wind turbine blade based on the CLT. By analyzing the existing blade, the optimized numbers of the spar cap layers in the blades are estimated. Furthermore, a parametric study for the axial and twist coupling stiffness coefficients for each material design is conducted. In addition, the design optimization procedure for blade sections to improve the existing cross-sectional design is followed.

3.2.1. Spar cap Thickness Estimation

The number of the plies used in the spar cap is selected as one of the design variables. Hence, multiple existing wind turbine blades [37-42] are examined to analyze the spar cap thickness characteristics via a comparison based on normalized spar cap thickness distribution. An analysis is performed under identical load conditions corresponding to the IEC Wind Class. Furthermore, it is assumed that the thickness increases linearly with the blade length, i.e., from smaller blades to larger blades. Therefore, if the thickness of a section of a blade is normalized with respect to the length of the blade, then this parameter can be compared for a variety of diverse blades. By comparing the spar cap thickness ratios of the existing blades with similar design conditions and capabilities, specific trends can be identified among the blades. This reduces the number of repetitive calculations that are required during the initial laminate design and shortens the development period for an optimal design.

Using this similarity or tendency of the existing blades, a trend line for the spar cap thickness is predicted and a higher-order curve fitting function is obtained. By using this function, the spar cap thickness ratio of the blade is estimated, and the final required number of plies are obtained by dividing the unit thickness of the unidirectional ply.

3.2.2. Stiffness Coefficient of the Spar cap

The computation is performed by using the information, such as the number of plies, angle and material properties of fibers (unidirectional or multi-axial), applied on the spar cap. Also, the axial and twist coupling stiffness coefficient results for each blade section are used as the design information of the blade. The stiffness coefficient prediction for a composite beam has been proposed by many researchers based on CLT [43-44] by applying the traditional assumptions for thin beams. Stress prediction on a composite beam composed of multiple plies with different materials and lamination directions is performed at the laminate level. By CLT, matrix A can be expressed as fol lows:

$$A_{ij} = \sum_{k=1}^{n} \left[\overline{Q}_{ij} \right]_k \qquad (i, j = 1, 2, 6) \tag{3.19}$$

In Eq. (3.19), n indicates the number of plies of the spar cap. Moreover, N_s is relatively small for a thin composite structure, and therefore, it is assumed to be zero and can be expressed as follows,

$$\begin{Bmatrix} N_z \\ N_{zs} \end{Bmatrix} = \begin{bmatrix} A_{11} - \dfrac{(A_{12})^2}{A_{22}} & A_{16} - \dfrac{A_{12}A_{26}}{A_{22}} \\ A_{16} - \dfrac{A_{12}A_{26}}{A_{22}} & A_{66} - \dfrac{(A_{26})^2}{A_{22}} \end{bmatrix} \begin{Bmatrix} \varepsilon_z \\ \gamma_{zs} \end{Bmatrix} \tag{3.20}$$

where, N_α is the sum of the composite laminate stress and the value from integrating the stress of the laminate in the thickness direction. When Eq. (3.20) is expressed as follows, each element of the matrix will be determined accordingly.

$$\begin{Bmatrix} N_z \\ \gamma_{zs} \end{Bmatrix} = \begin{bmatrix} H_{11} & H_{21} \\ H_{21} - H_{22} \end{bmatrix} \begin{Bmatrix} \varepsilon_z \\ N_{zs} \end{Bmatrix} \tag{3.21}$$

where,

$$H_{11} = \left(A_{11} - \frac{A_{12}^{\ 2}}{A_{22}} - \frac{H_{21}^{\ 2}}{H_{22}} \right) \tag{3.22}$$

$$H_{21} = \left(A_{16} - \frac{A_{12}A_{26}}{A_{22}} \right) H_{22} \tag{3.23}$$

$$H_{22} = \left(A_{66} - \frac{A_{26}^{\ 2}}{A_{22}} \right)^{-1} \tag{3.24}$$

H_{11}, in Eqs. (3.22) ~ (3.24), is an axial stiffness coefficient and is a value proportional to the flexural stiffness. H_{21} is a twist coupling stiffness coefficient that expresses the degree of triggering twist deflection and H_{22} is a shear stiffness coefficient, respectively.

3.2.3. Optimization for the Blade Sections

For the structural design of the blade, the specifications of the turbine system used in the design of the baseline blade is summarized in Table 3.1. In addition, the cross section of a regular wind turbine blade is shown in Fig. 3.2 and the material properties used in the design in this thesis are shown in Table 3.2. An improvement for the design of the blade is proposed by developing a cross sectional design-optimization framework. Figure 3.3 shows a flowchart of the present optimization procedure. The blade cross section is proceeded with the structural design using design variables. Subsequently, the sectional properties are obtained using VABS, and the strain/stress is estimated by applying the design load. Such calculation repeats several times of iteration and concludes the final result as the optimal design result, so that the result is within the range of not deviating from the contour.

Spar cap ply number, skin ply number, root ply number, shear web ply number, shear web location and shear web foam thickness are used as design variables. The objective function used in the current optimization framework is expressed in Eq. (3.25).

$$J = \min[2(m_{spar\,cap} + m_{skin} + m_{root}) + m_{1st\,shear\,web} + m_{2nd\,shear\,web}] \qquad (3.25)$$

In addition, as a constraint of computation, resonance avoidance and 2nd shear web location are applied.

3.3 Extraction of the sectional properties

In order to accurately predict the behavior of the blade, and replace the complex blade configuration with a simpler one, it is necessary to introduce the blade element concept. For blades that extend in the longitudinal direction, dividing into several sections and then estimating various properties of each section.

The sectional mass for the blade can be estimated using each blade element. Additionally, the center-of-mass location and reference of the inertia properties on the principal axes attached to the center of mass for each section can also be obtained. The flexural rigidities such as EI_x, EI_y, GJ *and* EA with regards the reference frame whose origin is at the blade reference axis are also estimated based on the blade element. The sectional edge-wise stiffness, EI_x, is computed with the following equations.

Edge-wise stiffness:
$$EI_x^{\,i} = \frac{M_x^{\,i}}{\Delta\theta_x / dz^i} \tag{3.26}$$

$$\Delta\theta_x = d\theta_x^{\,i} - d\theta_x^{\,i-1} \tag{3.27}$$

where $M_x^{\,i}$ is the unit moment for an edge-wise direction, dz^i is the sectional length and $d\theta_x^i$ is a rotation angle for the x axis, respectively.

Similarly, based on the procedures for the edge-wise stiffness, the sectional flap-wise stiffness can be obtained using the following equations.

Flap-wise stiffness:
$$EI_y^{\,i} = \frac{M_y^{\,i}}{\Delta d\theta_y / dz^i} \tag{3.28}$$

$$\Delta d\theta_y = d\theta_y^{\,i} - d\theta_y^{\,i-1} \tag{3.29}$$

where $M_y^{\,i}$ is the unit moment for flap- wise direction, dz^i is sectional length and $d\theta_y^i$ is the rotation angle for y axis, respectively.

The torsional and extension stiffness are also obtained as below.

Torsion rigidity: $$GJ^i = \frac{M_z^{\,i}}{\Delta d\theta_z / dz^i} \tag{3.30}$$

$$\Delta d\theta_z = d\theta_z^{\,i} - d\theta_z^{\,i-1} \tag{3.31}$$

Tension rigidity: $$EA^i = \frac{F_z^{\,i}}{\Delta d\delta_z / dz^i} \tag{3.32}$$

$$\Delta d\delta_z = d\delta_z^{\,i} - d\delta_z^{\,i-1} \tag{3.33}$$

where $M_z^{\,i}$, $F_z^{\,i}$ are the unit moment and force for a rotational direction and z-direction, respectively, and $d\theta_z^i$ is a rotation angle for the z axis and $\Delta d\delta_z$ is the strain for the z-direction. The sectional properties of each blade element should be obtained using the Eqs. (3.26) − (3.33), definition of load and the boundary conditions.

3.4 Structural Integrity Evaluation

It is necessary to check whether the blade is well tolerated to the load applied by the blade and whether it can be operated safely by targeting the results of the aerodynamic and structural design of the blades that are performed previously. Various evaluations are performed to secure structural stability for

blades whose structural design has been completed through diverse design procedures. This can be divided into ULS and FLS as a large classification, each of which is described in detail below.

3.4.1. Ultimate Limit State (ULS)

Various criteria such as Tsai-Wu, Tsai-Hill failure criterion, etc. are used to evaluate stability of the structures made of composite materials, but in this thesis, Puck's failure criterion known as the harshest evaluation method is applied for fiber and inter-fiber failure evaluation proposed by the IEC guideline [32, 45].

In the case of fiber failure, it occurs when the fiber direction stress-strain (σ_1) and fiber direction strain amplitude (ε_1) of a composite material, and failure occurs in two types of mode for tensile and pressure load as shown in Fig. 3.4(a). Equation (3.34) expresses this.

$$\frac{\sigma_1}{X_t} = 1 \ \ for\ \sigma_1 > 0 \ \ or \ \ \frac{\sigma_1}{X_c} = 1 \ \ for\ \sigma_1 < 0 \tag{3.34}$$

In the case of the inter-fiber failure, it refers to cracking of resin that wraps the fiber in a composite material, and as shown in Fig. 3.4(b), damage occurs due to a combination of the perpendicular stress-strain(σ_n) and shear stress-strain (τ_{nt}, τ_{n1}) in the stress-strain action plane. Inter-fiber failure will occur when the σ_2, τ_{21} combination goes out of the destruction curve. And the following is the mode A fracture condition that satisfies resin direction tensile stress-strain ($\sigma_2 \geq 0$), and a fracture angle of 0°.

$$\sqrt{\frac{\tau_{21}}{S_{21}}+\left(1-p_{\perp\mathrm{II}}^{+}\frac{Y_T}{S_{21}}\right)^2\left(\frac{\sigma_2}{Y_T}\right)^2}+p_{\perp\mathrm{II}}^{+}\frac{\tau_{21}}{S_{21}}=1 \tag{3.35}$$

where, τ_{21} is the shear stress-strain, S_{21} is the shear angle of the unidirectional layer. $p_{\perp\mathrm{II}}^{+}$ is the slope of the destruction curve when $\sigma_2 \geq 0$, $-\left(\frac{d\tau_{21}}{d\sigma_2}\right)_{\sigma_2=0}$. Y_T is the tensile angle of the unidirectional layer in the horizontal direction of the fiber.

Mode B is a fracture with a fracture angle (θ_{fp}) of that is caused by the fiber's horizontal direction pressure stress-strain ($\sigma_2 < 0$) and the following are the fracture conditions.

$$\frac{1}{S_{21}}\left(\sqrt{\tau^2{}_{21}+\left(p_{\perp\mathrm{II}}^{(-)}\sigma_2\right)^2}+p_{\perp\mathrm{II}}^{(-)}\sigma_2\right)=1 \tag{3.36}$$

where, $p_{\perp\mathrm{II}}^{(-)}$ is the destruction curve's slope when $\sigma_2 \leq 0$, $-\left(\frac{d\tau_{21}}{d\sigma_2}\right)_{\sigma_2=0}$

Mode C is the fracture in which the fractured plane has an inclination angle because pressure load is applied and the following are the fracture conditions.

$$\left[\left(\frac{\tau_{21}}{2\left(1+p_{\perp\perp}^{(-)}S_{21}\right)}\right)^2+\left(\frac{\sigma_2}{Y_c}\right)^2\right]\frac{Y_c}{-\sigma_2}=1 \tag{3.37}$$

where, angle of the fractured plane is $\cos\theta_{fp}=\sqrt{\frac{f_w R^A{}_{\perp\perp}}{-\sigma_2}}$, $p_{\perp\perp}^{(-)}=p_{\perp\mathrm{II}}^{(-)}\frac{R_{\perp\perp}^{A}}{S_{21}}$ and $R_{\perp\perp}^{A}$ is the resistance of the applied plane against fracture due to shear stress-strain, Y_c is the pressure strength of the unidirectional layer in the horizontal direction of fiber.

3.4.2. Fatigue Limit State (FLS)

In the meantime, wind turbines experience various fatigue loads over their 20-year lifetime. Therefore, it is necessary to evaluate whether the structural safety will be secured for those fatigue loads. In the case of fatigue evaluation, evaluation is performed by applying Miner's rule, which is generally used in fatigue analysis. The number of applied loads is expressed in the form of Markov matrix, which is known as a stochastic matrix, is used to represent steps in a probability chain. Each input of the Markov matrix represents the probability of an outcome. And the allowable number of applied loads at this time is obtained using Goodman diagram [46]. Fatigue life evaluation is conducted in the following procedure [47].

1. Compute the strain amplitude of each computation cross-section (strain/unit load) by applying unit load (M_x = 1kNm, M_y = 1kNm) to each section of the blade computation cross-section. [F_{MS}]
2. Compute the allowed cycle for each material using each of the value computed in Equation (3.38), Goodman diagram.
3. Find the Markov matrix with M_x , M_y components for the fatigue load condition in the pre-defined blade cross-section for fatigue life analysis.
4. Compute fatigue failure for each element of the blade by applying the cycle of the final Markov matrix and allowed cycle to Miner's rule. For fatigue failure not to occur, the "D" value should be 1 or smaller

as shown in Equation (3.39).

$$N = \left[\frac{R_{k,t} + \left| R_{k,c} \right| - \left| 2 \times \gamma_{Ma} \times S_{k,M} \times F_{MS} - R_{k,t} + \left| R_{k,c} \right| \right|}{2 \times \left(\gamma_{Mb} / C_{1b} \right) \times S_{k,A} \times F_{MS}} \right]^{m} \tag{3.38}$$

$$D = \sum \frac{n_i}{N_i} \leq 1 \tag{3.39}$$

Here, " N " is the number of allowed cycles of a specific load for which the composite material can withstand the load and n is the number of cycles of the specific load applied to the corresponding composite material. " D " refers to the fatigue life of the composite material and is expressed with the ratio of " n " and " N ".

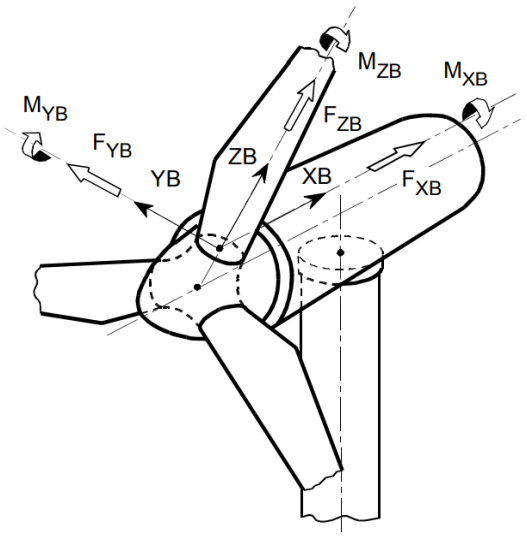

XB in direction of the rotor axis
ZB radially
YB so that XB, YB, ZB rotate clockwise

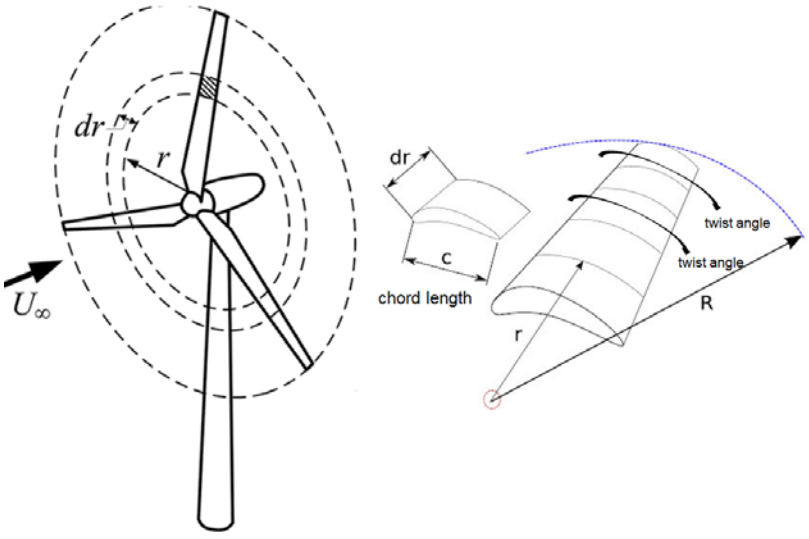

Figure 3.1. Blade coordinate system and blade elements

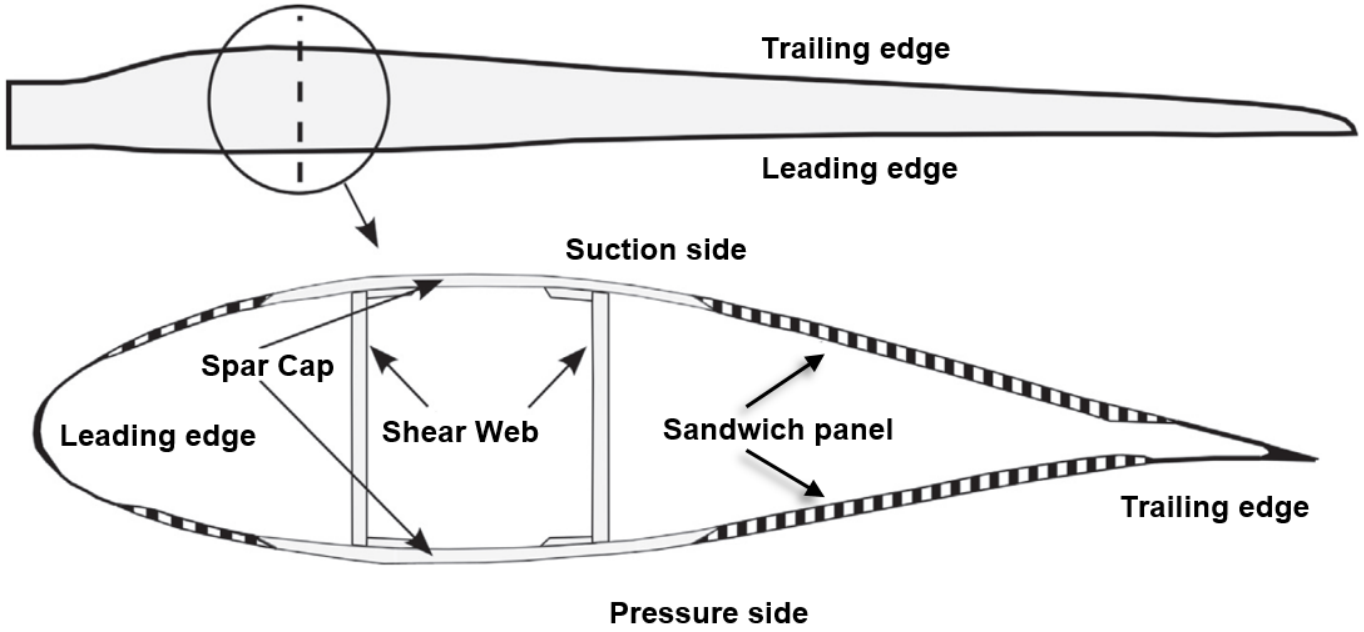

Figure 3.2. Cross-section of a wind turbine blade

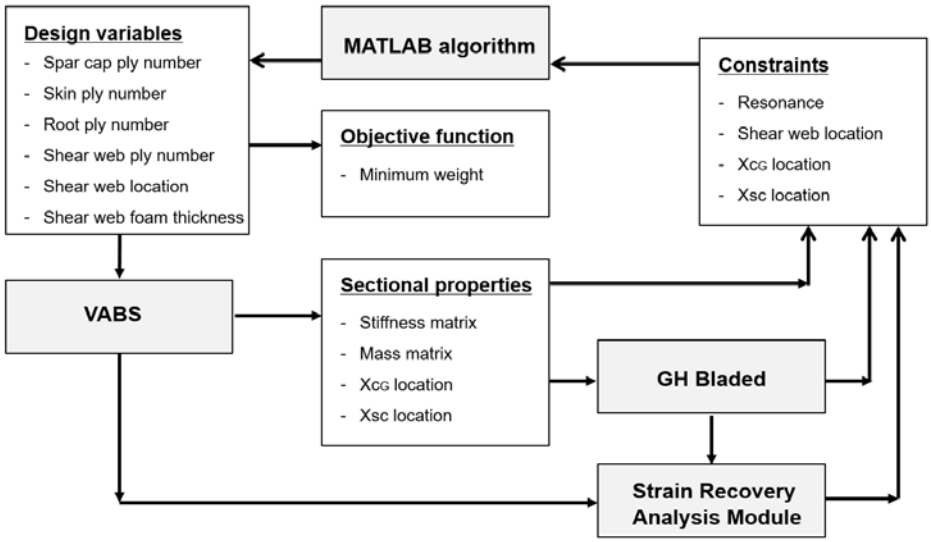

Figure 3.3. Flowchart of the optimal design for the blade sections

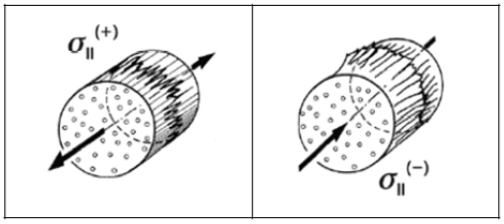

(a) Fiber failure mode

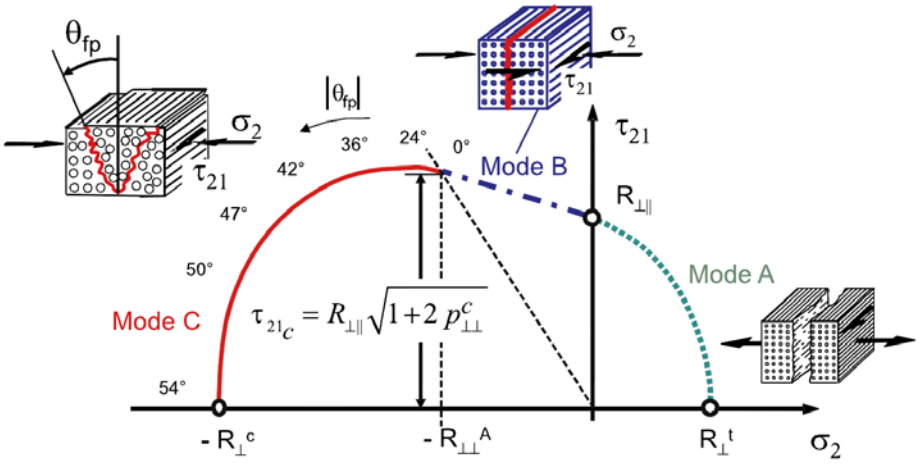

(b) Inter fiber failure mode

Figure 3.4. Fracture curve for fiber and inter fiber failure

Table 3.1. Specification for 2MW reference turbine

Item	Description
Type	3 bladed upwind
Rotor diameter	82.0 m
Rotor swept area	5281 m2
Hub height	78.0 m
Power regulation	Variable speed, pitch regulated
Rotor speed	17.47 RPM (rated)
Rated power	2,000 KW (2MW)
Cut-in wind speed	4 m/s
Cut-out wind speed	25 m/s
Rated wind speed	11.5 m/s
Design wind class	IIA (Vref=42.5 m/s, Iref=0.16)
Annual mean wind speed at hub height	8.5 m/s
Required turbine lifetime	20 years
Blade mass	7,838 kg
Blade length	40.1m
Tower clearance from the blade	5.85m
Max chord	3.2m

Table 3.2. Material properties for GFRP and CFRP

	Ply Thickness [mm]	E_x [MPa]	E_y [MPa]	G_{xy} [MPa]	ν_{xy} [-]	Density [Kg/m^3]
Glass Unidirectional fibers (UD)	0.47	41,800	14,000	2,630	0.28	1,920
Tri-axle	0.94	27,700	13,650	7,200	0.39	1,850
Bi-axle	1	13,600	13,300	11,800	0.49	1,780
Foam	1	256	256	22	0.3	200
Carbon Unidirectional fibers (UD)	0.47	114,500	8,390	5,990	0.27	1,220

Chapter 4

AERODYNAMIC DESIGN

Within the framework of the blade aerodynamic design, the maximum aerodynamic efficiency, power production, and the minimum thrust are the targets to obtain. This chapter describes an improved optimization procedure for the blade aerodynamic design. The aerodynamic design for the blade is performed primarily using BEMT. Then, RSM is applied to blades and the optimal design is performed while considering multiple parameters. The relationship between the objective function and the design parameters, such as the chord length, the maximum chord, and twist angle, are obtained by using the second-order RSM. The initial and optimized blade geometries are compared and showed that the performance of the optimized blade improved significantly.

4.1 Optimal Aerodynamic Design Procedures

In order to achieve the maximum blade efficiency of the wind turbine, multivariate statistical techniques are used in carrying out the optimization of the blade. For this, the second-order RSM in a commercial software, Minitab 18 [48], is applied to the design of experiment (DOE) approach. Moreover, GH Bladed [49] is used for the estimation of the blade efficiency (C_P). GH Bladed is a commercial code used for wind turbine design based on BEMT, and is commonly used in the field of wind turbines.

4.1.1. Initial Blade Design

For designing the baseline blade, the airfoils and the information used in this chapter are shown in Fig 4.1 and Table 4.1. Six types of airfoils are used, including the NACA and DU series, and NACA 64–618 is considered as an airfoil at the tip. The aerodynamic performance in terms of the Reynolds number at the blade tip region ($\mathrm{Re} = 4.5 \times 10^5$) is obtained using the aerodynamic table generator (ATG) [50]. The lift and drag coefficients (C_L, C_D) of various types of airfoil are applied to the airfoil section and predict the aerodynamic performance of the blades, which are functions of the angle of attack. Then, the angle of attack, blade efficiency, and thrust of the blade are calculated using BEMT. During this process, the governing equation is solved by repeatedly updating the axial induction and tangential induction factors until it converges. These procedures will also be repeated in the next elements, and the calculation will continue until all elements are completed. There exist

many computational codes, and GH Bladed is utilized in this thesis.

Through multiple iterations for the maximum efficiency (C_p) in the blade design, the chord length and the twist angle distribution along the blade are recognized as the most important design factors for the blade efficiency [4-7], which are 40.1 and 2.6 m, in length and chord, respectively. Additionally, the aerodynamic power is targeted as a 2 MW rated power and 221 kN maximum thrust. Even though that is a well-created blade based on BEMT, it is a blade that requires an improvement in terms of efficiency.

4.1.2. Objective Function

In the blade optimization design process, the objective function and constraint are established first. The objective function is chosen to maximize the efficiency of the blade in order for increased energy production. For that, the most fundamental target in the wind turbine blade optimal design is to obtain the blade design at its largest possible C_p values. The design variables are selected to be the chord length and the twist angle distribution, by referring to many existing studies. As a constraint, when all the designs are completed, the overall blade geometry should be designed smoothly.

- Objective function: To maximize the efficiency (C_P) of the blade
- Design variables: Chord length, twist angle (± 10% based on the calculation location)
- Constraints: Chord length and twist angle, not exceeding 3.5 m and 15°, respectively

4.1.3. Design Parameter and Calculation Locations

In the blade design procedure, the most significant design parameters are identified as the chord length and the twist angle distribution, as shown in [3] and [4]. Therefore, considering the effects of the two parameters on the wind blade performance, simultaneously, is required. Table 4.2 presents the baseline blade geometry and calculation location. The blade is divided into 16 sections (17 locations), and 14 locations, from 3 to 16, are regarded as optimization locations using RSM, as shown in Table 4.2. The other locations (1, 2, and 17) are excluded from calculation locations because the optimization effect is expected to be minimal from an aerodynamic point of view. The optimal design is performed by placing calculated optimization locations intensively from 40% to 90% span-wise location, which significantly affects the blade efficiency. The ranges and levels of the variables are decided based on the adjacent chord length and the twist angle for the calculation locations, as listed in Table 4.3. At the calculation location, the values of the chord length and twist angle are determined to be + 10% for −1 and −10% for +1, respectively. If this value is greater than 10%, inconsistency may occur such that the chord length and twist angle at the calculation location do not smoothly connect with those determined at the adjacent calculation location. In that case, considering the blade fabrication process using the infusion method, the result will become an impractical design.

4.1.4. Calculation Procedure

Thirteen simulations with different design parameters are conducted for each calculation location, from 3 to 16, and only calculation location 3 is shown as a sample in Table 4.4. The 9th–13th simulations are the central experiments, which are used to guarantee a reliable prediction. In it, an estimation of the relationship between the design variables and output responses is attempted by using the experimental design method with the RSM and GH Bladed results. The two main factors are determined as design variables, and the case of various combinations of these variables will be obtained. The last column shows C_P values by GH Bladed for each sample at multiple parameters. RSM calculation finds the number of optimal combinations of these two variables as "Variables" in 13 cases; the efficiency at this time is expressed as "Response" through BEMT calculation. Then, it chooses a case that indicates the maximum efficiency (C_P). The chord length and twist angle values are selected as geometries for the location and are reflected in the final design. These computations are performed for each calculation location, and 13 computations per location are performed, and thus, a total of 182 ($13 \times 14 = 182$) calculations are performed.

4.2 Optimal Aerodynamic Design

In this chapter, RSM uses a mathematical formulation to find combinations that may represent the best blade efficiency using two independent variables. The blade is divided into 17 locations, and 14 locations are regarded as optimization locations.

4.2.1. Surface and Contour Plot

Surface plots, which are a pairwise relationship between the chord length, twist angle, and C_P values, are shown in Fig 4.2. In this diagram, at location 3, an optimum efficiency is achieved at 2.6 m chord length and 14.9° twist angle, at which the maximum C_P will become 0.448. This diagram demonstrates the positive effects of increasing the chord length on the value of C_P, whereas the changes in the twist angle do not have such effect. It is estimated that increasing the chord length to a specific twist angle value, approximately 15°, will also increase the efficiency. In consideration of that, design should focus on the changes in the chord length rather than the twist angle near the blade root. However, other locations, such as Locations 4 through 15, have different tendencies. The diagram shows an inverse relationship between the two parameters. If the chord length increases and the twist angle decreases to a certain point, C_P will show an increased tendency.

The correlation between C_P values is shown in terms of the chord length and twist angle in Fig 4.3 as contour plots. In the diagram, it is straightforward to verify the relationship among the design parameters. At the calculation locations from 4 to 16, the dark color, which means a larger *Cp* value, is

mostly located on the left and top. This indicates increasing size of the chord length, while taking the twist angle smaller, rather than increasing the value of the twist angle. Based on such trends in the contour plot, the present blade optimization design is found to be appropriate.

4.2.2. Aerodynamic Design Result

The optimization results for each calculation location are listed in Table 4.5. The combination of the optimal design by all the calculation locations, i.e., the final optimal blade design result, shows a further increased value of C_P, as shown in Fig 4.4. In the case of the locations from 7 (14.327 m from the root, 36% of the blade length) to 14 (33.95 m from the root, 85% of the blade length), although optimized only at the respective locations, the overall efficiency is found to exceed 0.45. This means that most of the blade efficiency is rather influenced by that area, a length of approximately 40% to 90% from the root [51]. Thus, for the blade optimization, it will be effective to concentrate on the part that is responsible for most of the efficiencies and power of the blade, and then perform the optimal design. As shown in Figs 4.2 and 4.3, the present optimization progresses in the direction of increasing chord length and decreasing twist angle.

In this way, in Chapter 4, the shape design of the blade that generates the largest efficiency and target output of 2MW is completed. For the shape of the blade designed in this way, a structural design for the design of a relatively light blade while withstanding various applied loads will be performed.

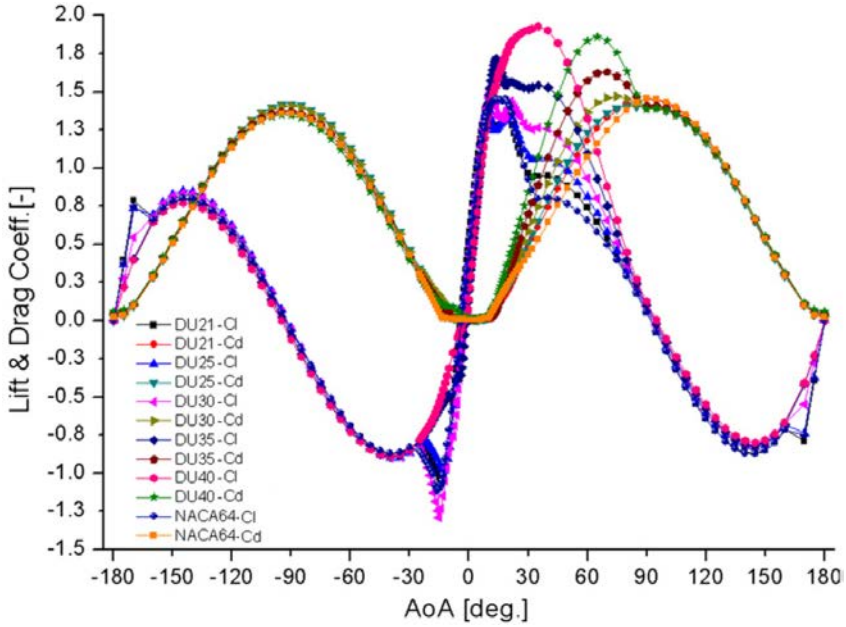

a) Aerodynamic coefficients of the airfoils.

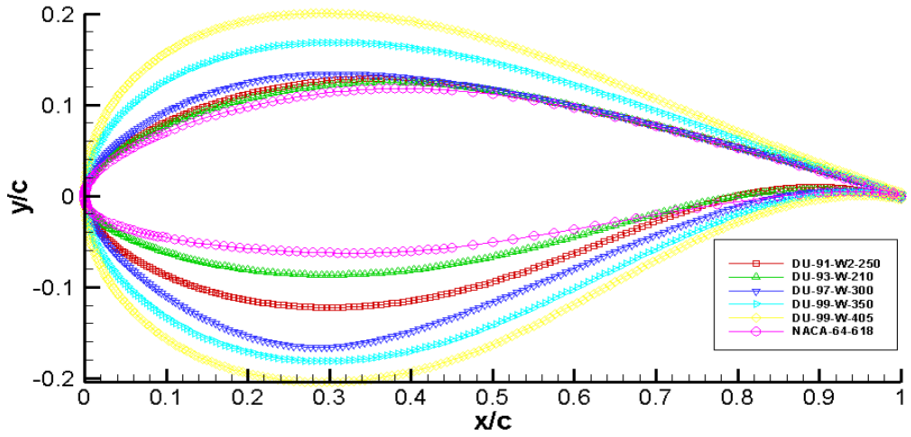

b) Airfoil shapes of NACA and DU series

Figure 4.1. Aerodynamic coefficients and airfoil shapes

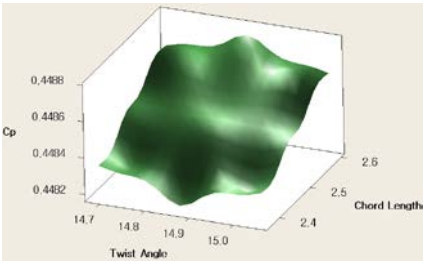

a) Location 3

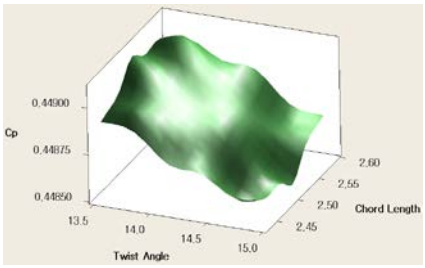

b) Location 4

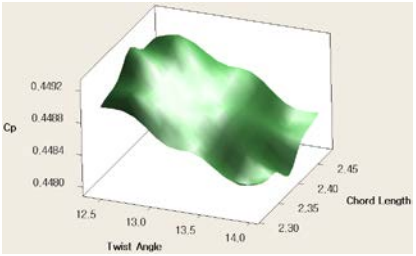

c) Location 5

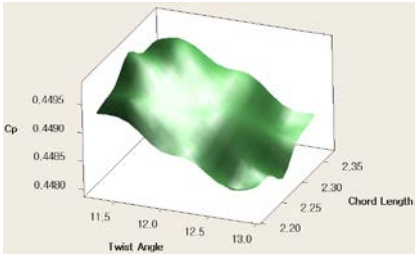

d) Location 6

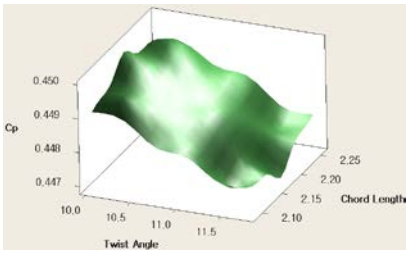

e) Location 7

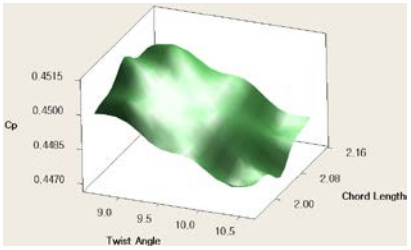

f) Location 8

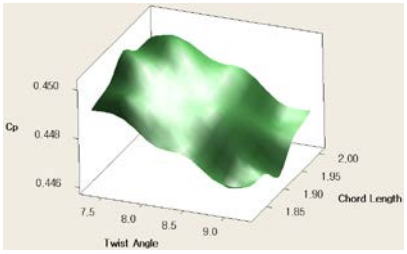

g) Location 9

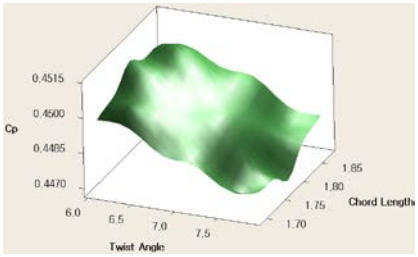

h) Location 10

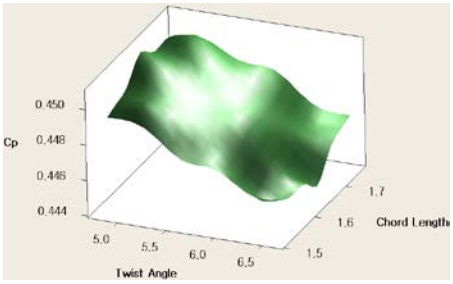

i) Location 11

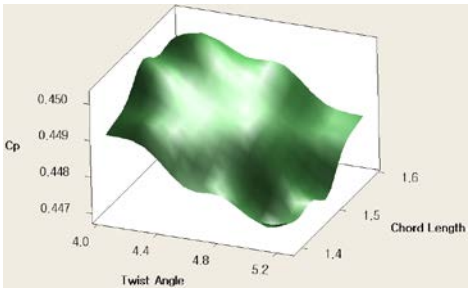

j) Location 12

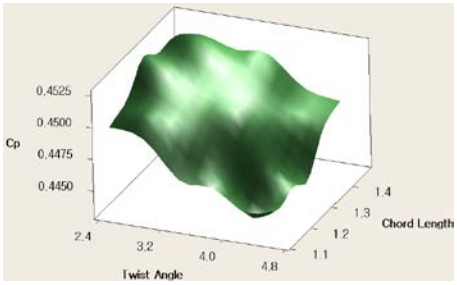

k) Location 13

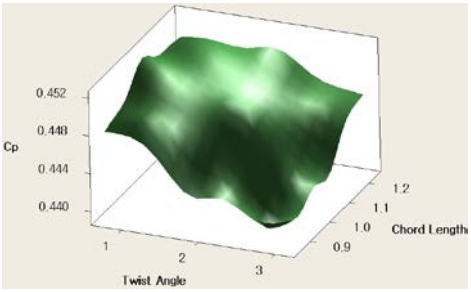

l) Location 14

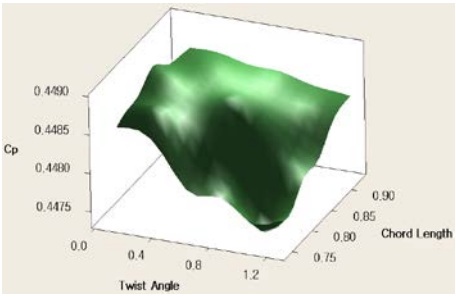

m) Location 15

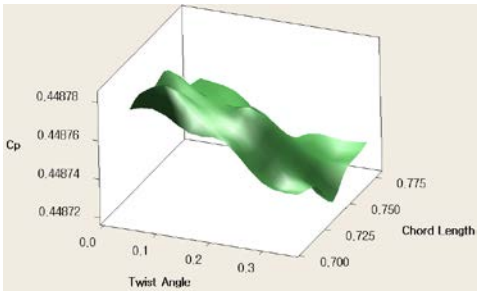

n) Location 16

Figure 4.2. Surface plots of C_p in terms of chord length and twist angle

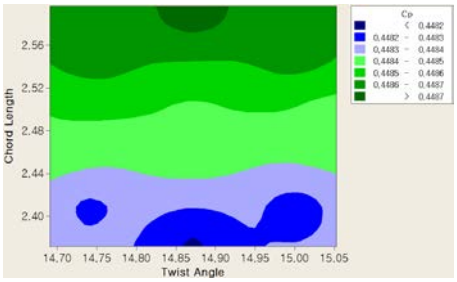

a) Location 3

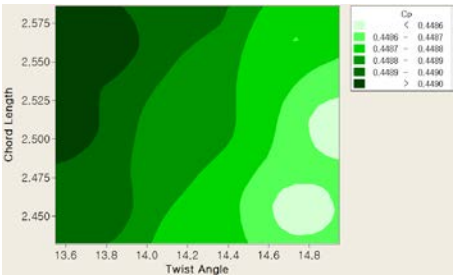

b) Location 4

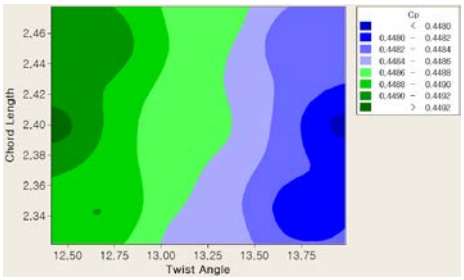

c) Location 5

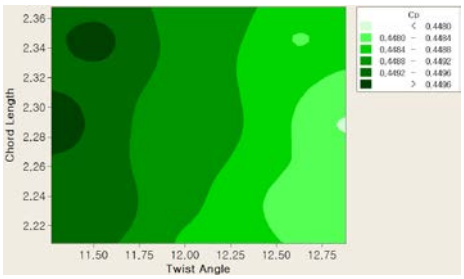

d) Location 6

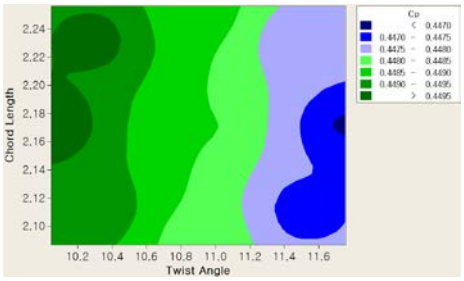

e) Location 7

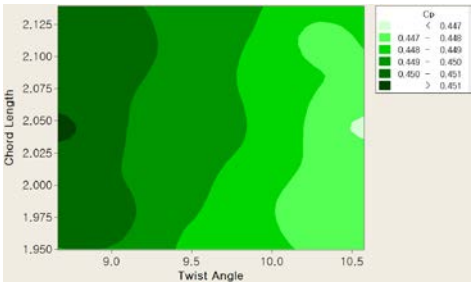

f) Location 8

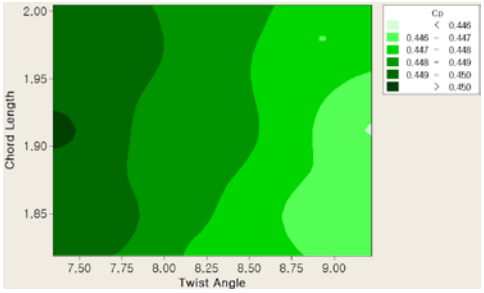

g) Location 9

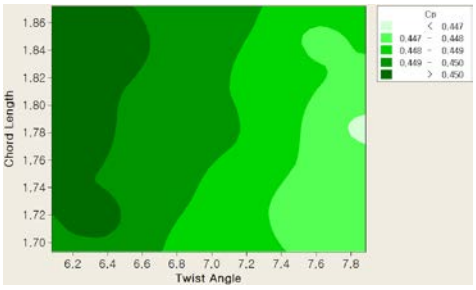

h) Location 10

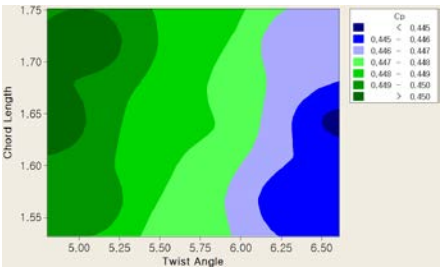

i) Location 11

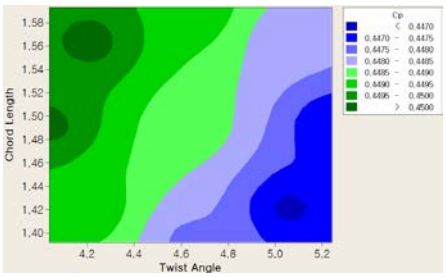

j) Location 12

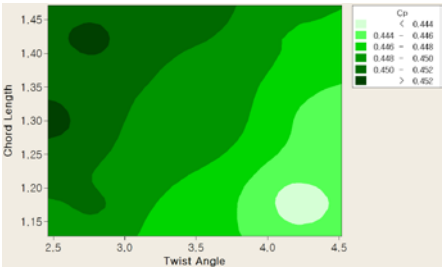

k) Location 13

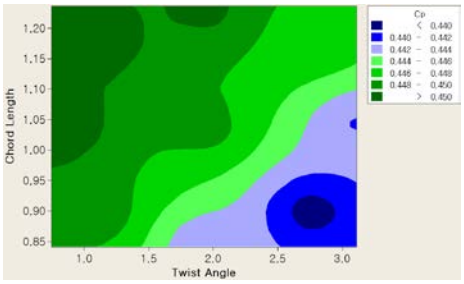

l) Location 14

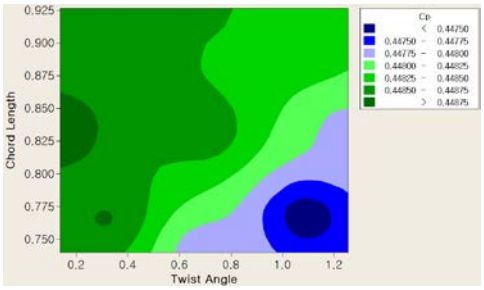

m) Location 15

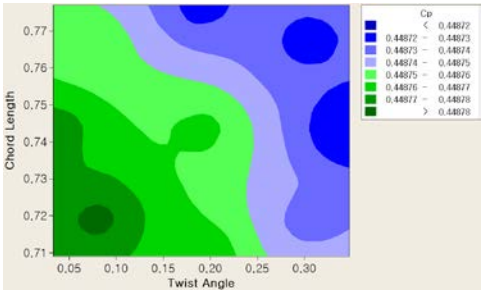

n) Location 16

Figure 4.3. Contour plots of C_P in terms of chord length and twist angle

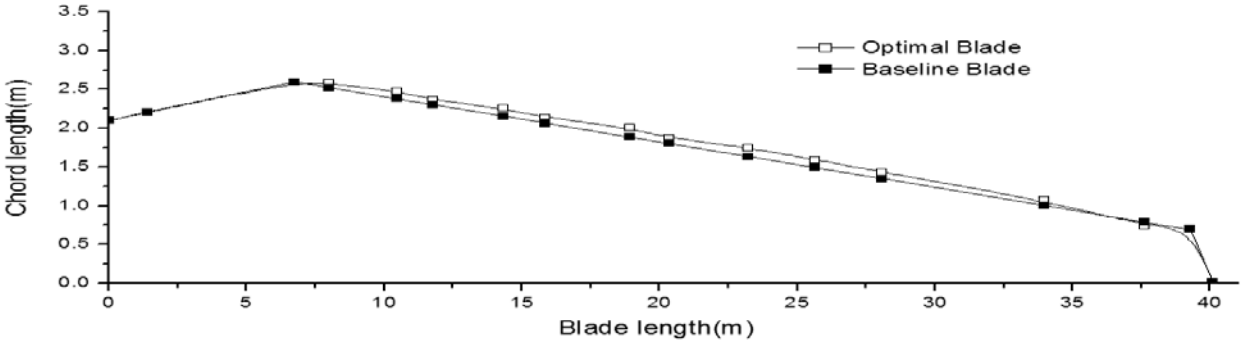

a) Chord length distribution

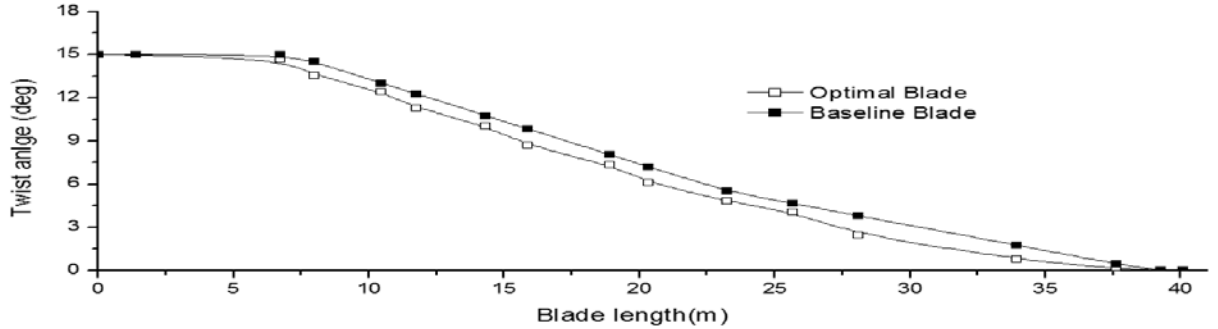

b) Twist angle distribution

Figure 4.4. Comparison between the optimal and baseline geometry

Table 4.1. Airfoil distribution

Airfoil Number	Position [μ]	Airfoil
1	0.0272	Cylinder
	0.0928	Cylinder
2	0.1574	DU-401
3	0.2326	DU-350
4	0.3177	DU-300
5	0.4153	DU-250
6	0.5305	DU-212
7	0.6585	NACA64618
	1.0000	NACA64618

Table 4.2. Baseline blade geometry and calculation location

Calculation location	Geometry		
	Distance from root(m)	Chord Length(m)	Twist Angle(°)
1	0	2.1	15
2	1.399	2.209	15
3	6.747	2.600	15
4	7.987	2.527	14.487
5	10.469	2.382	13.023
6	11.755	2.306	12.264
7	14.327	2.156	10.746
8	15.852	2.066	9.845
9	18.903	1.888	8.046
10	20.345	1.804	7.195
11	23.229	1.635	5.492
12	25.660	1.493	4.640
13	28.091	1.350	3.789
14	33.950	1.007	1.738
15	37.640	0.791	0.445
16	39.280	0.695	0
17	40.100	0.010	0

Table 4.3. Ranges and levels of variables, chord length (m) and twist angle (°)

	Location 3			Location 4			Location 5		
	Levels			Levels			Levels		
Variables	**-1**	**0**	**+ 1**	**-1**	**0**	**+ 1**	**-1**	**0**	**+ 1**
Chord Length	2.405	2.600	2.564	2.564	2.527	2.455	2.455	2.382	2.344
Twist Angle	15.000	15.000	14.743	14.743	14.487	13.755	13.755	13.022	12.643
	Location 6			Location 7			Location 8		
	Levels			Levels			Levels		
Variables	**-1**	**0**	**+ 1**	**-1**	**0**	**+ 1**	**-1**	**0**	**+ 1**
Chord Length	2.344	2.307	2.231	2.231	2.156	2.112	2.112	2.067	1.978
Twist Angle	12.643	12.264	11.505	11.505	10.746	10.296	10.296	9.846	8.946
	Location 9			Location 10			Location 11		
	Levels			Levels			Levels		
Variables	**-1**	**0**	**+ 1**	**-1**	**0**	**+ 1**	**-1**	**0**	**+ 1**
Chord Length	1.978	1.889	1.846	1.846	1.804	1.719	1.719	1.635	1.564
Twist Angle	8.946	8.046	7.620	7.620	7.195	6.343	6.343	5.492	5.066
	Location 12			Location 13			Location14		
	Levels			Levels			Levels		
Variables	**-1**	**0**	**+ 1**	**-1**	**0**	**+ 1**	**-1**	**0**	**+ 1**
Chord Length	1.564	1.493	1.421	1.421	1.350	1.179	1.179	1.007	0.899
Twist Angle	5.066	4.640	4.215	4.215	3.789	2.763	2.763	1.738	1.091
	Location 15			Location 16					
	Levels			Levels					
Variables	**-1**	**0**	**+ 1**	**-1**	**0**	**+ 1**			
Chord Length	0.899	0.791	0.767	0.767	0.743	0.719			
Twist Angle	1.092	0.445	0.302	0.302	0.158	0.079			

Table 4.4. Design of the parameters for the calculation location 3

Run	Variables		Response
	Chord Length(m)	Twist Angle(°)	Efficiency(C_P)
1	2.597	14.872	0.449
2	2.484	15.054	0.448
3	2.405	15.000	0.448
4	2.484	14.690	0.448
5	2.564	14.743	0.449
6	2.405	14.743	0.448
7	2.372	14.872	0.448
8	2.564	15.000	0.449
9	2.484	14.872	0.449
10	2.484	14.872	0.449
11	2.484	14.872	0.449
12	2.484	14.872	0.449
13	2.484	14.872	0.449

Table 4.5. Optimized results for each calculation location

Calculation location	Results		
	Chord Length(m)	Twist Angle(°)	Efficiency(C_P)
3	2.597	14.690	0.449
4	2.586	13.550	0.449
5	2.478	12.413	0.449
6	2.368	11.269	0.449
7	2.257	10.045	0.450
8	2.139	8.666	0.451
9	2.005	7.346	0.451
10	1.872	6.079	0.451
11	1.752	4.801	0.452
12	1.593	4.038	0.450
13	1.433	2.463	0.453
14	1.073	0.745	0.452
15	0.740	0.138	0.449
16	0.711	0.033	0.449

Chapter 5

OPTIMAL STRUCTURAL DESIGN

Structural design of the wind turbine blade is series of difficult tasks, for modeling and estimation of large composite turbine blades, huge computational resources and time are required. Additionally, a significant amount of design parameters will need to be handled, enforcing it difficult to perform systematic parametric study. In this regard, this chapter presents procedure for the structural design of a large-size wind turbine blade based on the CLT using baseline blade design, which is structurally completed initial design. By analyzing the existing blade, the optimized numbers of the spar cap layers in the blades are estimated. The sectional optimal design of blade is established on the basis of the ATR optimization framework and a cross sectional analysis is performed using VABS. In this chapter, blade structural design for increased rigidity and decreased weight is carried out based on the blade design in the previous chapter. Extreme load for structural design is derived as reference blade model as shown in Fig. 5.1, and based on that, the blade structural design is performed.

5.1. Structural Configuration

For the structural design of the blade, the specifications of the turbine system used in the design of the baseline blade is summarized in Table 3.1. In addition, the cross section of a regular wind turbine blade is shown in Fig. 3.2 and is divided into the skin, spar cap, and shear web depending on the supporting load. The skin requires maintaining the blade exterior and resistance against torsion load, so it has a sandwich structure made of bi-axle or tri-axle (2AX or 3AX) glass fibers and foam material. The foam material is used to enhance flexural stiffness and prevent buckling, and PVC foam or Balsa wood is mainly used. Spar caps are inserted into thick beams by stacking dozens of thin unidirectional fibers (UD), because it supports most of the bending moment that occurs due to the wind load. The shear web is located between skins, and has a sandwich structure consisting of bi-axle glass fiber and foam to support the shear load acting on the blade. For the efficiency of a blade structural design, the blade is divided into 11 detailed parts based on the major materials used in the design and their locations.

- Pressure side spar cap / suction side spar cap
- First shear web / second shear web
- Trailing edge
- Blade root / extra root
- Skin / foam / foam on spar cap / foam beside spar cap (total 11 components)

In addition, the material properties used in the design are shown in Table 3.2.

5.2. Structural Design for the Spar cap

For the design of a wind turbine blade, a diverse information (material properties, geometry, design load, etc.), related knowledge and experience will be required. Therefore, it will be a difficult engineering task without sufficient information inside or with little experience. In such a situation, comparison and obtaining information of the blade characteristics, such as stiffness, weight and thickness, from the existing blades will be a useful method. This will be an efficient approach in verifying the design when one's own blade design results are not sufficiently accumulated [52, 53].

5.2.1. Baseline Blade

For an initial structural design of the blade, an existing blade geometry with a proven aerodynamic and structural performance is selected as the baseline blade. It is designed in accordance with IEC wind class IIA, with a length of 40.1 m, mass of 7,838 kg and maximum chord length of 3.2 m as shown in Table. 3.1.

The blade is designed by an inverse design methodology. Specifically, a reference blade is designed using E-glass epoxy by ensuring that the sectional mass and stiffness properties of the three-dimensional blade are identical to those of NREL 5-MW turbine blade [54]. The blade skins in the leading and

trailing edge sections are composed of biaxial material oriented at ±45° with respect to the blade axis. Furthermore, the unidirectional material is used in the main spar caps. Based on the preliminary design of the spar caps, the number of composite material layers in each section of the blade is adjusted iteratively to obtain a blade with sectional properties that are identical to those of the baseline blade.

5.2.2. Spar Cap Thickness Estimation

To obtain a normalized spar cap thickness distribution, the various existing turbine blades [40-42, 54] are referred. And the thickness of these spar caps is to be compared. The thickness of a section of the spar cap is normalized with respect to the length of the blade, and then this parameter will be compared for a variety of diverse blades. By comparing the spar cap thickness ratios of the existing blades with similar design conditions and capabilities, specific trends can be identified among the blades.

The normalized spar cap thicknesses distribution and its trend lines are shown in Fig. 5.2. It shows that the spar cap thickness ratio exhibits similar tendency from Station 20 to 100 with respect to four types of existing blades. In the figure, similar normalized spar cap thickness of the existing blades indicates a similar normalized stiffness of the spar cap. Given that the material and stacking angle of the spar cap for all the blades correspond to GFRP with unidirectional fibers (0°) and the thickness of the normalized spar cap is similar, the normalized stiffness is also similar. There is a difference in the

thickness ratio at the root position of the blade. This is due to a variety of bolts, such as T-bolts or stud bolts that are used on the blade as per the designer and manufacturer.

In this thesis, the normalized spar cap thickness distribution of the existing blades is investigated to predict the trend line for the initial laminate design, as shown in Fig. 5.2, and the 6th order curve fitting function is obtained, as shown in Eq. (5.1). By using this, the spar cap thickness ratio of the blade is re-calculated, and the final necessary number of layers is calculated by dividing the unit thickness of the unidirectional fiber.

$$y = 8.22\times10^{-11}x^6 - 3.27\times10^{-8}x^5 + 5.07\times10^{-6}x^4 - 3.81\times10^{-4}x^3 + 1.38\times10^{-3}x^2 - 0.21x + 2.77 \quad (5.1)$$

In Eq. (5.1), y denotes the normalized thickness of the spar cap, and x denotes the normalized blade position along the blade length. This equation is used to determine the thickness of the spar cap with respect to the span-wise direction of the blade. It is a simple numerical expression and not a universal formulation. Additionally, as the design of the blade changes based on the changes in wind class and rated power, the formation also varies by based on the existing blade. When designing a blade structure, the spar cap thickness is one of the most important design variables [26] because it is used to determine the stiffness of the blade. With this trend line, it is possible to determine the spar cap thickness at the initial stage even though it is not familiar with the blade design due to less information and experience [52, 53].

5.2.3. Stiffness Coefficient of the Spar cap

A parametric study for the spar cap with respect to the material, such as GFRP and CFRP, and stacking angle, including 0°, 5°, 10°, 15° and 20°, is conducted based on the baseline blade. Among the main factors that determine the stiffness, only Young's modulus is considered in this section. The value of the second moment of inertia and the thickness of the spar cap are already considered in the previous section by Equation (5.1). Therefore, the present design optimization focuses on maximizing the Young's modulus. The computation is performed by using the information, such as the number of plies, angles, and material properties of fibers (unidirectional or multi-axial) that are accumulated on the spar cap, as per Eqs. (3.22) and (3.23). Furthermore, the axial- and twist coupling stiffness coefficient results for each blade section are used for redesigning the blade.

Figure 5.3 shows the axial stiffness coefficient for each computational location for GFRP and CFRP spar caps, respectively. In both cases, the axial stiffness coefficient decreases as the stacking angle of the unidirectional fiber increases. This is because when the stacking angle of a composite fiber differs from 0°, the main axial direction of the blade and the stiffness along the main axial direction decreases proportionately. Hence, it is important to concentrate on the 0° material in the spar cap to ensure compliance with the bending load, which acts along the main direction of the blade. As the angle increases from 0° to 20°, it is evident that the load bearing capacity of the fiber decreases and the axial stiffness coefficient decreases. Additionally, in Fig. 5.3(b), the axial

stiffness coefficient of the CFRP is twice as high as that of the GFRP, as shown in Fig. 5.3. This is because its high Young's modulus (E) is twice that of the GFRP, as shown in Table 3.2. Thus, when designing the spar cap of a blade, it is necessary to select the laminate angle and material to be used by considering the direction and magnitude of the load acting on the blade.

Figure 5.4 shows the twist coupling stiffness coefficients for GFRP and CFRP blades, respectively. The diagrams show that the twist-coupling coefficient tends to increase as the angle of the unidirectional fiber increases and converge at a certain angle, where it maintains its value. Therefore, considering the effect of bending-torsion required by the wind turbine blade, it is desirable to use the specific angle. Additionally, the twist-coupling stiffness coefficient of CFRP higher than that of GFRP, as shown in Fig. 5.3. In conclusion, the axial stiffness decreases as the stacking angle of a unidirectional fiber increases with respect to the main axial direction. However, the twist-coupling coefficient increases and converges at a specific angle in the range of 10° ~ 15°. This tendency varies depending on the material. For a certain structural design of a blade, flexural deflection and twisting deflection can be triggered at the same time due to a load by using these properties. Thus, using this technique, research on structural design that improves the output and reduces the fatigue load is being conducted [28].

In this study, a unidirectional material is used to cope with the bending moment (My), which is the main load applied to the blade. However, for the design of torsion–bending coupling (TBC) blades [40], the results in Fig. 5.4 can be used as a reference.

5.3. Optimal Structural Design for the Section

Using the blade with the initial structural design completed, the optimal cross-section design is performed for several sections in the blade span direction. This optimization procedure for the sectional design is established on the basis of the ATR optimization. An objective function is established to minimize the weight of the blade and the design variables are used such as ply number for spar cap, skin/shear web, and shear web location. By this optimal design procedure, design of the blade structure is conducted. Design of the structure will be completed if the final objective function is satisfied through various iterative calculations. In addition, a cross sectional analysis is performed using GT/VABS, which is a general asymptotically correct finite-element-based cross-sectional analysis intended to model arbitrary geometries.

5.3.1. Present Algorithm

Among the various optimization algorithms supported by MATLAB, calculations are performed using the genetic algorithm and Nelder-Mead simplex algorithm, respectively, which are typically used in the blade design, and the comparison of the results is also carried out.

In the genetic algorithm, a population of candidate solutions to an optimization problem is evolved toward better solutions. Each candidate

solution has a set of properties which can be mutated and altered; traditionally, solutions are represented in binary as strings of 0s and 1s. The evolution usually starts from a population of randomly generated individuals, and is an iterative process, with the population in each iteration called a generation. In each generation, the fitness of every individual in the population is evaluated; the fitness is usually the value of the objective function in the optimization problem being solved.

Meanwhile, Nelder-Mead simplex method is a commonly applied numerical method used to find the minimum or maximum of an objective function in a multidimensional space. It is a direct search method based on function comparison and Nelder–Mead technique is a heuristic search method that can converge to non-stationary points on problems that can be solved by alternative methods.

5.3.2. Optimal Cross Section Design

Blade structural design for increased rigidity and decreased weight is carried out based on the optimal cross section design method. As shown in Fig. 3.4, the following 9 design variables are considered in the optimization procedure. The outer/inner plies for skin and shear web are fixed as a bi-axle ±45° ply of glass fiber, and UD is only used for the spar cap. Table 5.1 summarizes the design variables used in the present optimization framework. The above is summarized as follows.

- Objective function: minimum weight

- Design variables: ply number for spar cap, skin, shear web, root and shear web location, thickness for shear web foam
- Constraints: resonance, shear web location

5.3.3. Results Comparison based on Designing Algorithm

The blade structural optimization using two types of optimization algorithms is conducted. The optimal design obtained by the genetic algorithm is found to be inferior in terms of its weight decrease, but it also has a disadvantage that takes a relatively long time to calculate. In addition, the baseline blade for the design optimization are the ones with the optimal design of the spar cap, by referring to the existing reference blades. Due to that, the weight decrease is not as significant as expected. However, the design results obtained by Nelder-Mead simplex show rather increased weight. It is a result obtained by a local optimization based on Nelder-Mead simplex method, which focuses on increasing the rigidity locally rather than on reducing the weight of the structure. Therefore, in this thesis, the design is further conducted on the optimal design blade by the genetic algorithm, and structural integrity will be evaluated.

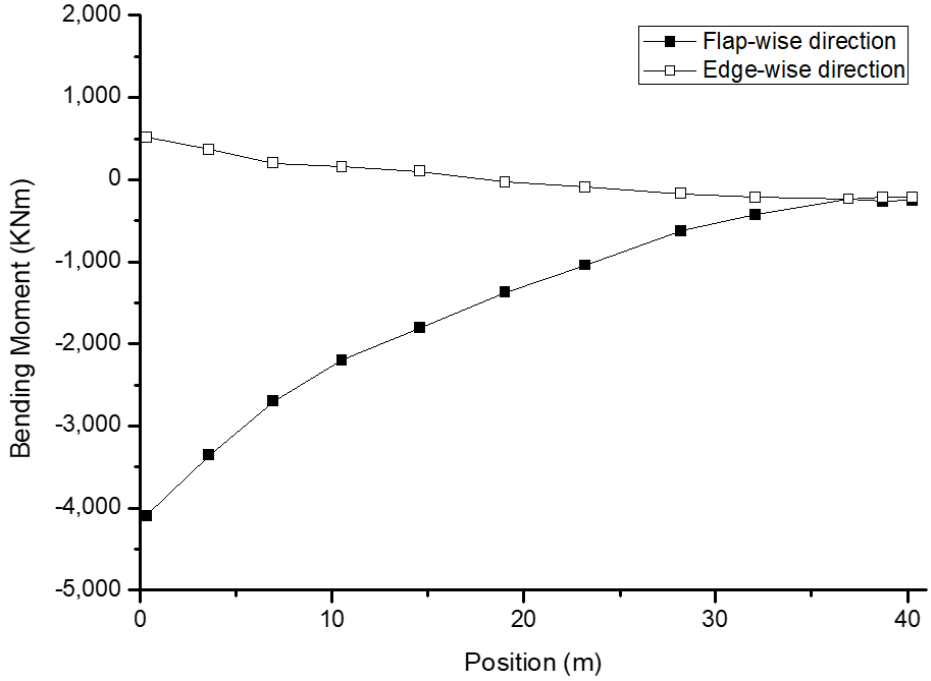

Figure 5.1. Design load for the blade structural design

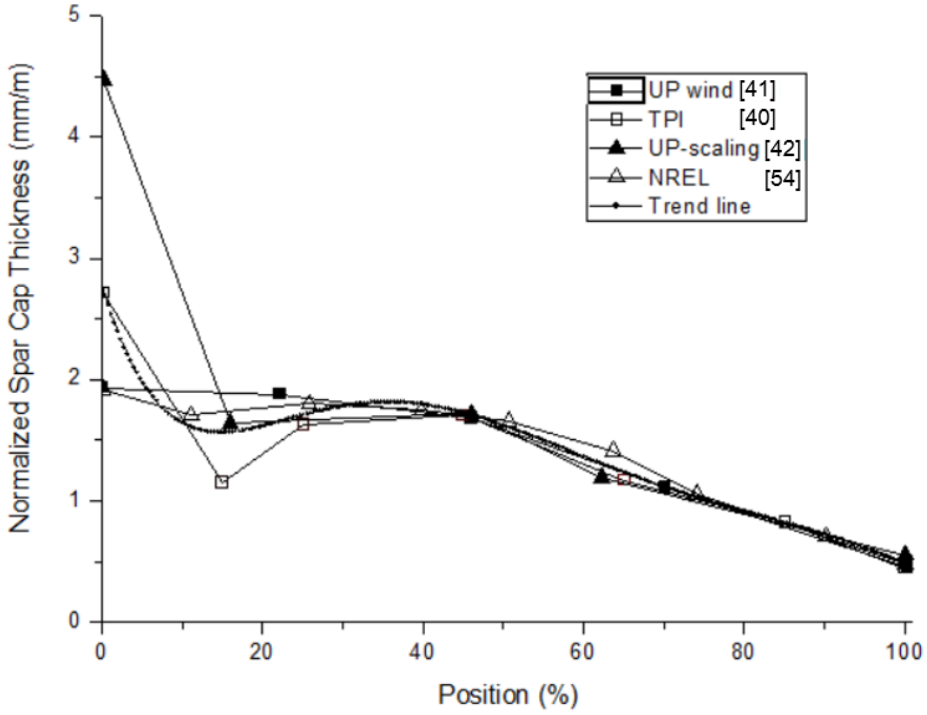

Figure 5.2. Comparison of the spar cap thickness in the existing turbine blades

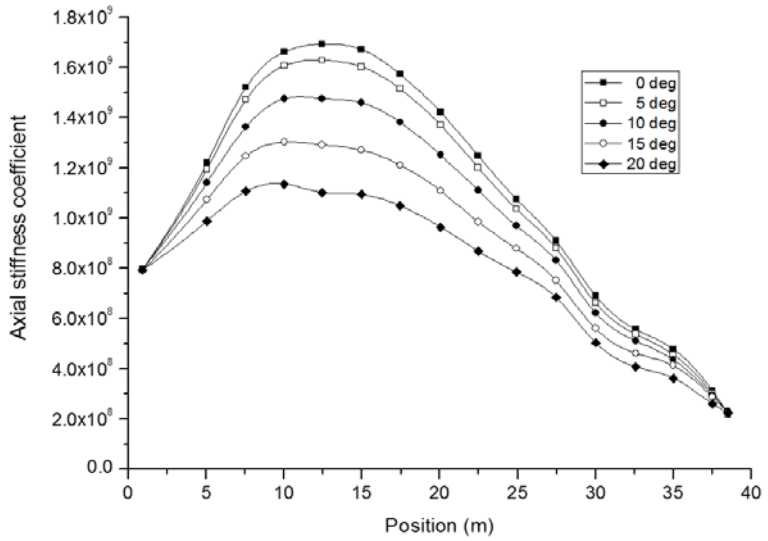

(a) Result of GFRP

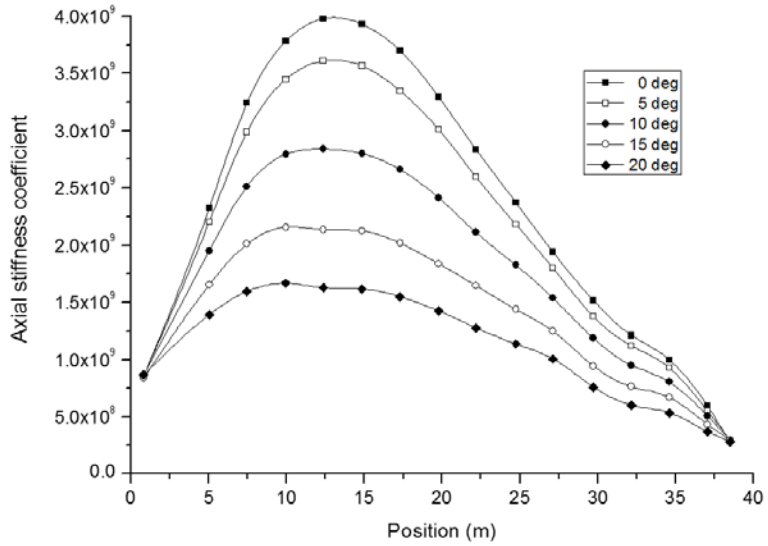

(b) Result of CFRP

Figure 5.3. Axial stiffness coefficient of the spar cap

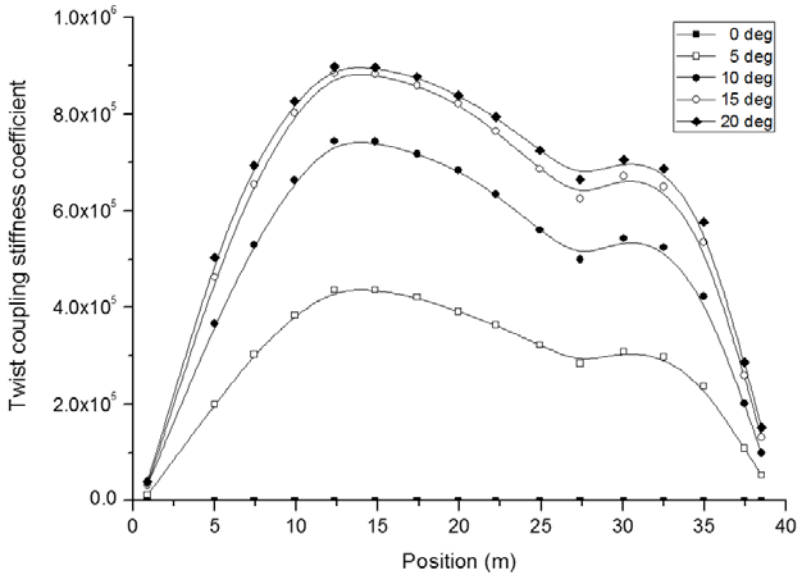

(a) Result of GFRP

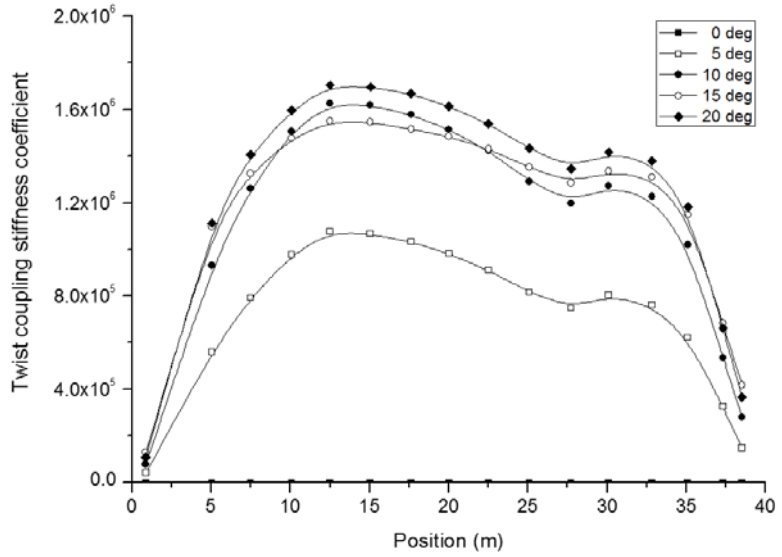

(b) Result of CFRP

Figure 5.4. Twist coupling stiffness coefficient of the spar cap

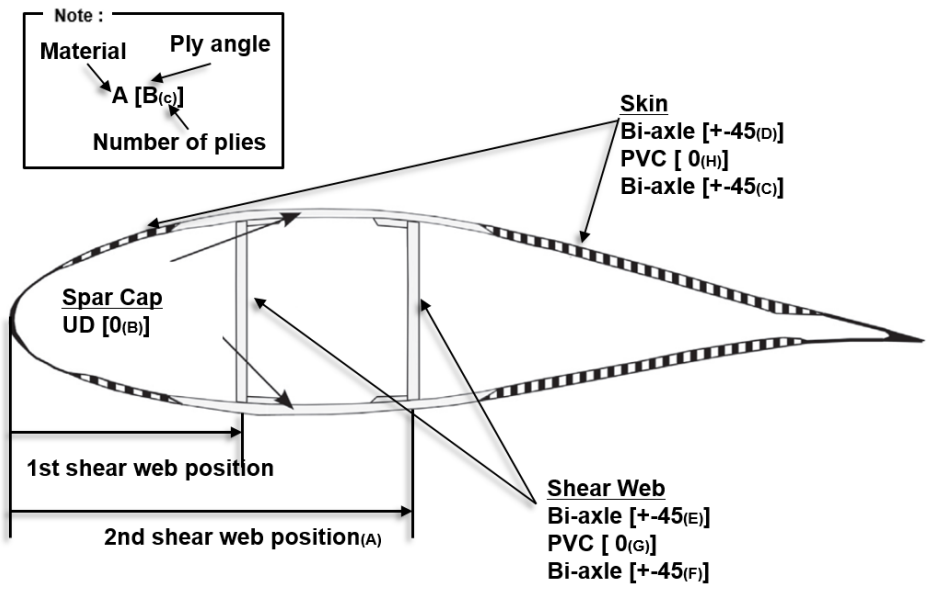

Figure 5.5. Design variables used in the present optimization

Table 5.1. Design variables used in the present optimization

Symbol in Fig. 4.8	Design variable	Lower boundary	Upper boundary
A	2nd Share web position	0.30c	0.7c
B	Number of piles for spar cap	5	70
C	Number of piles for skin inner	1	5
D	Number of piles for skin outer	1	5
E	Number of piles for shear web inner	1	3
F	Number of piles for shear web outer	1	3
G	Foam thickness for shear	5mm	20mm
H	Foam thickness for skin	5mm	40mm
I	Number of piles for blade root	10	100

Chapter 6

STRUCTURAL EVALUATION

In this chapter, various structural integrity evaluations are conducted on the results of the blade structural design performed in Chapter 5. In order to evaluate the structural integrity of the present blade, the load acting on the blade is obtained based on BEMT. However, CFD should be adopted to consider the effects that have a significant impact on the prediction accuracy, such as the three-dimensional swirl effect, blade-vortex interaction, and tip loss effect, but are not fully covered in BEMT. In addition, by CFD, the streamlines/pressure distribution in terms of the wind speed will be evaluated. Then, using the load calculation results, design evaluation such as fiber failure, inter fiber failure, stability, etc., is carried out. Fatigue life evaluation for the FLS condition for life time of 20 years of wind turbines is also processed. For such design assessment, based on IEC61400-1[55], -5[32], international standards[56, 57] for wind turbine systems and blade, the results of the structural design are discussed further.

6.1 Extraction of the Sectional Properties

For the calculation of the section properties from the blade, it is divided into several sectional elements in accordance with the span direction. Each sectional element is connected with MPC 184 on the right and left sides as shown in Fig. 6.1 as the boundary and load conditions, respectively, depending on the computational purposes. Such method applies the unit load to the right nodal point of each blade element and processes the results of nodal displacements/rotation angle to generate 4 × 4 stiffness matrices for the specified beam discretization.

The sectional mass and moment of inertia for z-direction are computed in line with the blade span length. The mass and moment of inertia for 33 individual sections will be calculated in an individual manner. The results of the sectional mass distribution and moment of inertia for 33 sections are shown in Fig. 6.2(a) and (b), respectively. The blade root area in Fig 6.2(a), which is composed of more than 80 composite material layers to connect the blade and a hub of the wind turbine, is heavier than other regions because it is thicker than others. The moment of inertia for z-direction is also similar to the mass distribution in terms of shape as shown in Fig 6.2(b) since it is also influenced by the sectional mass distribution. Then, the stiffness of edge wise, flap wise, torsion and sectional rigidity are shown in Fig 6.2(c) to 6.2(d). The edge-wise stiffness is larger than flap-wise one as shown in Fig 6.2(c) due to its slender shape.

The mass, moment of inertia, and stiffness of the elements are divided into several sections along the span of the blade. Those values are processed in the form required and used by the load analysis. In practice, it is possible to use VABS to extract the corresponding values from the desired position, but in this case, the number of the calculation positions for VABS will be significantly increased to represent the entire blade. Therefore, in this thesis, the blade sectional element is adopted.

6.2 Load Prediction

Prediction of the load on a structure within the design of a structure is one of the important elements in the design procedure. Likewise, in the design of wind turbine, it is important to predict the load on wind turbine and its blade. Then, using the obtained load analysis results, the structural integrity will be evaluated by substituting the blades into various load conditions. In this chapter, by using the commercial load calculation program, GH-Bladed, the load calculation for the wind turbine is performed on the 2MW wind turbine. And by using that result, the blade structural design will be evaluated.

6.2.1 Ultimate Limit State (ULS)

For load analysis for wind turbine design, consideration of various situations such as wind shape and operating conditions is required. In the case of the

wind shape, several formulas were suggested based on the following wind conditions: normal turbulence model (NTM), extreme turbulence model (ETM), extreme coherent gust with direction change (ECD), extreme wind shear (EWS), extreme operating gust (EOG), extreme direction change (EDC), and extreme wind speed model (EWM). Along with such wind model, a design load case (DLC) is obtained by combination of various operating conditions, such as yaw error, grid disconnection, and operating wind speeds. There is difference in DLC applied based on the size and operating conditions of the blade. However, since most of the blade extreme load occurs under ETM or EWM conditions, DLC 1.3 and DLC 6.2 which consider an extreme wind speed condition should be included. A specific DLC for load analysis is selected by referring to the one that was applied in SANDIA project [58] and UPWIND project [59]. Among the 14 DLC's proposed by IEC for an extreme load analysis, DLC's included in either SANDIA or UPWIND project are reflected in this thesis. A total of 8 DLC's are ultimately selected, and those are summarized in Table 6.1.

Extreme loads are obtained by a system load calculation, as shown in Fig. 6.3. It is a polar load envelope (PLE) that shows 360° distribution of the resultant moment along the length of the blade when viewed from the blade root area to tip. The moment applied to the blade is largest at the root part and becomes smaller toward the tip, and then the extreme moment curve becomes closer to the origin of the graph as the load computation location gets further away from the root of the blade. With PLE, a representative case with the highest

representative load is selected as a design load case, i.e., 93.8° (My_{max}), 138.1° (Mx_{min}), 280.7° (My_{min}), 342.9° (Mx_{max}), respectively. It is chosen to have the maximum and minimum load that represent four directions under a 360°direction load applied to the blade.

In addition, in PLE, the four design load cases selected are designated again in the direction of the blade length as *My* moment and *Mx* moment components, respectively, as shown in Fig. 6.4(a) ~ (d). Those four DLC's are applied in the direction of the length of the blade, and will be used to evaluate the blade structure.

6.2.2 Fatigue Limit State (FLS)

Wind turbine is exposed to a variety of loads, including wind loads, over a 20-year lifetime. In the case of the ultimate load experienced during the life of 20 years, it acts on the structure instantaneously, and the ultimate structural strength evaluation is performed considering such characteristics. However, in the case of fatigue load, it acts steadily to the wind turbine for a period of 20 years.

Annual wind speed distribution for fatigue load condition is shown in Table 6.2. The table describes the type of load that the wind turbine may experience for one year (8,760 hours) by DLC, and the wind speed conditions at that time, such as the smaller wind speed, larger wind speed, and the mean wind speed, may be set. In addition, for each DLC, time is indicated for how many hours per year DLC will be applied. Meanwhile, utilizing the probability density

function called as Weibull formula, the annual wind speed distribution applied to the wind turbine is shown in Fig. 6.5. By the DLC, which lasts for one year shown in Table 6.2, application to the annual wind speed distribution in Fig. 6.5 provides the fatigue load that wind turbines can experience for 20 years. As a result, fatigue loads are computed for six degrees of freedom.

In the direction of the span of the blade, the fatigue load result of *My* component, which acts at 3.5 m, is shown in Fig. 6.6 in the form of Markov matrix. In that regard, for the fatigue loads acting in the direction of blade span, the action loads are separated into the mean values and the range values. The horizontal axis of the table refers to an average moment value, while the vertical axis refers to the range of the moment. And the numbers in the internal cells are the design lifespan, which represents the number of repetitions for the corresponding mean-range load when expanding the analysis result. Markov matrices can be obtained for each blade length direction computation location and load component. In this thesis, 14 ($2\times7=14$) Markov matrices are obtained in consideration of the load components (Mx, My) of 2 and 7 fatigue assessment points.

6.3 CFD Computation

Evaluation of the accuracy of the load calculation results using BEMT and CFD analysis is performed and the two results are compared. In addition, to calculate the blade surface pressure, the computation is performed using the

finite volume method based on the commercial program ANSYS FLUENT. Three-dimensional incompressible Reynolds averaged Navier-Stokes (RANS) equation with the realizable k-ε two-equation model is used as a turbulence model. The RANS equations are time-averaged equations of motion for fluid flow and it primarily used to describe turbulent flows. And the k-ε turbulence model is the most common model used in CFD to simulate mean flow characteristics such as wind turbine, aerodynamics field, etc., for turbulent flow conditions.

Pressure-based segregated algorithms named semi-implicit method for pressure-linked equation algorithm is employed. For gradient computation and spatial discretization, least squares cell-based scheme and second order upwind scheme are used, respectively. By the standard wall model, the y+ value on the blade surface is adjusted to meet the conditions of the turbulence model, and a grid of 20 stories is built with a gradient rate of 1.2 from the blade surface for accurate flow prediction within the boundary layer.

6.3.1 Computational Grid and Calculation Conditions

A numerical grid on the blade surface and surroundings are shown in Fig. 6.7. It secures enough distance for disturbance by securing six-dimensional space in the radial direction, and securing two- and three-dimensional space in the axial direction around the blade, respectively. The blade is given the no-slip (wall) condition, and a rotating body is given to the domain that surrounds the blade. The entrance is subjected to the uniform inflow condition, and the exit

to the mean constant pressure condition is assigned. The circumferential boundary is subjected to the slip wall condition. The total number of grids in the analytical domain is approximately 4.5 million, and all the grids are composed of unstructured grids.

To conduct numerical simulation, rotational speed of the rotor blade is fixed at the rated value of 17.5 RPM and 4 cases of the wind speed are chosen from cut-in to rated (4 m/s ~ 12.1 m/s). Uniform velocity inlet condition, averaged static pressure outlet condition and rotational body are applied as the boundary conditions. As a criterion for determining whether the results converged, the range of the RMS residual value is set to 3×10^{-4}.

6.3.2 Stream Line and Pressure Distribution

The streamlines and pressure distribution in terms of the inflow velocity are shown in Figs. 6.8 and 6.9, respectively. By the streamlines in terms of the inflow wind speed, it is found that the detachment occurs at the root of the blade as the inflow wind speed increases. And the forced stalls are carried out by the pressure distribution difference and the radial flow caused by the centrifugal force. Generally, power performance is affected negatively due to radial flow, but BEMT assumes that there is no radial interaction between adjacent elements. Therefore, corrections for aerodynamic results considering the blade rotation effect should be included to perform BEMT analysis.

However, as shown by the pressure distribution in terms of the rate of inflow in Fig. 6.9, the output is predicted to increase due to the fact that the impact on

the aerodynamic efficiency is smaller inboard. Efficiency of the wind turbine is greatly affected by the shape of 40 - 100% span locations [51].

6.3.3 Thrust and Torque Comparison

The flow field velocity contour is shown in Fig. 6.10 with respect to the inflow velocity. Velocity intensity will increase as the wind speed increases and it is concentrated mainly in the region around the 50% or outboard of the blade span length. It is shown that as the wind speed increases, the magnitude of velocity intensity and the effective range for generating torque will also increase. In case of the rated condition, most of the blade torque occurs mainly in 30% ~ 90% spanwise stations. The results of thrust and torque are compared, and the value obtained by BEMT in Chapter 4. 221 kN shows approximately 4.4% discrepancy.

Therefore, by comparing the results of the load analysis by using both BEMT and CFD, the load used in the design of the blade will be properly obtained.

6.4 Structural Integrity Evaluation

In the results of load calculation in Sections 6.2 and 6.3, four types of the load conditions (the maximum in-plane direction, the minimum in-plane direction, the maximum out-plane direction, the minimum out-plane direction) that show increased load distribution in the blade span direction from PLE are selected for extreme strength evaluation. Using the load calculation results, the

blade structural integrity is evaluated by extreme conditions such as stability, modal, the maximum tip deflection, and fatigue strength analysis.

6.4.1 Maximum Tip Deflection

The blades are subjected to various loads, including wind loads, during operation, resulting in displacement. In any case, the maximum tip deflection occurring in the blade will be maintained at the minimum distance from the tower to ensure the safety of the entire wind turbine system. Therefore, the blade maximum displacement assessment is one of the important and basic procedures.

Evaluation of the blade tip deflection under an extreme load condition is critical for evaluating the structural integrity, and should be strictly evaluated in the design verification and evaluation stage. The maximum tip deflection evaluation on 4 types of extreme load conditions is applied, and Fig. 6.11 shows both the tip deflection result and PLE to check the deflection shape based on the applied load direction. The maximum deflection occurs in $My\_\min$ condition, design load case, i.e., 280.7°, the tower clearance with blade is 5.85m as shown in Table. 3.1, whereas the maximum displacement result is 3.74m. Therefore, based on the results of the calculation, it is confirmed that the maximum displacement of the blade is within a safe range.

6.4.2 Laminate Failure Evaluation

The laminate failure evaluation is performed using Eqs. (3.34) – (3.37) introduced in Section 3.4.1. The fiber failure and inter-fiber failure assessment is performed in each laminate, and the result are summarized in Figs. 6.12~6.15. The concept of the inverse reserve factor (IRF) is introduced. It is the ratio between the stress caused by the loading action and the allowable stress, which is the inherent ability of the material, meaning that the structure will be safe when the result is less than 1.

Most of the results under 4 types of design load cases show a value of less than 1, and it is confirmed that there is no fiber and inter-fiber failure in extreme load conditions. In the fiber damage analysis, a relatively high failure index appeared in the blade root and spar cap, while for inter-fiber failure analysis, high failure index appears in the shear web that receives high torsion load and the root part. Also, a relatively high failure index occurred in the flap-wise direction extreme load condition. The maximum fiber and inter-fiber failure evaluation results are 0.39 and 0.68, respectively, in $My\_\max$ condition, design load case, i.e., 280.7°, thus the present blades secure sufficient safety margin in the extreme load conditions.

6.4.3 Fatigue Evaluation Results

The wind turbines experience various fatigue loads over their 20-year lifetime during operation, including wind loads. Therefore, it is necessary to evaluate whether the structural safety is secured even for those fatigue loads. The fatigue evaluation is performed using Eqs. (3.38) – (3.39) introduced in

Section 3.4.2, and evaluation is performed by applying Miner's rule, which is generally used in fatigue analysis. But the allowable number of applied loads at this time is calculated using the Goodman diagram in Equation (3.38).

With regard to the international standards and most certification guidelines, fatigue evaluation for wind turbine blades is regulated as a mandatory item. In detail, fatigue evaluation is conducted by using load time series data obtained through the load calculation, and the definition of fatigue load conditions is described in detail in Section 6.2.2. In this thesis, the load values in two directions only consider the flap-wise direction bending moment and edge-wise direction bending moment which consist of fatigue load among the six degrees of freedom. Schematic diagram of fatigue evaluation is shown in Fig. 6.16.

The fatigue evaluation is conducted for a total of 56 conditions, with the combination of 7 fatigue evaluation cross-sections, 2 load (Mx , My) conditions, 2 evaluation parts (spar cap and trailing edge) and 2 maximum/ minimum transformation rate ($7 \times 2 \times 2 \times 2 = 56$). The final evaluation result for the spar cap and trailing edge are shown in Tables 6.3 and 6.4. It is found that the analysis result of fatigue evaluation due to My is the weakest at the spar cap, which is located at 18.9m in the blade span direction. It is 10^{-6} , and it is found that fatigue failure does not occur. Thus it is confirmed that it is structurally safe for fatigue loads.

6.4.4 Stability Evaluation

Composite products are vulnerable to buckling. Therefore, for structures made of composite materials, buckling stability is of paramount importance. By the buckling analysis, the buckling stability under the 4 types of extreme load condition is to be analyzed. According to the guideline of IEC 61400-5, the buckling stability evaluation is carried out and the results are evaluated based on the safety margin of 1.25.

Buckling analysis is conducted with the extreme load conditions (DLC 93.8°, 138.1°, 280.7°, 342.9°), and the results are shown in Fig. 6.17 based on the critical load coefficient for buckling. By having a critical load coefficient of 1.25 or above in all the load conditions, the result of buckling stability is regarded as safe and it is located within a stable range.

The most extreme condition, the flap-wise direction maximum load ($My_{\max}$) condition, confirms that the critical load coefficient will be 1.5. In addition, the components vulnerable to buckling are the leading/trailing edge close to the blade root, and the spar cap which is located approximately 70% from the blade root. The leading and trailing edge close to the root are the locations that the largest bending moment is applied. Buckling occurs at the leading and trailing edges, which have relatively lower stiffness compared to the spar cap at the corresponding location. For the case of the location 70% from the root, the thickness of spar cap layer is designed to be smaller considering that the applied load, which becomes smaller towards the blade tip. However, the thickness difference that occurs as the foam thickness of the leading and trailing edges in the corresponding location is maintained at a constant value is regarded as the main reason for buckling occurring at the spar cap area. As a

result, the leading and trailing edges close to the blade root where the compressive load due to bending moment is a weak point of the blade, and the spar cap area which has a large thickness difference with its surrounding also has significant buckling risk.

As shown above, the foam material may reinforce stiffness and thickness of a specific component of the blade while minimizing the increase in mass, optimal design of the foam thickness and placement is important to satisfy the final goal in terms of the weight and buckling stability.

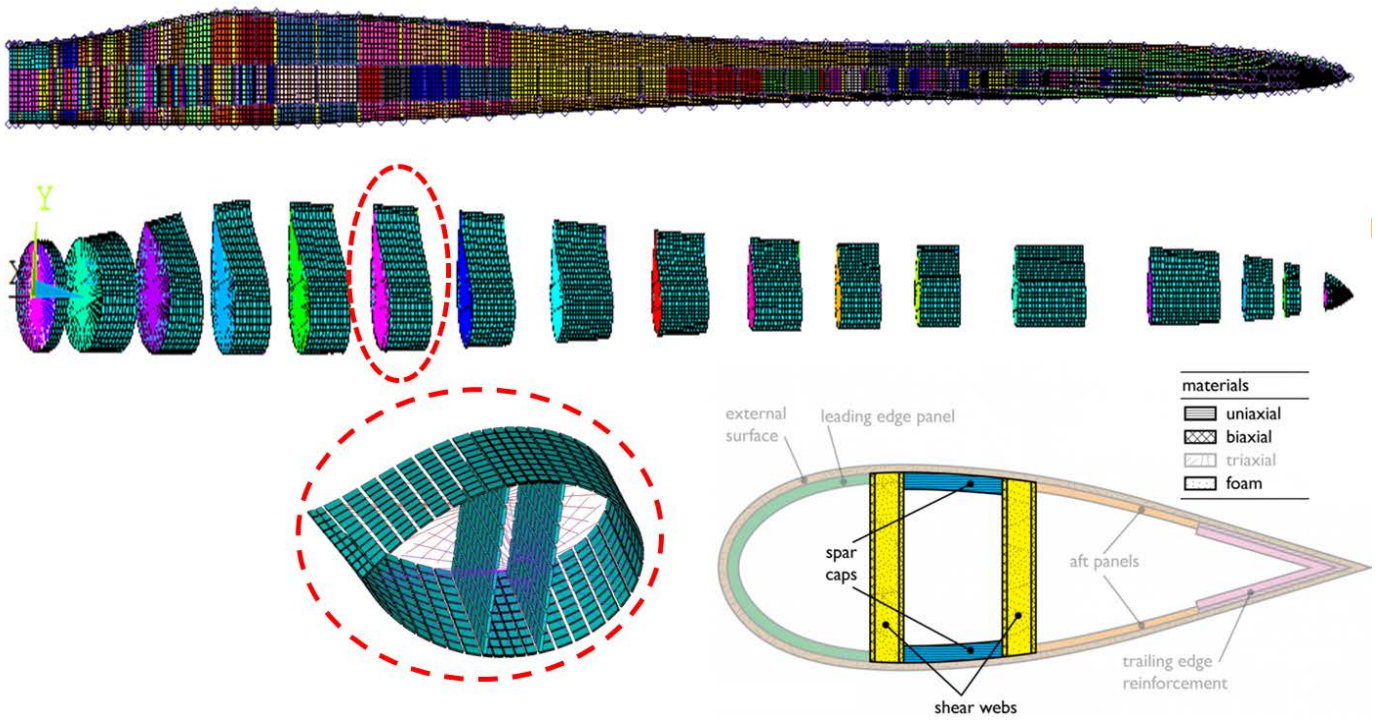

Figure 6.1. Finite element discretization for the wind turbine blade

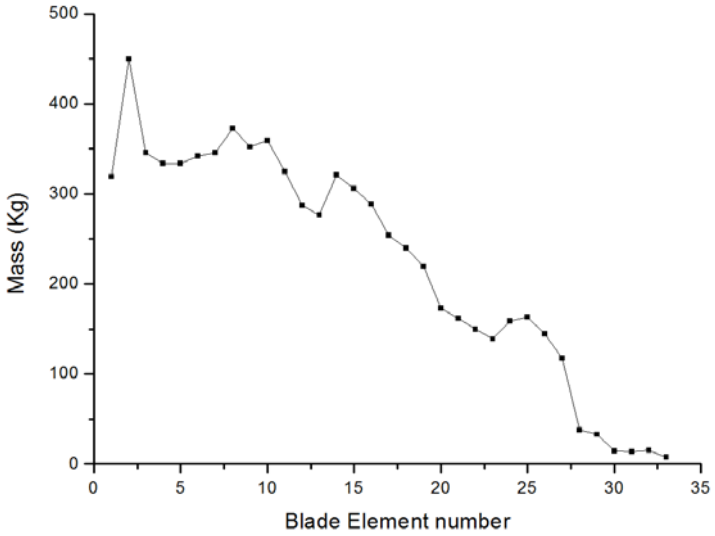

(a) mass distribution

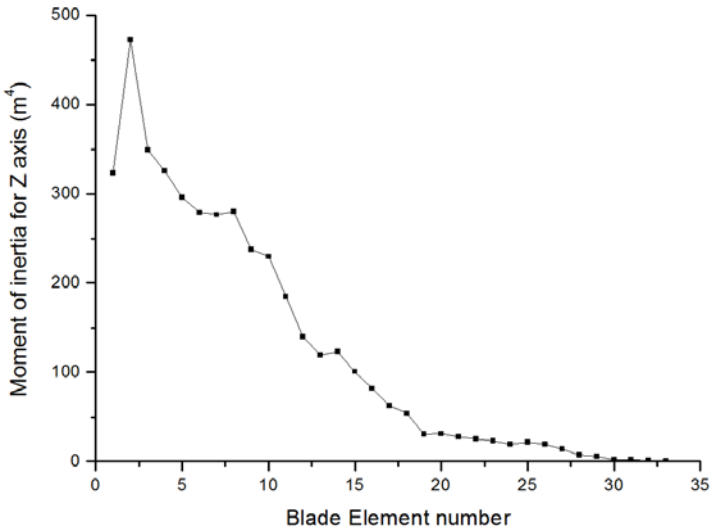

(b) moment of inertia

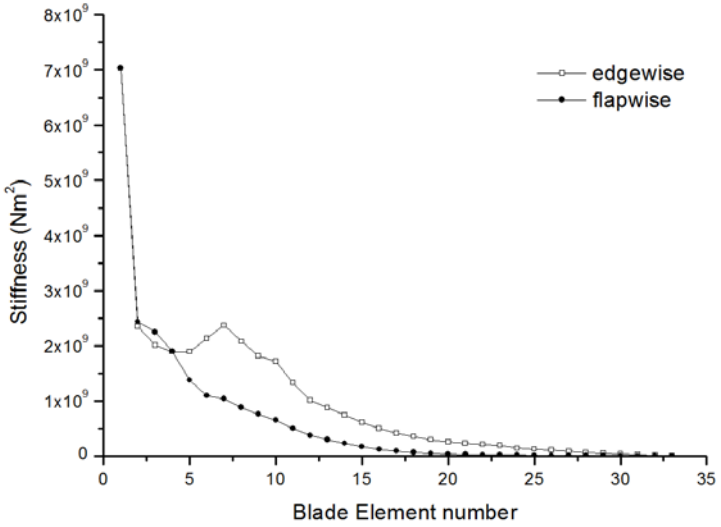

(c) edge- and flap-wise stiffness

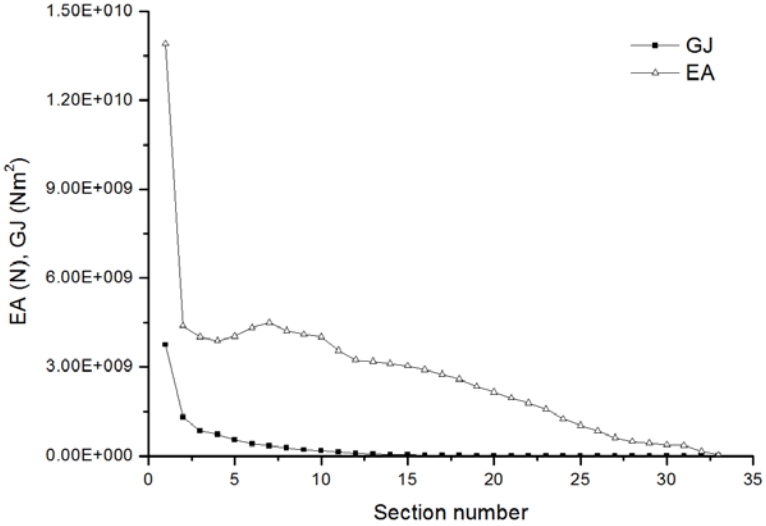

(d) torsion and tensional rigidity

Figure 6.2. Sectional distribution results along the blade span

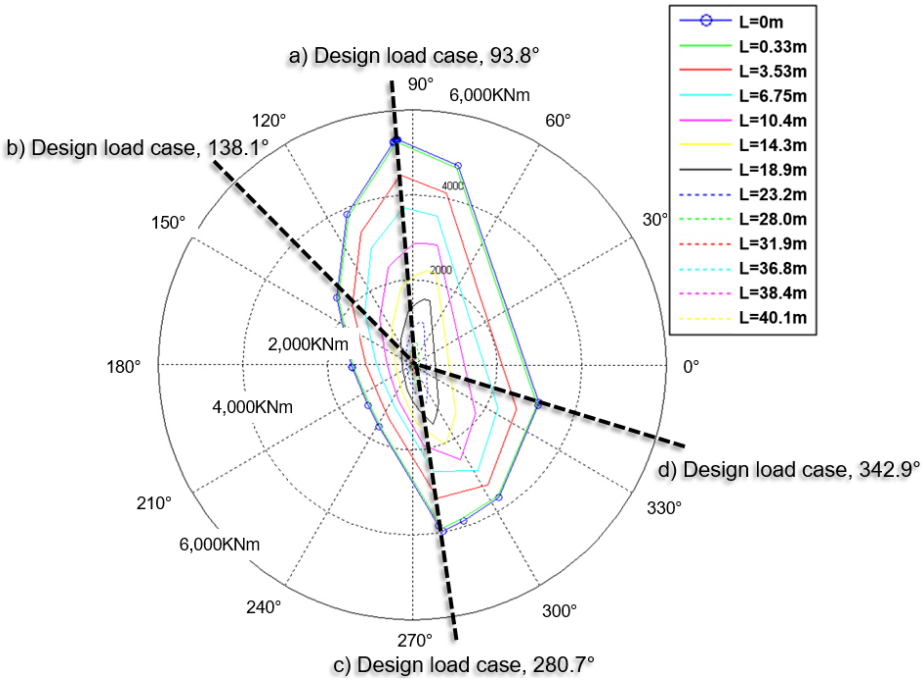

Figure 6.3. Extreme load calculation result of the blade

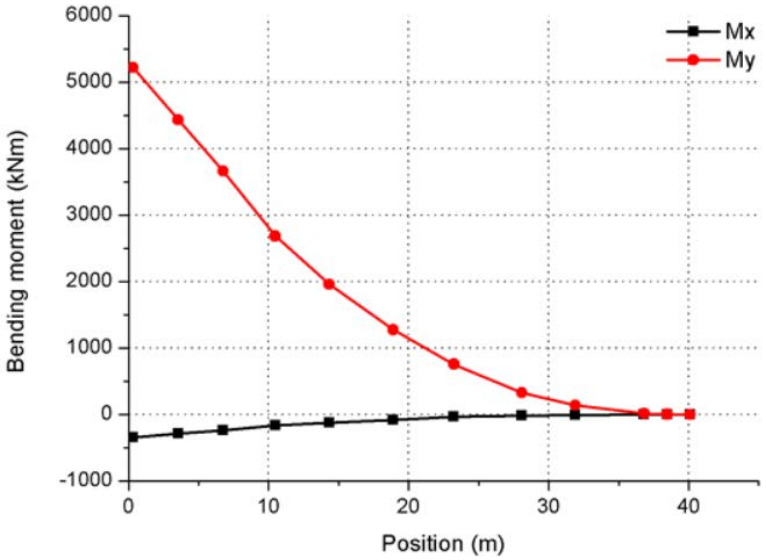

(a) Accumulated moment distribution, 93.8°

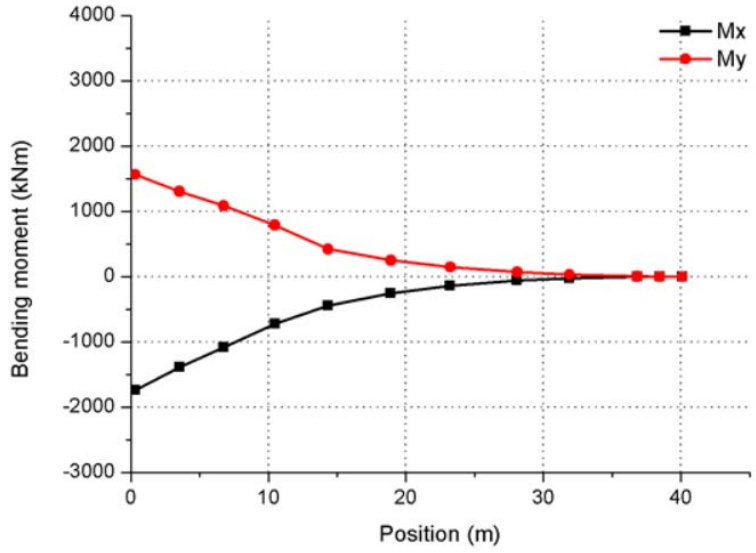

(b) Accumulated moment distribution, 138.1°

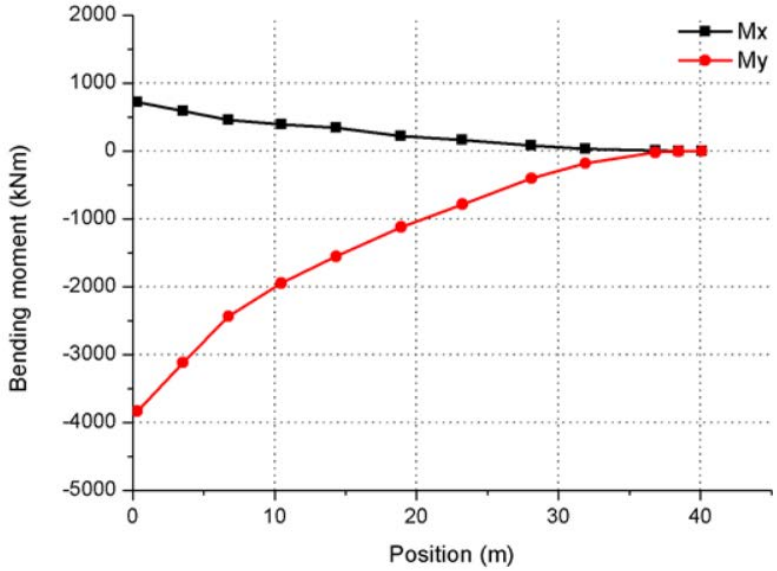

(c) Accumulated moment distribution, 280.7°

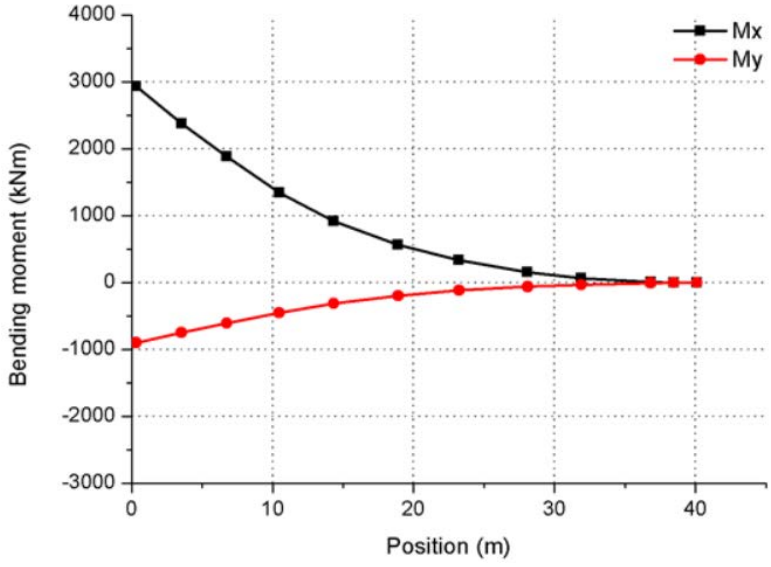

(d) Accumulated moment distribution, 342.9°

Figure 6.4. Accumulated moment distribution for the extreme load case

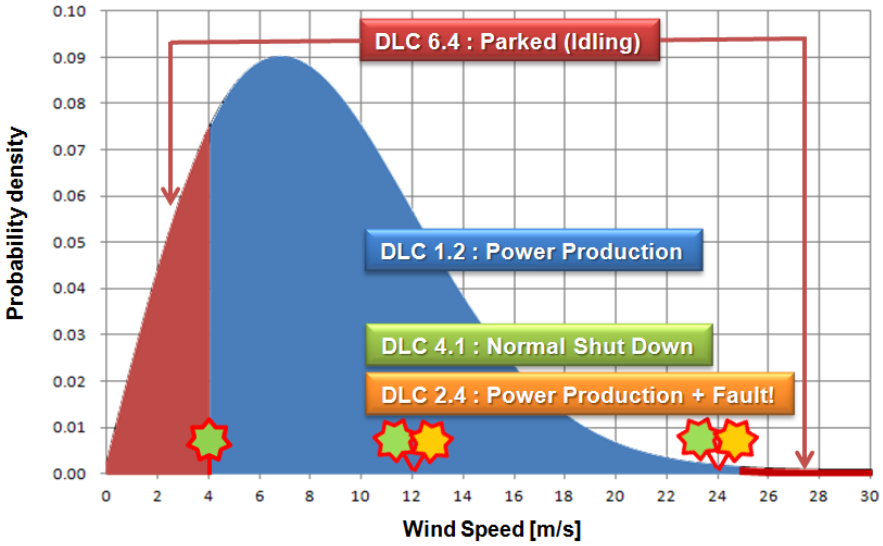

Figure 6.5. Annual wind speed distribution (Weibull function)

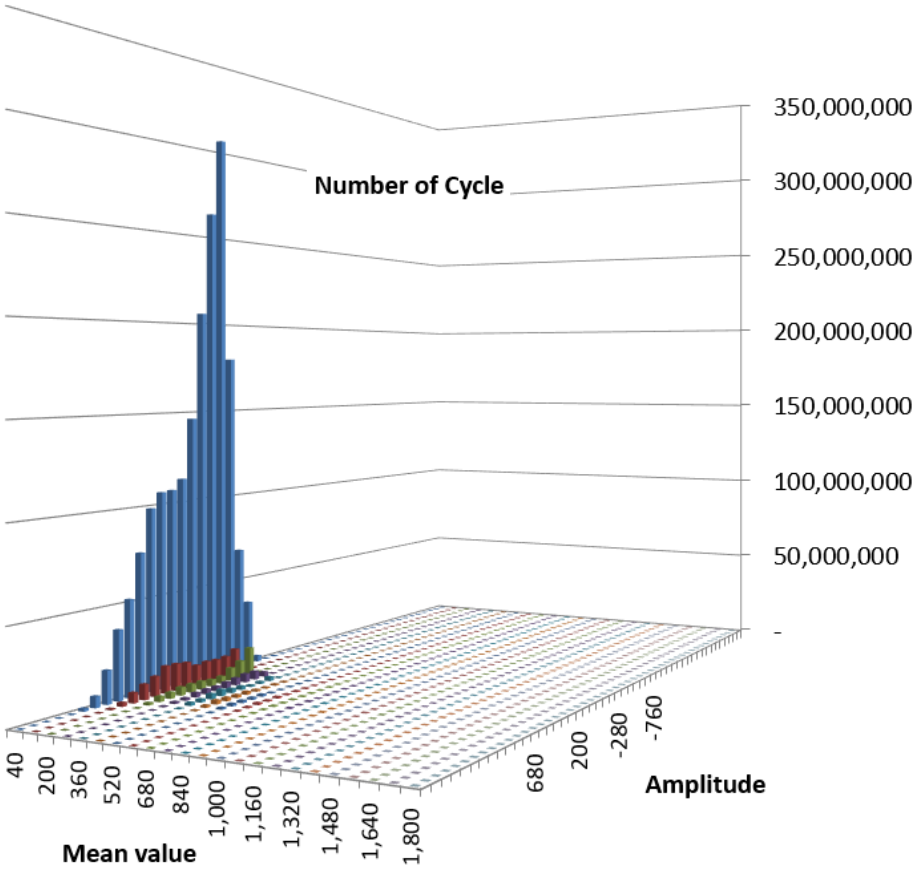

Figure 6.6. Fatigue load result as Markov matrix (*My* at L=3.539m)

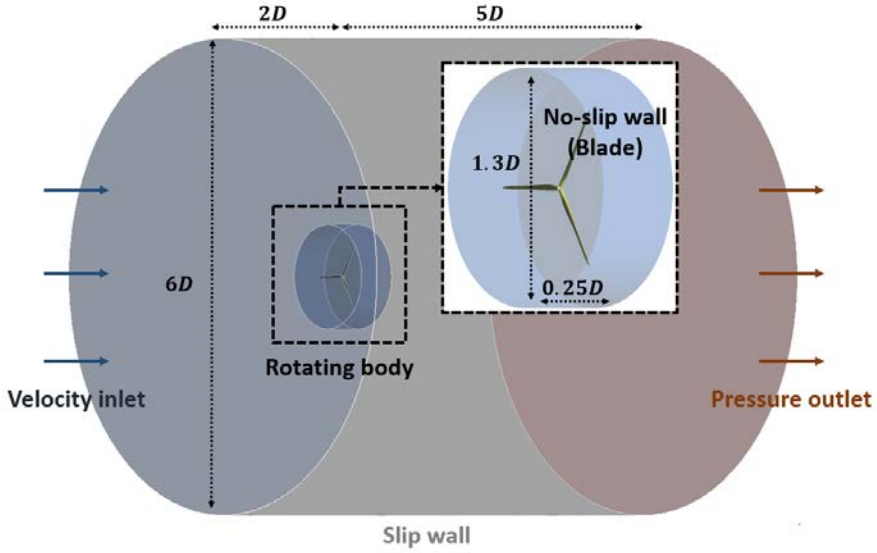

(a) Domain condition

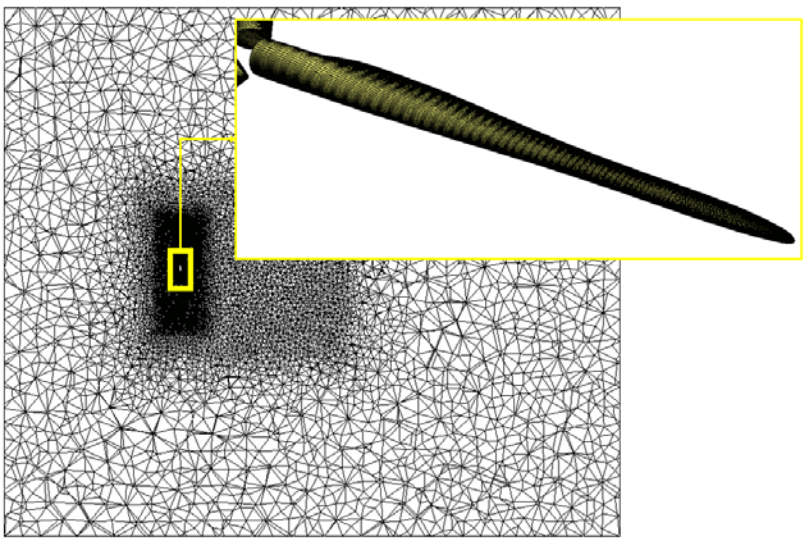

(b) Grid distribution and surface grids on the blade

Figure 6.7. Computational domain for CFD calculation

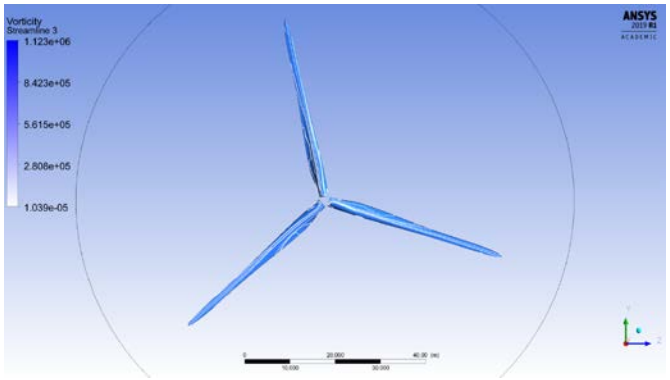

a) V_{in} = 4m/s

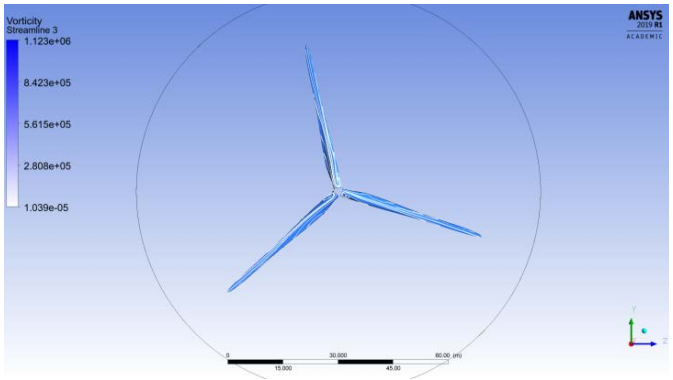

b) V_{in} = 6m/s

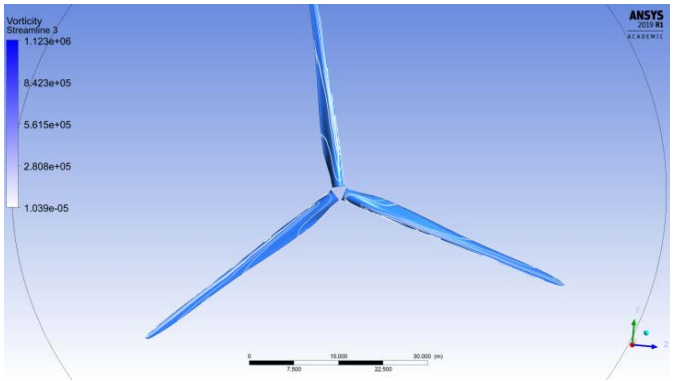

a) V_{in} = 8m/s

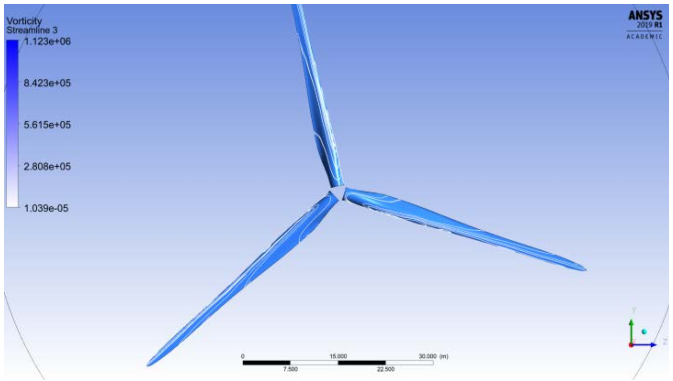

b) V_{in} = 11.5m/s

Figure 6.8. Stream line distribution in terms of the inflow velocity

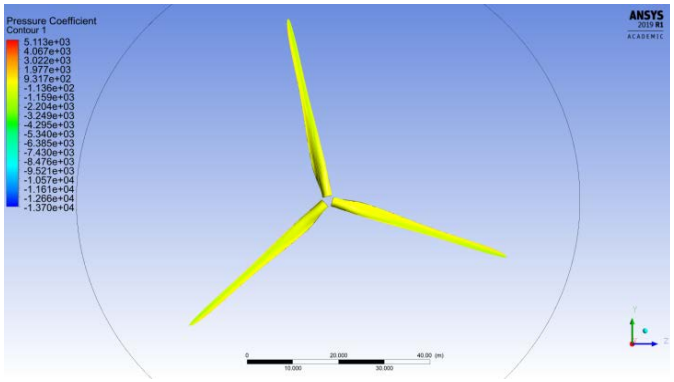

a) V_{in} = 4m/s

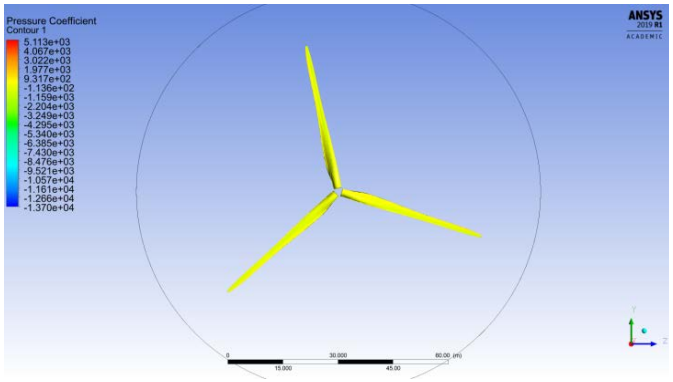

b) V_{in} = 6m/s

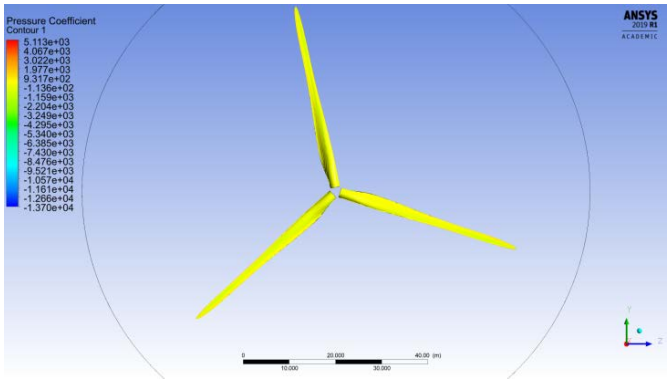

a) V_{in} = 8m/s

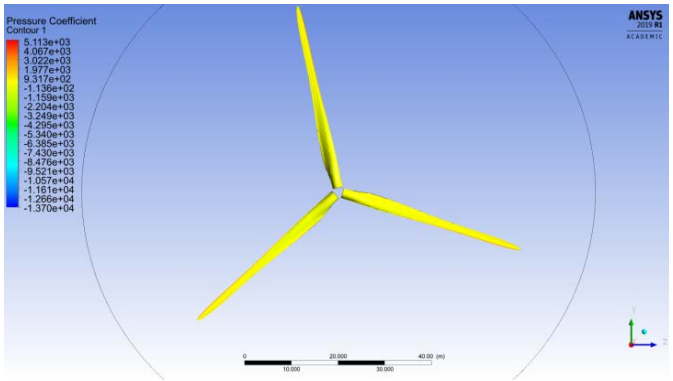

b) V_{in} = 11.5m/s

Figure 6.9. Pressure distribution in terms of the inflow velocity

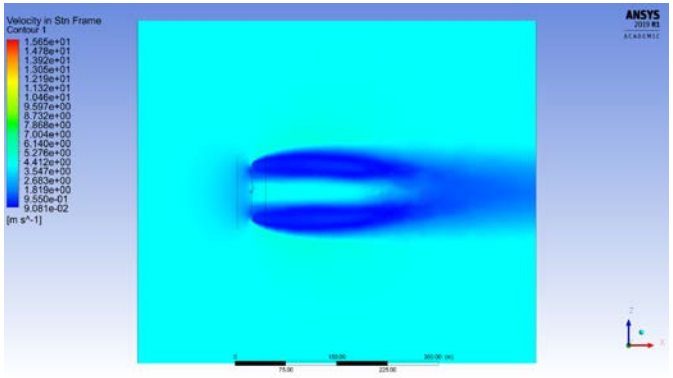

a) V_{in} = 4m/s

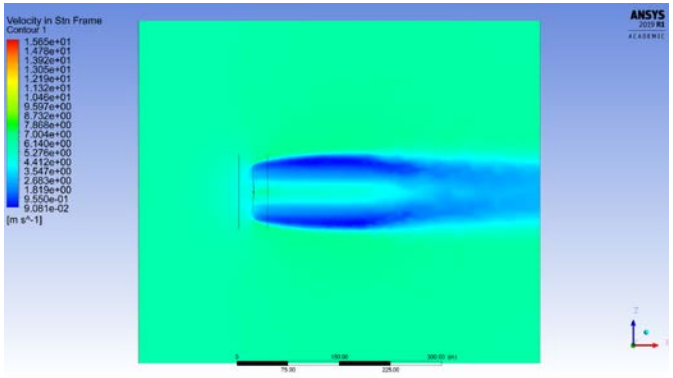

b) V_{in} = 6m/s

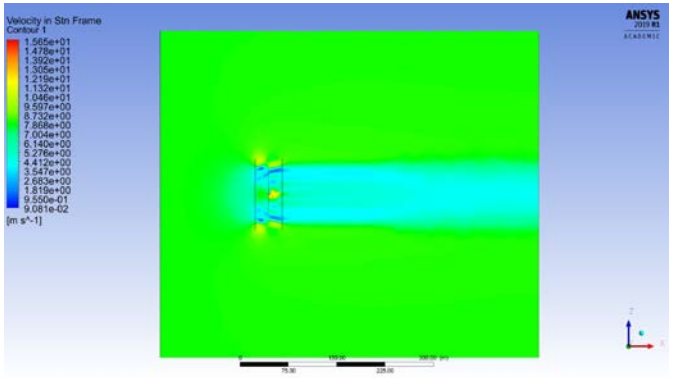

a) V_{in} = 8m/s

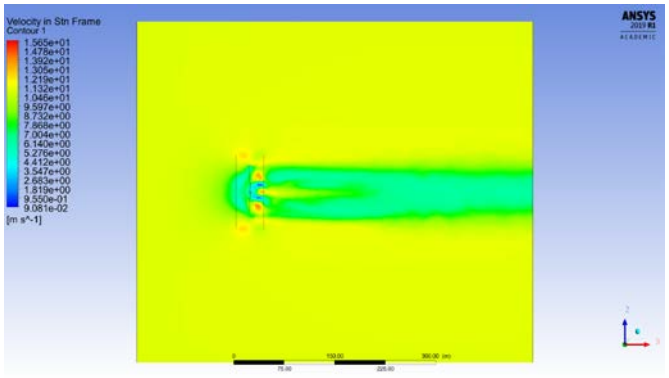

b) V_{in} = 11.5m/s

Figure 6.10. Flow field velocity contour in terms of the inflow velocity

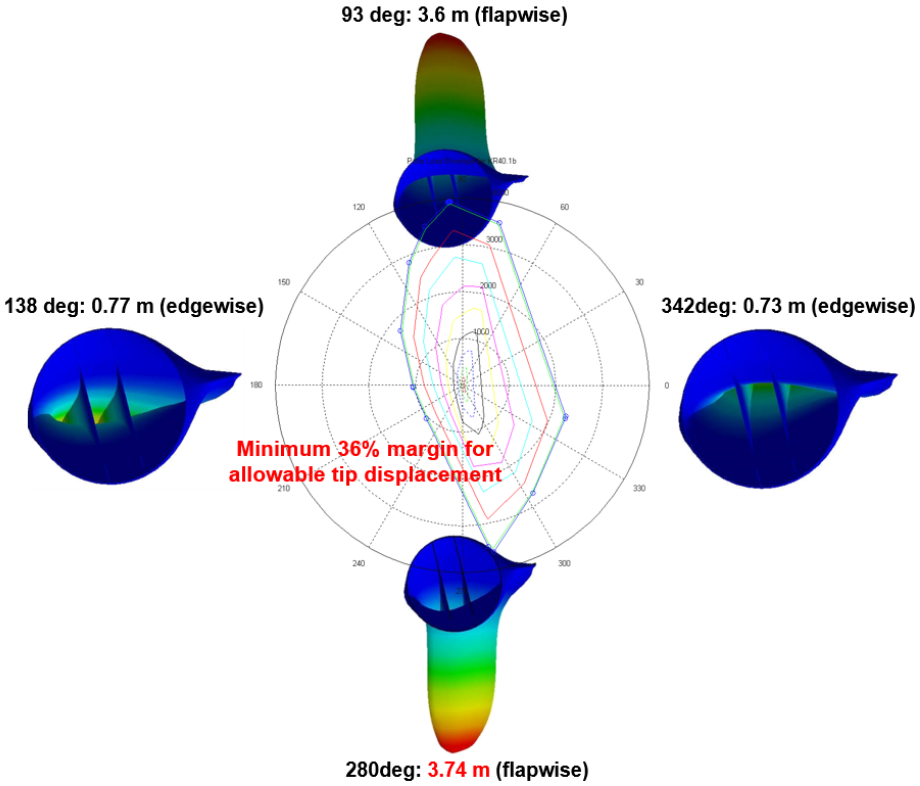

Figure 6.11. Tip deflection results for four extreme load conditions

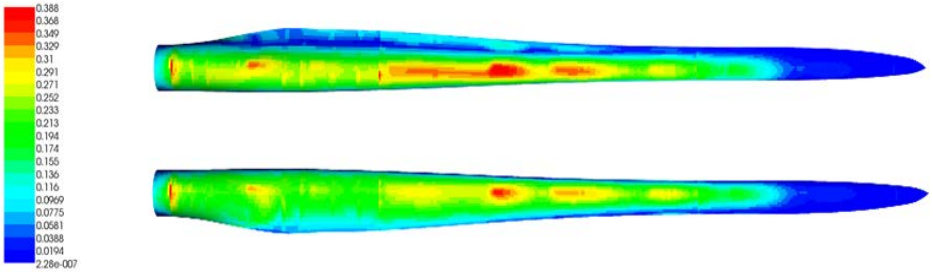

(a) Results of the fiber failure (max. IRF: 0.39)

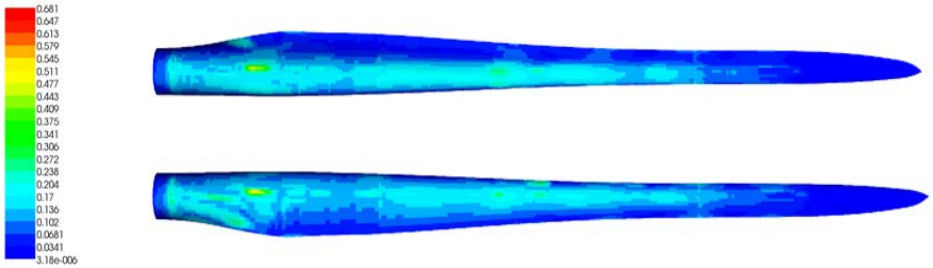

(b) Results of the inter-fiber failure (max. IRF: 0.68)

Figure 6.12. Evaluation result for DLC 93.8° condition

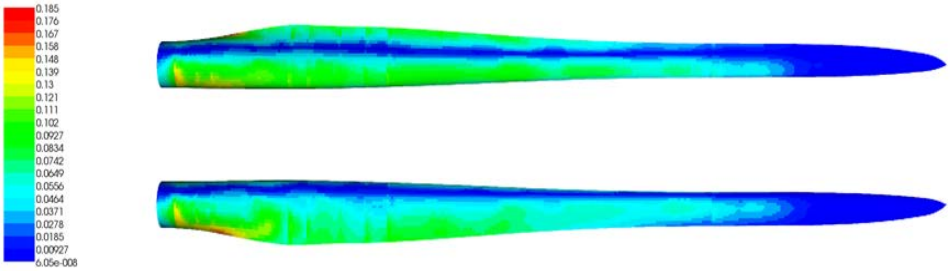

(a) Results of the fiber failure (max. IRF: 0.19)

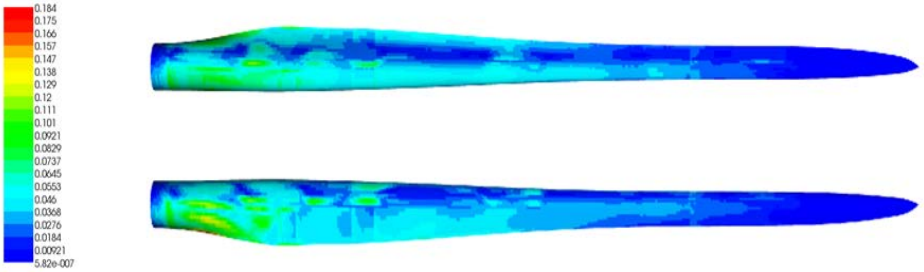

(b) Results of the inter-fiber failure (max. IRF: 0.18)

Figure 6.13. Evaluation result for DLC 138.1° condition

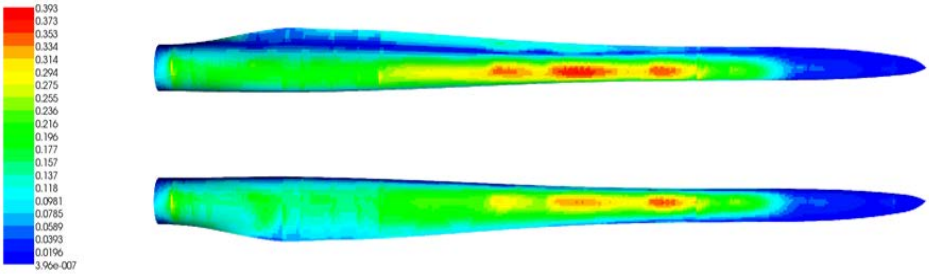

(a) Results of the fiber failure (max. IRF: 0.39)

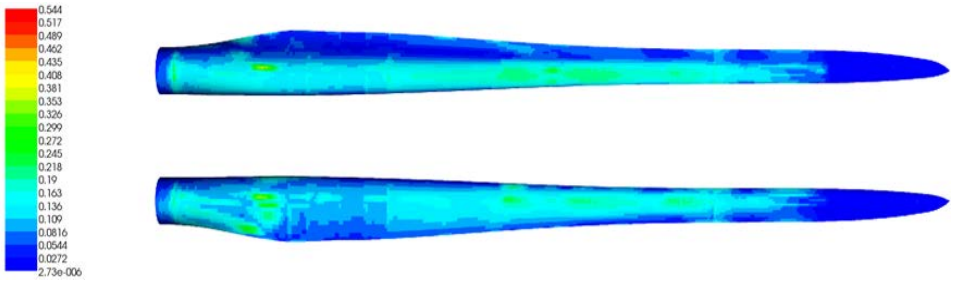

(b) Results of the inter-fiber failure (max. IRF: 0.54)

Figure 6.14. Evaluation result for DLC 280.7° condition

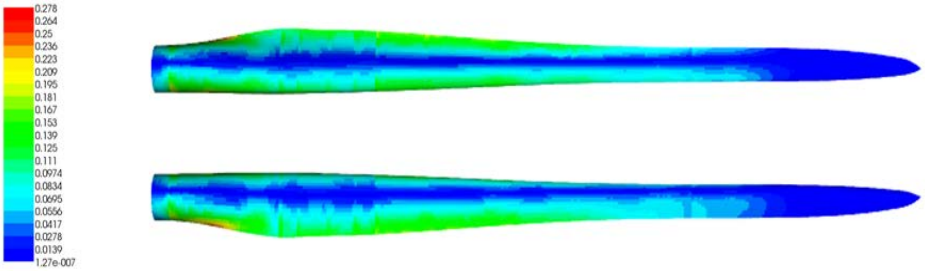

(a) Results of the fiber failure (max. IRF: 0.28)

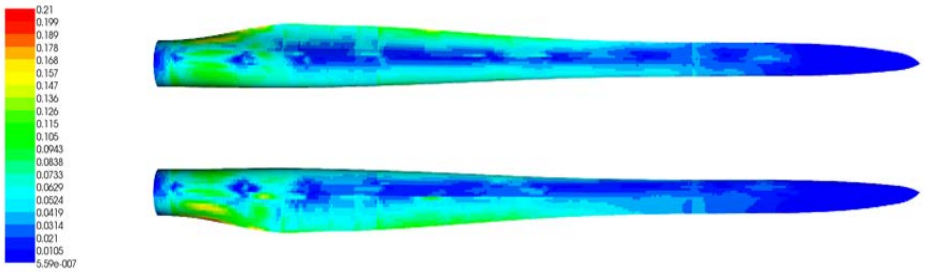

(b) Results of the inter-fiber failure (max. IRF: 0.21)

Figure 6.15. Evaluation result for DLC 342.9° condition

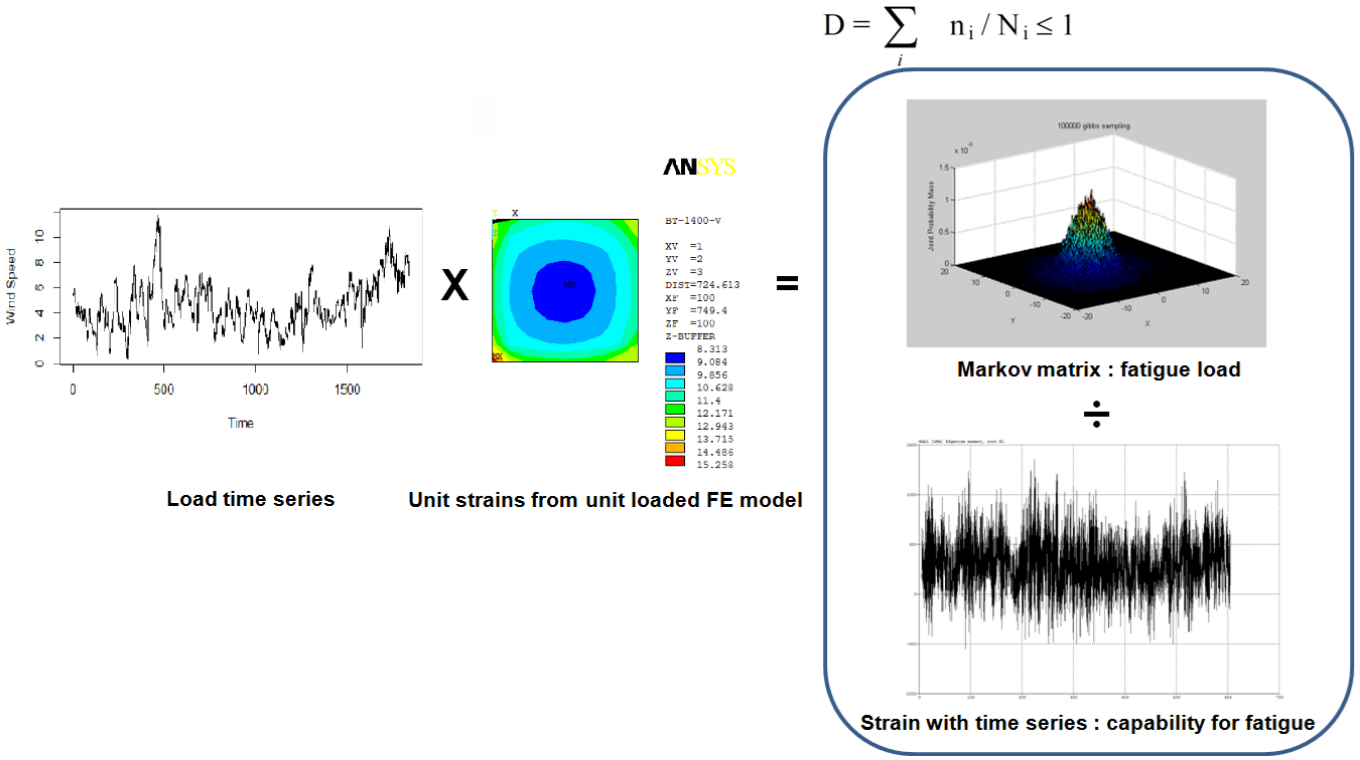

Figure 6.16. Schematic diagram of the fatigue evaluation

(a) DLC 93.8° condition, 1.5 of load factor

(b) DLC 138.1° condition, 3.0 of load factor

(c) DLC 280.7° condition, 2.9 of load factor

(d) DLC 342.9° condition, 5.0 of load factor

Figure 6.17. Buckling analysis result

Table 6.1. Comparison of the selected design load cases

No.	Design load case	Wind condition	IEC	SANDIA	UPWIND	Present
1	1.1	NTM	○	-	-	
2	1.3	ETM	○	○	○	●
3	1.4	ECD	○	○	○	●
4	1.5	EWS	○	○	-	●
5	2.1	NTM	○	-	-	-
6	2.2	NTM	○	-	-	-
7	2.3	EOG	○	-	-	-
8	3.2	EOG	○	○	-	●
9	3.3	EDC	○	○	-	●
10	4.2	EOG	○	-	-	-
11	5.1	NTM	○	-	-	-
12	6.1	EWM	○	-	○	●
13	6.2	EWM	○	○	○	●
14	6.3	EWM	○	○	-	●

Table 6.2. Annual wind speed distribution for the fatigue load condition

DLC	Lower wind speed (m/s)	Upper wind speed (m/s)	Mean wind speed (m/s)	hours/year
DLC 6.4	0	4	3	1,399.4
DLC 1.2	4	5	4	686.5
DLC 1.2	5	7	6	1,533.9
DLC 1.2	7	9	8	1,511.8
DLC 1.2	9	11	10	1,281.4
DLC 1.2	11	13	12	956.4
DLC 1.2	13	15	14	636.6
DLC 1.2	15	17	16	380.7
DLC 1.2	17	19	18	205.6
DLC 1.2	19	21	20	100.6
DLC 1.2	21	23	22	44.6
DLC 1.2	23	25	24	18.0
DLC 6.4	25	∞	29.75	9.8
				8,760 hours

Table 6.3. Fatigue evaluation result for the spar cap

Cross section	Calculation point [mm]	Spar cap			
		Mx		*My*	
		Max	Min	Max	Min
1	3,539	5.41×10^{-19}	2.53×10^{-21}	2.08×10^{-10}	3.10×10^{-10}
2	6,747	6.17×10^{-20}	1.50×10^{-22}	8.81×10^{-12}	3.07×10^{-11}
3	10,469	2.94×10^{-24}	5.37×10^{-26}	1.00×10^{-10}	3.70×10^{-10}
4	14,327	6.07×10^{-20}	1.08×10^{-22}	1.83×10^{-9}	1.80×10^{-8}
5	18,903	6.23×10^{-31}	2.43×10^{-21}	2.77×10^{-7}	1.20×10^{-6}
6	23,229	1.02×10^{-21}	1.83×10^{-27}	5.90×10^{-7}	9.33×10^{-7}
7	28,091	7.66×10^{-23}	2.17×10^{-27}	8.07×10^{-7}	2.95×10^{-7}

Table 6.4. Fatigue evaluation result for the trailing edge

Cross section	Calculation point [mm]	Trailing edge			
		Mx		*My*	
		Max	Min	Max	Min
1	3,539	3.19×10^{-15}	2.73×10^{-15}	2.18×10^{-14}	8.39×10^{-22}
2	6,747	5.16×10^{-19}	6.70×10^{-15}	2.16×10^{-19}	1.59×10^{-28}
3	10,469	5.69×10^{-18}	4.28×10^{-15}	8.41×10^{-15}	2.56×10^{-23}
4	14,327	2.38×10^{-17}	4.02×10^{-14}	1.22×10^{-14}	1.18×10^{-20}
5	18,903	2.29×10^{-8}	2.51×10^{-14}	7.78×10^{-32}	2.64×10^{-9}
6	23,229	8.20×10^{-13}	4.72×10^{-15}	1.23×10^{-15}	9.78×10^{-11}
7	28,091	2.43×10^{-20}	3.27×10^{-17}	1.69×10^{-17}	4.82×10^{-10}

Chapter 7

NUMERICAL RESULTS

In this chapter, it is necessary to discuss in more detail the originality of the design and its evaluation process, and the advantages of design results.

7.1 Extraction of the Sectional Properties

Based on the numerical results, the structural characteristics are compared between the three-dimensional blade and the equivalent beam models to obtain the total mass, mode shapes, and natural frequencies. The three-dimensional model and the simplified beam model estimate the total weight to be 7,125 kg and 7,138 kg, respectively. In addition, Fig. 7.1 and Table 7.1 shows the results of the modal analysis using the present stiffness and mass properties. The natural frequencies and mode shapes are found to agree well within 2.6 % discrepancy. The differences are dominant for the higher modes since the warping, shear, and the geometric non-linear characteristics are related to the

flap bending-twist coupling. Also, the results based on the blade element concept shows good agreements with the three-dimensional analysis in spite of the simplicity. Most BEMT-based load analysis programs perform calculations on the blades in the form of simplified beams. Thus, in order to accurately predict the behavior of the wind turbine, it is important to accurately simulate the characteristics of the realistic blade.

7.2 Optimal Aerodynamic Design

The combination of the calculation locations, from Locations 3 to 16, are listed as the results of the optimum blade design in Table 7.2. It shows the geometric comparison between the initial and the optimum blade with respect to the chord length and the twist angle. The chord length is increased by approximately 5% as compared to that of the baseline blade. However, the built-in twist angle is decreased dramatically specifically, 69% at 37.6m span of the blade. By examining the results of the optimal design, comparison of the efficiency (C_P) is shown in Fig 7.2.

In addition, the power curve comparison between the two blades is shown in Fig 7.3. The rated wind speed of the optimized blade is dereased from 12.5 to 12.0 m/s, which is the rated wind speed shifted to the left at 4%. This indicates that the rated power of 2 MW will be obtained at a lower wind speed, which indicates increase of AEP. 2 megawatts are the maximum energy produced in the optimum condition for the wind turbine. The turbine with a lower rated

wind velocity means that 2 MW of electricity can be produced at a relatively lower speed, as compared to a high rated wind speed turbine. This represents a highly desirable design. As an optimal power is generated at relatively lower wind speeds, it is possible to obtain more energy production and, therefore, an increased efficiency.

In Table 7.3, the efficiency (C_P) is increased approximately by 8.7%, and the rated wind speed is decreased by 4% from 12.5m/s to 12m/s. Because of those results, AEP shows increase of approximately 7%.

7.3 Optimal Structural Design

The final structural design, which is obtained by an optimal design of the spar cap, and the optimal cross section design, shows to have weight 7,124 kg with increased rigidity and decreased weight. The composite material layer patterns of the blade are shown in Figs. 7.4 and 7.5.

7.3.1. Present Algorithm

The blade structure optimization results calculated using two types of optimization algorithms are summarized in Table 7.4. Calculations shows that genetic algorithm is more suitable for the present design. Both genetic algorithm and Nelder-Mead simplex satisfy the required numerical stability. However, the total weight by the genetic algorithm is reduced by about 200kg,

while Nelder-Mead simplex results in increase of about 500kg. Nelder-Mead simplex focuses on the local optimization. It can be identified by comparing the layup number of the section. When comparing the number of the spar cap plies, which plays the important role in the blade stiffness, the maximum number for the spar cap ply, which is 71 at the baseline blade, shows increase to 75 plies by Nelder-Mead simplex. This has a similar tendency not only in the spar caps but also in the other components such as shear web. It results in increase in the overall weight of the blade. However, in the case of genetic algorithm, for the maximum number of the spar cap ply, it is drastically reduced to 45 plies, and it is inferred that the weight of the blade is reduced.

7.3.2. Discussion for the Blade Component

The schematic description of the blade layer patterns is shown in Fig. 7.4. The skin uses bi-axle ±45° plies of glass fiber, and resists the torsional load that is applied to the blade and maintains the three-dimensional shape of the blade. In addition, the gel goat layer that protects the blade from external environments such as sun light. The spar cap is composed of UD fiber layers and supports most of the bending load, which is the major load applied to the blade. Foam material is applied to withstand the local buckling and maintain airfoil cross section shape. Since the blade root component is a section where a relatively large load is applied, either fiber failure, resin failure, or local buckling is expected to occur. Therefore, lamination reinforcement by using bi-axle fiber is attempted as shown in Fig 7.4. The layer pattern of the root

contract component is illustrated and its thickness is about 9 cm, which is much larger than the thickness of a regular blade skin. The section with such thickness difference seems to have stress-strain concentration, and thus it is necessary to maintain an insignificant thickness variation. Three-dimensional configuration of the blade and spar cap lay-up pattern are shown in Fig. 7.5.

7.3.3. Comparison of the Blade Weight

Comparison the weight of the major component to total weight of the blade is shown in Fig 7.6. The material usage among the major components of the blade, the spa cap and skin account for about 50% of the total weight. In the case of the spa cap, it is possible to expect relatively heavy weight due to the use of a dense UD product. It is found that the percentage of skins is considerably large at 22%. This is a component made of bi-axle, which covers the entire blade for skin. And it is observed that the weight ratio is also large due to its relatively frequent usage of the blade surface. In case of the blade root, the application area is relatively small, but due to the small thickness, it is assumed that the ratio of the blade root is increased. Finally, in the case of foam, despite being used in most areas of the blade with skin and shear web, it is found that the weight is relatively small due to the low density.

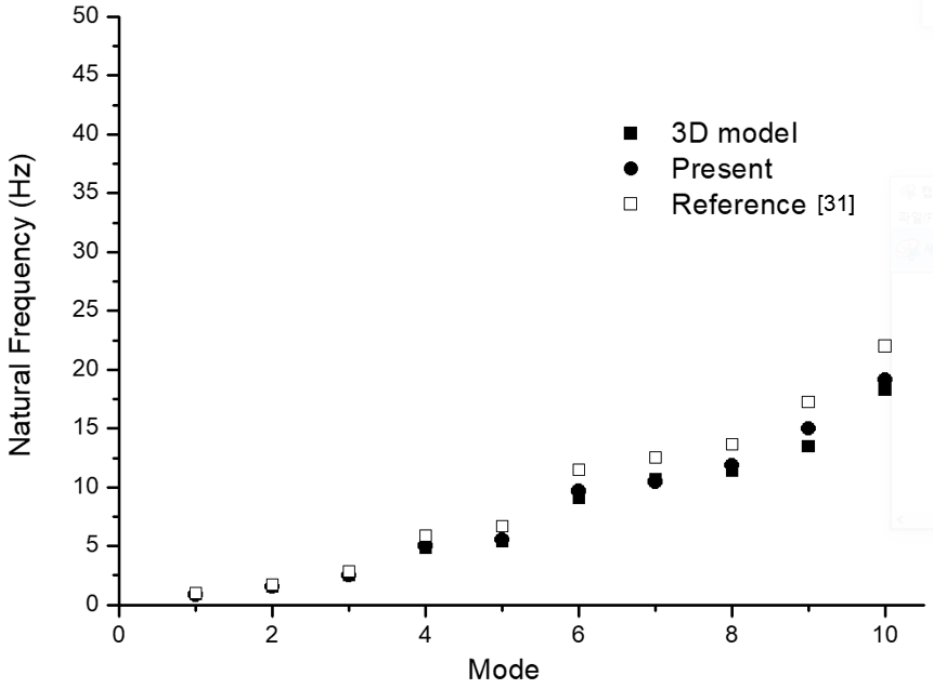

Figure 7.1. Comparison of the natural frequencies

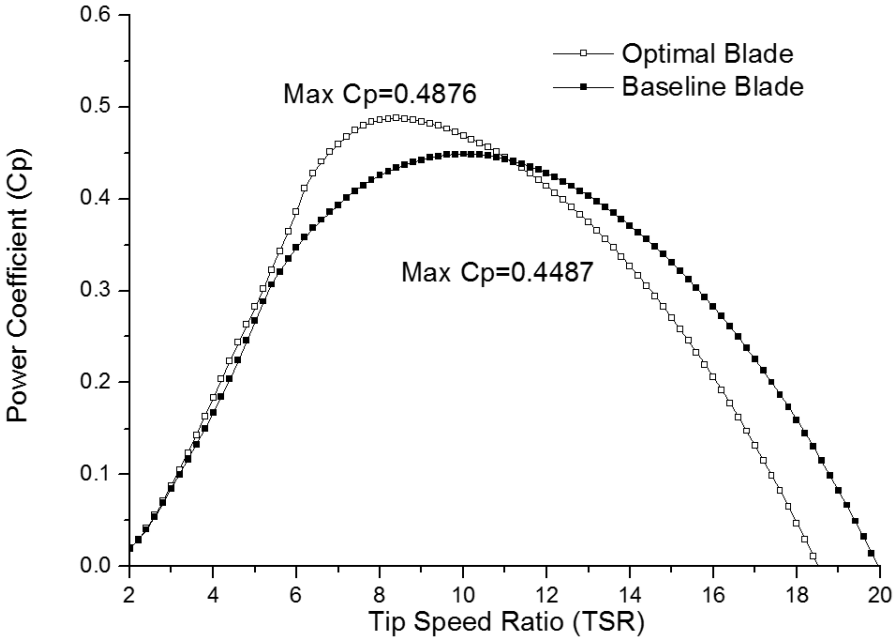

Figure 7.2. Power efficiency comparison between the optimal and baseline blades

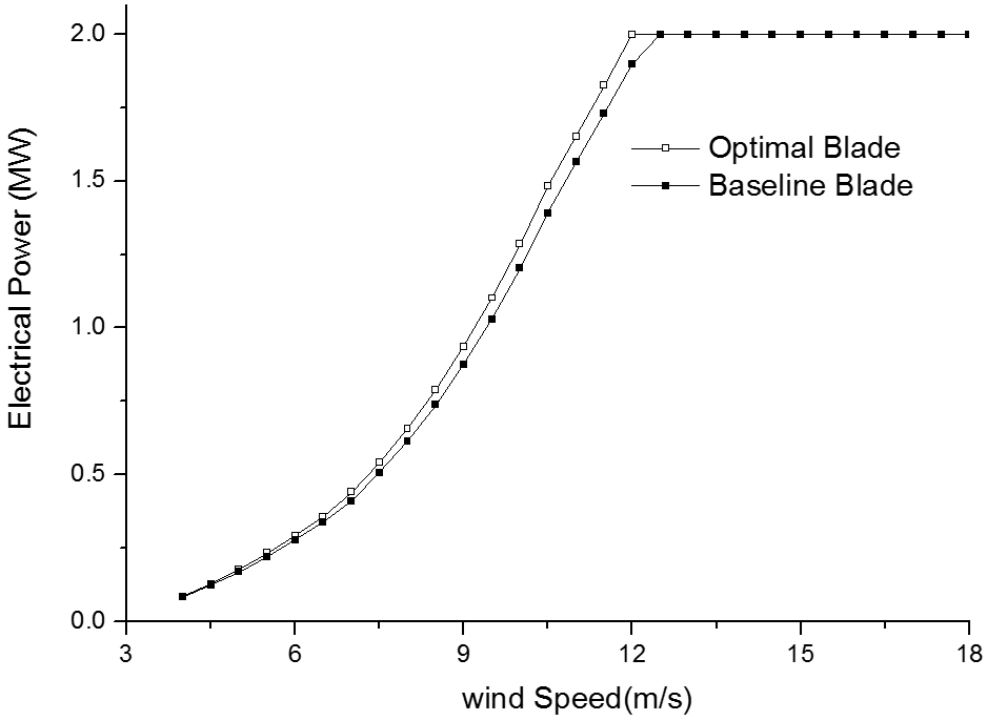

Figure 7.3. Power curve comparison between the optimal and baseline blades

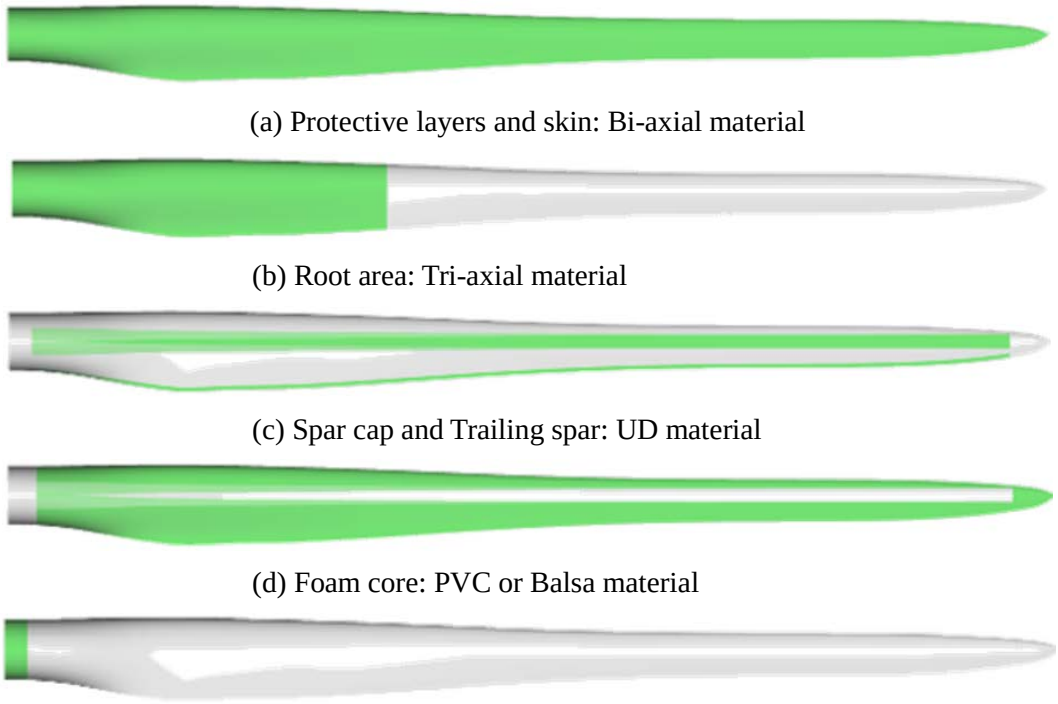

(a) Protective layers and skin: Bi-axial material

(b) Root area: Tri-axial material

(c) Spar cap and Trailing spar: UD material

(d) Foam core: PVC or Balsa material

(e) Extra root: Tri-axial material

Figure 7.4. Schematic description of the blade layer patterns

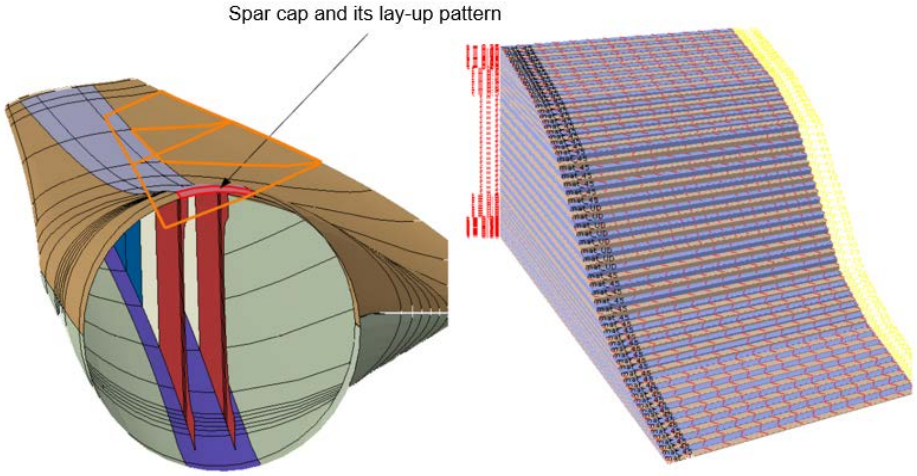

(a) Three-dimensional configuration and spar cap lay-up pattern

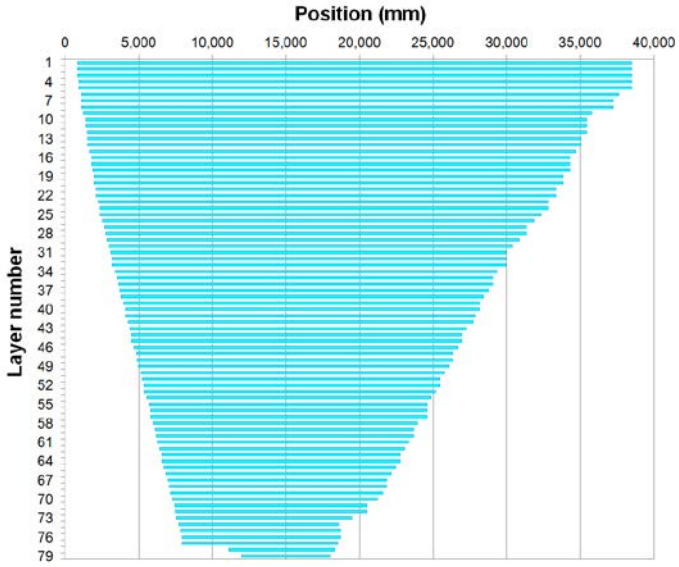

(b) Partial drawing for the spar cap lay-up pattern

Figure 7.5. Spar cap layer pattern

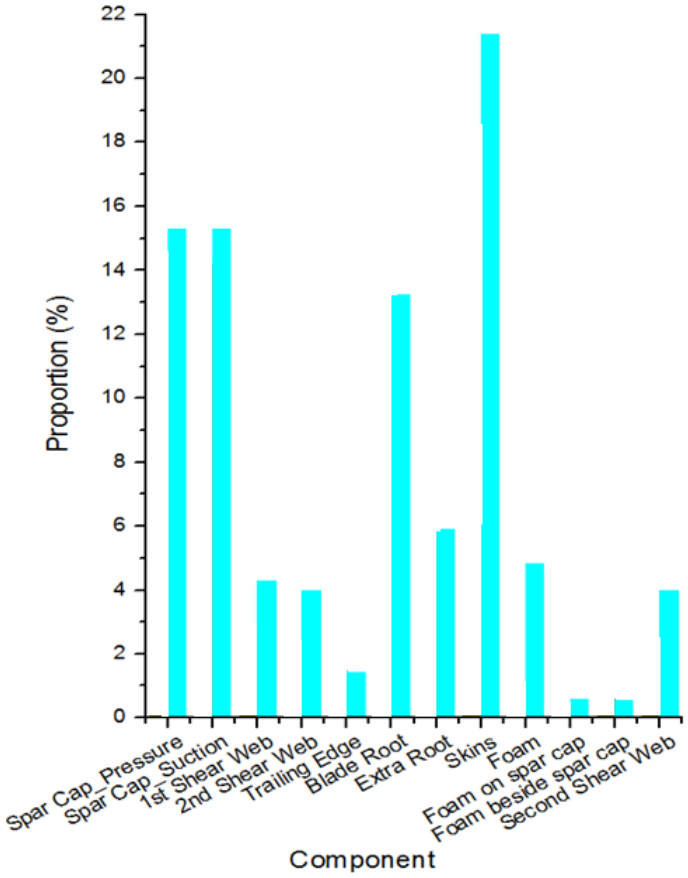

Figure 7.6. Weight composition ratio for the major components of the blade

Table 7.1. Modal analysis results

Mode	three-dimensional result (Hz)	Reference [31] (Hz)	Discrepancy (%)	Present (Hz)	Discrepancy (%)
1	0.857	0.965	-12.53	0.851	0.77
2	1.505	1.709	-13.60	1.507	-0.17
3	2.474	2.818	-13.91	2.485	-0.45
4	4.854	5.859	-20.71	4.983	-2.65
5	5.382	6.673	-23.99	5.526	-2.68

Table 7.2. Geometric comparison

Distance from root (m)	Baseline Blade		Optimum Blade		Comparison (%)	
	Chord Length(m)	Twist Angle(°)	Chord Length(m)	Twist Angle(°)	Chord Length	Twist Angle
0	2.100	15.000	2.100	15.000	-	-
1.399	2.209	15.000	2.209	15.000	-	-
6.747	2.600	15.000	2.597	14.690	-0.1	-2.1
7.987	2.527	14.487	2.586	13.550	2.3	-6.5
10.469	2.382	13.023	2.478	12.413	4.0	-4.7
11.755	2.307	12.264	2.368	11.270	2.6	-8.1
14.327	2.156	10.746	2.256	10.046	4.6	-6.5
15.852	2.067	9.846	2.139	8.666	3.5	-12.0
18.903	1.888	8.046	2.005	7.346	6.2	-8.7
20.345	1.804	7.195	1.872	6.079	3.8	-15.5
23.229	1.635	5.492	1.752	4.801	7.1	-12.6
25.660	1.493	4.640	1.593	4.038	6.7	-13.0
28.091	1.350	3.790	1.434	2.463	6.2	-35.0
33.950	1.007	1.738	1.073	0.745	6.5	-57.1
37.640	0.791	0.445	0.740	0.138	-6.5	-68.9
39.280	0.695	0.000	0.711	0.033	2.3	-
40.100	0.010	0.000	0.010	0.000	-	-

Table 7.3. Comparison of the aerodynamic design results

	Baseline Blade	Optimum Blade	Improvement
Rated Power	2MW	2MW	-
Rated Wind speed	12.5 m/s	12.0 m/s	- 4.00 %
Efficiency (C_P)	0.4487	0.4876	+ 8.67 %
Annual energy production (AEP)	4,665 MWh/y	4,975 MWh/y	+ 6.65%

Table 7.4. Structural design results by the optimization algorithms

	Initial blade	Baseline blade (optimized spar cap)	Applied optimization algorithm	
			Genetic algorithm	Nelder-Mead simplex
Total weight	7,838 kg	7,214kg	7,124kg	7,711kg
Calculation time	-	0.5days	2.5days	1days
Maximum number for the spar cap layer	92 plies	71 plies	45 plies	75 plies
2nd shear web location	-	-	Move 6% to the left	Move 18% to the left
Failure criterion	Safe	Safe	Safe	Safe

Chapter 8

CONCLUSIONS

The bigger the blades, the more energy the turbine may generate. Greater rotor area suggests that the turbine be capable of collecting more amount of the wind. Therefore, the manufacturers seek to create turbines that is capable of generating more energy either by reaching the faster wind speeds in loftier heights, or by increasing the rotor size.

Thus, the design of the blades for wind turbines should consider the interaction among power production, efficiency, blade tip deflection, buckling stability, and fatigue limit conditions. Although complex blade design is carried out in consideration of those various design variables, it is conducted by the present blade design and its optimization method. Those are arranged with optimal aerodynamic design, initial structural design, and optimal cross-sectional design, and their details are summarized as follows.

Regarding the optimal aerodynamic design, in this thesis, the blade efficiency,

rated power, and thrust are calculated based on BEMT and improved blade design scheme is introduced. It considers multiple design parameters, such as the chord length and the twist angles along the blades for an optimal design of the wind blades by using the second-order RSM. Through the proposed optimization methodology, the blade efficiency and AEP result in improvement, and the rated wind speed is also enhanced.

In the field of the initial structural design, design for increased rigidity and decreased weight is carried out. This thesis proposes a preliminary structural design scheme based on CLT for an initial structural design of a multi-MW wind turbine blade. Diverse design approaches, such as the trend line forecast of the normalized spar cap thickness distribution, prediction of the axial- and twist coupling stiffness coefficient for the spar cap, and one-dimensional beam formulation for the tip deflection prediction, are suggested for the present structural design.

For the initial blade, optimal cross-sectional design is performed for several optimization points in the longitudinal direction of the blade. The optimization method is established on the basis of ATR optimization procedure and a cross sectional analysis is performed using the commercial program, VABS. To achieve the objective function of the minimum weight, design variables, such as the number for the spar cap plies, skin, shear web, root/shear web location, and thickness for shear web foam are used.

The design procedures presented in this thesis show advantages over the conventional blade design procedures. Those are summarized as follows.

- ✓ Less engineering work: for calculations using VABS, only 9,814 elements, or about 39% of ANSYS, are used. Conversely, ANSYS finite element model contains 24,366 nodes and 25,041 elements. Hence, large amount of computational resources and time are required. However, the design method proposed in this thesis does not require complicated and time-consuming procedures.
- ✓ Reduced design period: only 2 months are needed for this design procedure. Conversely, it typically takes more than 12 months for the three-dimensional procedure. For the three-dimensional FE analysis, CAD program is used to illustrate the blade, and then, it requires mesh operations for the three-dimensional modeling. Hence, large amount of computational resources and time will be required. However, the design method proposed in this paper does not require complicated and time-consuming procedures. Based on the beam constitutive equation, an analytical approach for a laminated composite blade is suggested. Relatively small amount of calculations is required for VABS and the improved optimization framework. Therefore, it is possible to reduce the design period because it takes only 16% of the time required for a three-dimensional procedure.
- ✓ Excellence of results: Through the proposed optimization methodology, the blade efficiency is increased by 8.7% and the rated wind speed is also enhanced by 4% from 12.5m/s to 12m/s. AEP shows an increase of approximately 7%. In addition, the initial blade weight is 7,838 kg, and the final optimal cross-sectional design result is only 7,124 kg, which is

about 700 kg (9.11%) in a reduction compared to the initial weight.

- ✓ High accuracy: tip deflection prediction is performed, and the results of one-dimensional beam formulation and FEA correspond to 4.1 m and 3.74 m, respectively, for the flap-wise direction of the blade. The discrepancy in the results of the present and finite element analysis is 8.8%. Thus, the discrepancy is not significant in the initial structural design phase.

However, there are many other objectives which are not considered in this thesis such as the consideration of the blade manufacturing method and design evaluation through the full scale blade test. The blade design method introduced in this thesis is conducted based on the resin infusion method, which is the most common blade manufacturing method. However, as the blades continues to grow larger and the weight increases accordingly, it is expected that production of the blades using the pultrusion process will become more common in the future. In case of resin infusion method, skin, shear web, and spar cap are made separately and combined into bonding. However, in the case of the pultrusion process, the spar cap part is formed in a square shape with the skin, and due to this difference, the current design method based on the resin infusion method will need to be changed. Therefore, it will be necessary to change the design methods appropriate for such new fabrication methods. Finally, carrying out design verification on the various items such as the maximum displacement, modal test, buckling stability through full scale blade test will also be topics of the future study.

Bibliography

[1] Anonymous, "International Wind Energy Development-Supply Chain Assessment 2015-2018," *BTM Consult*, April 2019.

[2] Anonymous, "Wind Energy Market 2010/2011," German Wind Energy Association (*BWE)*, April 2019.

[3] Glauert, H., “Airplane Propellers, In Division L of Aerodynamic Theory,” *Springer-Verlag*, 1976.

[4] Maalawi, K. Y., and Badawy, M. T. S., “A Direct Method for Evaluating Performance of Horizontal Axis Wind Turbines,” *Renewable Sustainable Energy*, 5, 175-190, 2001.

[5] Kim, B.S., Kim, W.J., Bae, S.Y., Park, J.H., and Kim, M.E., "Aerodynamic Ddesign and Performance Analysis of Multi-MW Class Wind Turbine Blade," *Journal of Mechanical Science and Technology*, 2011.

[6] Jerson, R., João, T.P., and André, L.A., "An extension of BEM method applied to horizontal-axis wind turbine design," *Renewable Energy*, 36(6), 1734-1740, 2011.

[7] Lanzafame, R., and Messina, M., “Fluid Dynamic Wind Turbine

Design: Critical Analysis, Optimization and Application of BEM Theory,” *Renewable Energy*, 32, 2291-2305, 2007.

[8] Patrick, M.S., and Choi, Y.D., "Numerical Analysis for a Proposed Hybrid System with Single HAWT, Double HATCT and Vertical Oscillating Wave Energy Converters on a Single Tower," *Journal of Mechanical Science and Technology* ,30(10), 4609-4619, 2016.

[9] Mostafa, F., Mahdi, N.A., Omid, N., Ali, M., and Kim, K.C., “Aerodynamic Performance Improvement of Wind Turbine Blade by Cavity Shape Optimization,” *Renewable Energy*, 132, 2019.

[10] Ozge, P., and Ismail, H.T., "Aerodynamic Shape Optimization of Wind Turbine Blades Using a Parallel Genetic Algorithm," *Procedia Engineering*, 61, 28-31, 2013.

[11] Wei, J.Z., Wen, Z.S., and Jens, N.S., "Integrated Airfoil and Blade Design Method for Large Wind Turbines," *Renewable Energy*, 70, 172-183, 2014.

[12] Krishnil, R.R., Sunil, P.L., and Rafiuddin, M.A., "Design and Optimization of Airfoils and a 20kW Wind Turbine Using Multi-Objective Genetic Algorithm and HARP_Opt Code," *Renewable Energy*, 2018.

[13] Vincent, D., Mohamed, L.L., Jonathan, S., and Hachimi, F., "Application of the Blade Element Momentum Theory to Design Horizontal Axis Wind Turbine Blades," *Journal of Solar Energy Engineering*, 140(1), 2017.

[14] Bai, C.J., Chen, P.W., and Wang, W.C., "Aerodynamic design and analysis of a 10-kW horizontal-axis wind turbine for Tainan, Taiwan," *Clean Technologies and Environmental Policy*, 18, 1151-1166, 2016.

[15] Li, J.Y., Li, R., Gao Y, and Huang, J., "Aerodynamic Optimization of Wind Turbine Airfoils Using Response Surface Techniques," *Proceedings of the Institution of Mechanical Engineers, Part A: Journal of Power and Energy*, 224(6), 827-838, 2010.

[16] Toft. H.S., Svenningsen, L., Moser, W., Sørensen, J.D., and Thøgersen, M.L., "Assessment of Wind Turbine Structural Integrity Using Response Surface Methodology," *Engineering Structures*, 106, 471-483, 2016.

[17] Tabatabaeikia, S., Ghazali, N.N.B.N., Chong, W.T., Shahizare, B., Izadyar, N., Esmaeilzadeh, A., and Fazlizan, A., "Computational and Experimental Optimization of the Exhaust Air Energy Recovery Wind Turbine Generator," *Energy Conversion and Management*, 126, 862-874, 2016.

[18] Huang, B., Usui, Y., Takaki, K., and Kanemoto, T., "Optimization of Blade Setting Angles of a Counter-Rotating Type Horizontal-Axis Tidal Turbine Using Response Surface Methodology and Experimental Validation," *International Journal of Energy Research*, 40(5), 610-617, 2016.

[19] Sun, H.S., "Wind Turbine Airfoil Design Using Response Surface Method," *Journal of Mechanical Science and Technology*, 25(5), 1335-

1340, 2011.

[20] Chattopadhyay, A., "Application of optimization methods to helicopter rotor blade design," *Structural Optimization*, 2, 11-22, 1990.

[21] Eun, W.J., Sim, J.S., Lee, S.W., and Shin, S.J.," Further Improvements in the SNUF Blade Design by Numerical Design Optimization Framework," *ASCE Journal of Aerospace Engineering*, 31,1-15, 2018.

[22] Lim, J.H., Shin, S.J., and Kee, Y.J., "Optimization of Rotor Structural Design in Compound Rotorcraft with Lift Offset," *Journal of the American Helicopter Society*, 1, 2016.

[23] Friedmann, P.P., Glaz, B., and Palacios, R., "A moderate deflection composite helicopter rotor blade model with an improved cross-sectional analysis," *International Journal of Solids and Structures*, 46, 2186-2200, 2009.

[24] Kovalovs, A., Barkanov, E., and Gluhihs, S., "Numerical optimization of helicopter rotor blade design for active twist control," *Aviation*, 11(3), 2007.

[25] Kang, J. P., Eun, W. J., Lim, J. H., Visconti, U., and Shin, S.-J., “Design improvements of smart active trailing-edge flap for rotating test,” *Proc., 56th AIAA/ASME/ASCE/AHS/ASC Structures, Structural Dynamics and Materials Conf.-Adaptive Structures Forum, AIAA*, 2005.

[26] Perry, R.J., Wirz, R.E., and Lin, E., "Structural design of spars for 100-m biplane wind turbine blades," *Renewable Energy*, 71, 133-155, 2014.

[27] Barnes, R.H., and Morozov, E.V., "Structural optimisation of composite wind turbine blade structures with variations of internal geometry configuration," *Composite Structures*, 152(15), 158-167, 2016.

[28] Maheri, A., Noroozi, S., and Vinney, J., "Combined analytical/FEA-based coupled aero structure simulation of a wind turbine with bend-twist adaptive blades," *Renewable Energy*, 32(6), 916-930, 2007.

[29] Maheri, A., Noroozi, S., and Vinney, J., "Application of combined analytical/FEA coupled aero-structure simulation in design of wind turbine adaptive blades," *Renewable Energy*, 32(12), 2011-2018, 2007.

[30] Barr, S.M., and Jaworski, J.W., "Optimization of tow-steered composite wind turbine blades for static aeroelastic performance," *Renewable Energy*, 139, 859-872, 2019.

[31] Liao, C.C., Zhao, X.L., and Xu, J.Z., “Blade layers optimization of wind turbines using FAST and improved PSO algorithm,” *Renewable Energy*, 42, 227-233, 2012.

[32] Anonymous, “Wind turbine part5: wind turbine blades,” *International Electro-technical Commission*, IEC: 61400-5, 2017.

[33] Tabassum A., Premalatha M., Tasneem A., Abbasi S.A., "Wind energy: Increasing deployment, rising environmental concerns," *Renewable and Sustainable Energy Reviews*, 31, 270-288, 2014.

[34] Cesnik, C. E. S., Shin, S.-J., and Wilbur, M. L. “Dynamic response of active twist rotor blades,” *Smart Mater. Struct.*, 10(1), 62–76, 2001.

[35] Yu, W., Hodges, D. H., Volovoi, V., and Cesnik, C. E. S. “On

Timoshenko-like modeling of initially curved and twisted composite beams," *Int. J. Solids Struct.*, 39(19), 5101–5121.2002.

[36] Armanios, E.A., and Badir, A.M., "Free Vibration Analysis of Anisotropic Thin-Walled Closed-Section Beams," *AIAA Journal*, 33(10), 1905-1910, 1995.

[37] Pirrera, A., Capuzzi, M., and Buckney, N., Weaver, P.M., "Optimization of Wind Turbine Blade Spars", *53rd AIAA/ASME/ASCE/AHS/ASC Structures, Structural Dynamics and Materials Conference, AIAA* 2012-1500, 2012

[38] Zhu, J., Cai, X., Pan, P., and Gu, R., "Optimization design of spar cap layup for wind turbine blade", *Frontiers of Structural and Civil Engineering*, 6(1), 53-56, 2012.

[39] Griffin, D.A., and Ashwill, T.D., "Alternative Composite Materials for Megawatt-Scale Wind Turbine Blades: Design Considerations and Recommended Testing ", *Journal of Solar Energy Engineering*, 125(4), 515-521, 2003.

[40] Anonymous, "Cost Study for Large Wind Turbine Blades: WindPACT Blade System Design Studies", *SANDIA report, SAND2003-1428, TPI Composites Inc*., 2003

[41] Lekou, D. J., "Scaling limits & costs regarding WT blades", *Upwind*, 2010.

[42] Chaviaropoulos, P.K., Langen, P.J., and Jamieson, P., "Similarity rules for W/T up-scaling", *UPWIND report*, 2007

[43] Berdichevsky, V., Armanios, E.A., and Badir, A.M., “Theory of Thin-Walled Anisotropic Beams,” *Journal of Composite Materials*, 5(2), 411-432, 1992.

[44] Libove, C., “Stress and Rate of Twist in Single-Cell Thin-Walled Beams with Anisotropic Walls,” *AIAA Journal*, 26(9), 1107-1118, 1998.

[45] Puck, H.S., “Failure analysis of FRP laminates by means of physically based phenomenological models,” *Composites Science and Technology*, 58(7), 1045-1067, 1998.

[46] Herbert, J. S. and John, F. M., “Optimized Goodman diagram for the analysis of fiberglass composites used in wind turbine blades," *AIAA*, 0196, 1-10, 2005.

[47] Mahmood, M.S. and Roham, R., "Simulation of fatigue failure in a full composite wind turbine blade," *Composite Structures*, 74, 334-339, 2006.

[48] http://www.minitab.com

[49] https://www.dnvgl.com/services/wind-turbine-design-software-bladed-3775

[50] Bot, E T.G., "Aerodynamics Table Generator; Handleiding," *ECN-C-01-077*, 2001.

[51] https://www.lmwindpower.com/en/stories-and-press/stories/innovation/innotip-at-the-tipof-innovation

[52] Cox, K., and Echtermeyer, A., “Structural Design and Analysis of a 10MW Wind Turbine Blade”, *Energy Procedia*, 24, 194-201, 2012.

[53] Song, F., Ni, Y., and Tan, Z., “Optimization Design, Modeling and Dynamic Analysis for Composite Wind Turbine Blade”, *Procedia Engineering*, 16, 369-375, 2011.

[54] Lee, K., Huque, Z., Kommalapati, R., and Han, S.E., "Evaluation of Equivalent Structural Properties of NREL Phase VI Wind Turbine Blade," *Renewable Energy*, 86, 796-818, 2016.

[55] Anonymous, Wind energy generation systems - Part 1: Design requirements, IEC 61400-1:2019.

[56] Anonymous, "Design and manufacturing of wind turbine blades, offshore and onshore wind turbines," *Rules and Guideline*, Det Norske Veritas (DNV), 2010.

[57] Lloyd, G., “Guideline for the Certification of Wind Turbines Edition," *Rules and Guideline*, 2010.

[58] Griffith, D.T and Ashwill, T.D., "The Sandia 100-meter all glass baseline wind turbine blade: SNL100-00", 2011.

[59] Anonymous, "Finding design solutions for very large wind turbines," *UPWIND project*, RISO-DTU, 2011.

국문 초록

다양한 설계 요소를 고려한 풍력터빈 블레이드 최적 설계

이상래

서울대학교 대학원

기계항공공학부

본 논문에서는 풍력 터빈이 20 년의 경제 수명 동안 작용할 수 있는 다양한 하중을 고려하여, 풍력 블레이드의 최적 설계에 관한 연구를 수행하였다. 블레이드 최적 설계를 위해 블레이드의 형상을 결정하는 공력설계, 안전도를 보장하는 구조설계와 같은 설계 단계와 함께 이를 이용한 하중 해석, 하중 해석 결과를 이용한 구조 건정성 평가를 각각 수행하였다.

최적 블레이드 공력설계를 위해 반응표면분석법(RSM)을 적용하여 최적의 시위 길이와 비틀림 각도의 조합을 블레이드 길이 방향으로 각각 계산하였으며, 이렇게 계산된 블레이드 형상을 이용하여 연간 에너지 생산(AEP) 계산 등을 수행하였다. 구조 설계의 경우, 현재

운영중인 상업용 블레이드를 참고하여 블레이드 구조 설계의 가장 핵심인 Spar cap 을 대상으로 최대의 강성과 최소의 중량을 가지는 최적 설계를 진행하였으며, 이렇게 설계된 블레이드 섹션을 대상으로 VABS 를 이용하여 다양한 설계변수(적층 개수,전단 웹 위치등)를 고려한 최적 설계를 추가로 수행하였다. 설계가 완료된 블레이드를 대상으로, 블레이드를 길이방향으로 여러 개의 섹션으로 구분, 하중 해석에 필요한 정보(단위 무게, 굽힘 강성, 비틀림 강성)를 각각 추출하였으며, 이 값들을 이용해서 블레이드 요소 모멘텀 이론(BEMT)과 CFD 를 활용하여 하중 해석을 수행하였고, 결과는 블레이드 구조 건전성 평가를 위해 사용되었다. 블레이드 구조건전성 평가의 경우, 타워와의 간섭을 피하기 위한 최대변위 평가, 좌굴, 섬유 및 수지 파손, 피로 평가 등의 항목으로 블레이드 구조에 대한 평가를 수행하였으며, 이를 통해 블레이드의 최적 설계와 안전도 평가를 수행하였다.

주요어: 풍력발전시스템, 블레이드, 최적설계, 블레이드 요소 모멘텀 이론(BEMT), 반응표면분석법(RSM), 공탄성 해석, 등가보 모델, VABS, 연간에너지생산(AEP)

학 번: 2013-30951